Delft University of Technology

Analysis and Optimization of Transverse Post-Tensioning in Immersed Concrete Tunnels

Natalia Vilanova Hanusaik

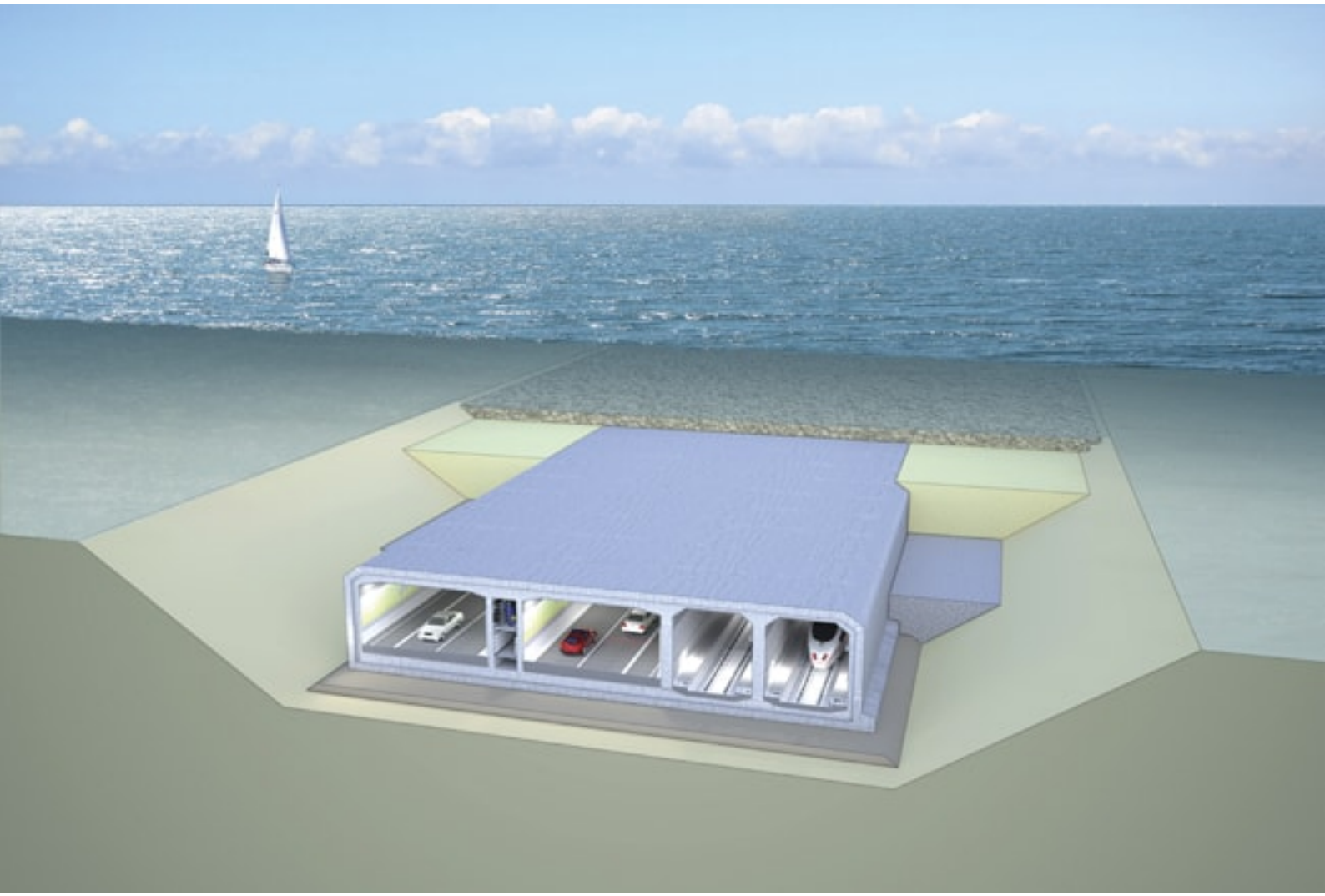

TU Delft

Royal HaskoningDHV
Enhancing Society Together

Analysis and Optimization of Transverse Post-Tensioning in Immersed Concrete Tunnels

by

Natalia Vilanova Hanusaik

to obtain the degree of Master of Science

at the Delft University of Technology,

to be defended publicly on Tuesday June 29, 2021 at 10:30 AM.

Student number:	4793498	
Thesis committee:	Dr. ir. Y. Yang,	TU Delft, Chair
	Dr. ir. C.B.M. Blom,	TU Delft, Supervisor
	Prof.dr.ir. J.G. Rots,	TU Delft, Supervisor
	Ir.C. M. P. 't Hart,	Royal HaskoningDHV

TU Delft

Royal HaskoningDHV
Enhancing Society Together

Acknowledgements

This thesis was written as part of the Master of Science in Structural Engineering (Concrete Structures) at the Technical University of Delft. I would like to acknowledge and express my gratitude to the people who have made this possible.

Firstly, I would like to thank Royal Haskoning DHV who offered me the incredible opportunity to work alongside them on this research. This thesis would not have been possible without their support. I would especially like to thank Marcel, my daily supervisor, for his ongoing patience, feedback and unwavering dedication to answering all my questions in a prompt and friendly manner. Thank you to Yuguang Yang, my chairman, for the enlightening guidance he's provided me throughout my progress and steering me in the right direction. I want to thank Kees Blom for his critical and constructive feedback, always helping me keep the broader picture in mind. Finally, thank you to Jan Rots for his interest in my research and his support.

I want to especially thank my mom, my dad, my brother and my sister for always supporting me in my choices. I cannot express how thankful I am to all my friends and how lucky I have been to have them this past year. To my friends from Delft, thanks for having been there from the start and I am sure for the many years to come. I am grateful for the support and the unbelievable student experience. Thank you to housemates who made this difficult last year of lockdown bearable and putting up with me. Special thanks to my friends who indulged in my queries about the workings of python and all things concrete, Berber, Geovanny, Nate, Giulia and Marco. Finally thanks to friends who are always with me in spirit from afar and have provided endless support and helped me through this rollercoaster. It goes without saying that I would have never made it this far without you all.

Natalia Vilanova Hanusaik
Delft, June 2021

Abstract

Due to the recent increase in traffic capacity requirements, the need for larger spans in immersed concrete tunnels has become a pressing matter. Although commonly used in Europe, reinforced concrete has a structural capacity limit when it comes to the transverse span length. The implementation of post-tensioning could allow for longer spans and a reduction in the overall concrete used. This technique is however rarely used in industry due to the complexity of applying it to underwater environments and the varied loading conditions an immersed tunnel element is subjected to. When implementing post-tensioned tendons, the curvature creates additional distributed loads which compensate for the high hydrostatic pressures and backfilling weight present at the final immersed stage of the tunnel. Due to the absence of these loads during the initial stages, prior to transportation, high tensile stresses are exhibited which can lead to severe cracking. Crack mitigation can be achieved by implementing permanent additional reinforcements in the opposite face of the post tensioning tendon. Additionally, another method is installing a temporary system connecting top and bottom slabs to replicate the final loading conditions. The objective of this research is to investigate the governing limitations of implementing transverse post-tensioning and evaluate when it is a structurally viable option. A case study is done at the end of this research to investigate the methods of improving the limitations and increase the structural capacity.

Using finite element modelling, a linear analysis was carried out to evaluate the behavior of the structure after implementing post-tensioning loads in the cross section and to identify the critical areas. The assumptions for the analytical moment distribution were found to overestimate the rigidity of the structure and made for larger moments at the wall-top slab connections, which were adjusted for the remaining parts of the study. An analysis into the effect of adding post-tensioning in the lower bottom slab revealed a substantial improvement in the final stage stress distribution, and was observed to be in full compression. A nonlinear analysis was used to provide insight into the global structural behaviour for both final immersed and dry dock stages. The final immersed stage exhibited linear elastic behaviour, whereas, the onset of cracking was observed at the top of midspan at the dry dock stage.

In a further analysis of the critical dry dock stage, the relation between partial prestressing, curvature of post-tensioning tendons and the effects on the cracking behaviour at midspan was explored. The results show that when maximum curvature and percentage of prestressing are simultaneously present, the crack width limit is reached. When slightly lowering either of these parameters, a substantial decrease in the amount of reinforcement is needed to mitigate these cracks. Since lowering the curvature implies an increase in required prestressing force, the more economical option is to lower the percentage of prestressing. This entails increasing the flexural longitudinal reinforcement to maintain the structure's capacity. Based on the assumptions made during the study, a maximum span length of 25m with a height of 1.3m was achieved. When increasing the inner tunnel height and span height, a length of 29m could be reached. An approximate 25% increase in slenderness was observed over the reinforced concrete tunnel, analyzed in this study.

Lastly, a case study was carried out on the Fehrmanbelt Fixed Link to analyze two methods to improve the dry dock critical sections when applying post-tensioning. An optimization of the top slab reduced the height by 0.08m through the implementation of post-tensioning with a reduction in both curvature and prestressing percentage. Due to it's unique two storey design, the possibility of utilizing temporary tendons as a method to mitigate midspan cracking at the dry dock was considered. Using a nonlinear analysis, three different models were analyzed: no additional reinforcement, top slab reinforcement and temporary tendons connecting top to middle slab. The results of these models showed that the temporary tendons increased the capacity locally of the midspan, however the additional reinforcement exhibited an overall improvement in both the midspan and the global capacity of the structure. This study found that implementing transverse post-tensioning was feasible when reducing the curvature of the tendons, reducing amount of prestressing and implementing additional reinforcement, which helped increase structural capacity of the critical areas in the dry dock stage.

List of Tables

List of Figures

Contents

1 Introduction

1.1. Immersed Tunnels

Immersed tunnels are recently becoming a more viable option in the transportation industry, with the development of construction techniques, making it a safer and cheaper option. They are increasing in size as well as the immersion depth, offering many benefits over the alternative options, namely bridges and bored tunnels.

An immersed tunnel consists of multiple segments constructed in a casting basin and then floated out to the final location and immersed into place using the immersed tube technique. This means the elements are placed on the river or sea bed and then backfilled to keep it in place and avoid collisions. With rivers and canal crossings, immersed tunnels have proven to be the best choice over bridges and bored tunnels in some circumstances.

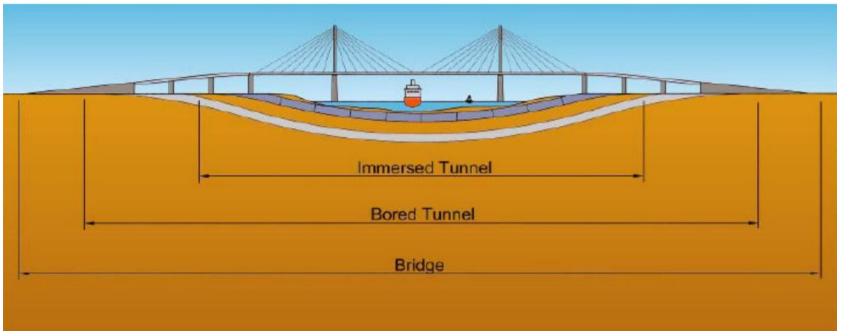

Figure 1.1: Comparison between different types of fixed links[1]

One of the benefits, as seen in Figure1.1, is the length of the tunnel itself. In some instances, since the tunnel lies close to the water bed level, this will limit construction depth. When comparing the option to a bored tunnel, the immersed tunnel onramps will be considerably shallower, resulting in a reduction in cost associated with the minimized dredging and length [13].

Bridges have a higher impact on existing land and water traffic. They might be seen as visually intrusive or results in too much disruption with the existing structures on land. Other issues could be the large clearance that might be required due to ship traffic, disturbance of the piers with water exchange, and impacts on its environment.

Comparing it to a bored tunnel, typically, the dredging of bored tunnels in the approaches causes more hindrance than immersed tunnels. However, the disturbance of dredging required along the water bed for an immersed tunnel can have a negative impact as well. Immersed tunnel construction relies on dredging, element casting and installation, all of which can happen simultaneously. Bored tunnels, on the other hand,

have limited planning to work with. However, immersion tunnels require a dry dock to cast all the elements; this takes place on a large piece of land not far from the final location, which is not always feasible.

The Netherlands is one of the leading countries in Europe for immersed tunnel design and has primarily focused on reinforced concrete tunnels. Starting with the Maastunnel, completed in 1942, the first tunnel of its kind, using reinforced concrete with a rectangular box shape. There were already five tunnels built prior in North America, but these had a circular shape and were made predominantly out of steel[14].

The main types of immersed tunnels built today are mainly out of reinforced concrete, steel plates or a steel-concrete-steel sandwich composite. Concrete tunnels are predominantly found in Europe vs. steel in North America. Another leading country for constructing immersed tunnels has been Japan, where both steel and concrete are being used.

1.2. Immersed Tunnel Options

The most widely used tunnel material in Europe and the focus of this thesis is the segmental concrete immersed tunnel. This means that the concrete tunnel elements are divided into segments which help mitigate longitudinal shrinkage cracks. The alternative, most commonly used in the past, consists of monolithic concrete elements which are not broken down into smaller elements.

In addition to concrete tunnels, some tunnels incorporate steel which are: single steel shell, double steel shell and composite concrete steel sandwich. The shells use an outer watertight layer of steel, and in the case of the double, also an inner layer. The steel-concrete-steel composite sandwich tunnel is composed of both internal and external steel. The middle is filled with non-shrink self-compacting concrete, connected by steel studs and plates to the external steel.

1.3. Tranverse Post-tensioning

Reinforced concrete immersed tunnels have limited span slenderness for the top, and bottom slabs, which is where transverse post-tensioning could be an option to optimize its size. Post-tensioning would allow for higher capacity concrete slabs, making them more slender and ultimately allowing for a wider tunnel cross-section.

One of the main challenges with using post-tensioning for immersed tunnels is the difference in loading from the dry dock stage, where the elements are cast on land, to the final immersed stage, which include the hydrostatic and backfilling loads. Typically in prestressed bridge beams, the dead load of the weight encompasses 80-90% of the final stage, which includes the live loads. When it comes to immersed tunnels, the self-weight of the tunnel can be anywhere from 10-40% of the tunnel's final loading. This is an issue when designing post-tensioning for the final design, as additional reinforcement is required to mitigate cracks that would form due to the camber from the high prestressing loads.

1.4. Previous Projects

The following projects have implemented transverse post-tensioning in their design:

- Louis-Hippolyte tunnel in Montreal, Canada
  - Transverse post-tensioning was used to minimize the tunnel height, which helped to shorten the tunnel over 65m, a crucial aspect for the designers. A temporary system was used where prestressed bars were placed to prevent the roof from bucking upward due to the prestressed forces. These ties were then gradually relaxed as the elements were immersed.
- Kennedy/Schelde tunnel in Belgium

– In this case, tunnel approaches had to be as short as possible due to limitations at the embankments. Post-tensioning was implemented in both the top and bottom slab prior to immersion. The final layout is seen below in Figure 1.2. Additional reinforcement was installed at the opposite faces in order to mitigate the counteracting prestressing loads.

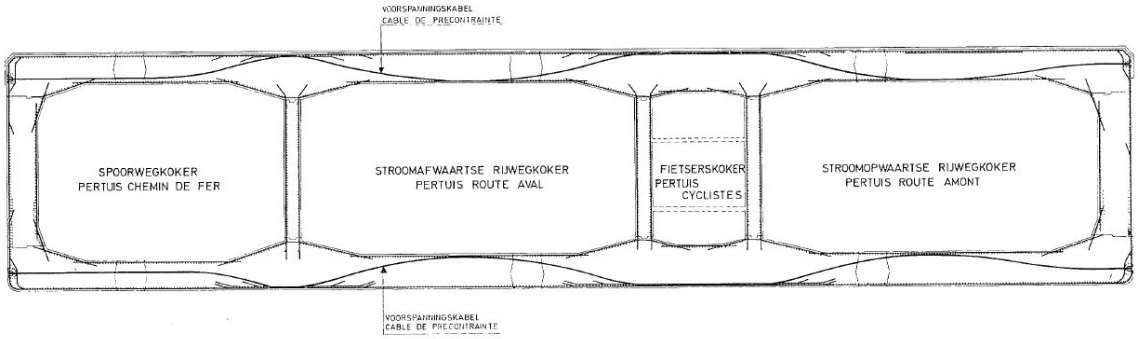

Figure 1.2: Post-tensioning layout in the Kennedy tunnel [2]

- Rupel Tunnel in Belgium
  - This tunnel was subjected to heavy surcharge ground loads, and transverse post-tensioning was used to increase capacity.
- Bjorvika tunnel in Norway
  - Only used in the first two segments of an element that were located at a shallow depth. Both the top and bottom slabs were post tensioned, to withstand the additional loading of a quay that was constructed on top of the tunnel at those particular locations.

Looking at the past projects that have used transverse post-tensioning, primarily used it to reduce the tunnel's height or to increase the capacity of the section for larger external loads. In the more recent project, when the width of the tunnel was large, transverse prestressing was considered in the initial stages. However, the amount of additional reinforcement required to compensate for the excess loading prior to immersion was not beneficial compared to regular concrete reinforced cross-sections.

1.5. Problem Definition

The use of transverse post-tensioning in immersed concrete is scarcely used due to its delicate mechanism for underwater usage, but more importantly, due to the difference in loading at the time of post-tensioning compared to the final stage after immersion. The need for larger spans in immersed concrete tunnels is increasing due to more significant traffic capacity requirements. Using reinforced concrete, which is largely used for immersed tunnels, especially in Europe, has a structural capacity limit regarding the transverse span length. The use of post-tensioning would allow for longer spans and a reduction in the overall concrete.

1.6. Research Project

This project aims to optimize the design of transverse post-tensioning in immersed concrete tunnels, identifying when it would be a structurally viable option. The curvature of the post-tensioning tendons creates additional loads, which are designed to compensate the high hydrostatic pressures and backfilling weight that is present at the final stage of the immersed tunnel. However, right after prestressing and up until the moment the element begins the immersion, it is predominantly the self-weight of the structure that counteracts the additional prestressing loads. As a result, very high tensile stresses are exhibited due to the post-tensioning at the initial stages, and this can lead to severe cracking if not mitigated with additional reinforcement. The

additional required reinforcement would only be in use temporarily. Transverse post-tensioning also adds a level of complexity to the constructibility of the element.

A few existing projects have utilised transverse post-tensioning, typically due to a design constraint that involved reducing the height of the tunnel. In most cases lowering the height and including an additional reinforcement resulting in considerable savings. In Montreal, Canada, Louis-Hippolyte Lafontaine tunnel utilized a temporary system in which post-tensioned tendons were installed, joining the top and bottom slab. The tendons were then cut as the elements were in their final position, making it possible to avoid implementing permanent additional reinforcement. This solution is not desirable due to the constructability issues that arise since the connection on the bottom slab interferes with the ballast tanks.

For most projects to date, reinforced concrete has had adequate capacity for the design, which is why post-tensioning is seldom required. Shenzhong, one of the widest tunnels designed will have an individual span length of approximately 18.5m using reinforced concrete for a 4-lane highway. As tunnels require larger span,s it is crucial to know where the governing limitations lie with reinforced concrete and what thresholds could be determined when switching to post-tensioning design. These would relate directly to the slenderness of the beam desired for the design. It is crucial to identify an adequate balance between the amount of prestressing, the curvature and the additional reinforcement. By optimizing these parameters, transverse post-tensioning could be a powerful alternative for immersed tunnel construction moving forward.

1.7. Research Questions

- What parameters limit the design widths of reinforced concrete immersed tunnels?
- What are the governing stages of the element when considering the effects of post-tensioning on thecross-section?
- What are the governing sections influenced by the implementation of post-tensioned loading?
- What methods can be used to increase the capacity in the governing sections?
- Optimize the degree of curved tendons in relation to the additional reinforcement required and prestressing losses. What is the optimal balance between amount of prestressing and curvature to minimize the impact at the dry dock stage?

1.8. Aims and Objectives

This research aims is to investigate the governing limitations of transverse post-tensioning and to evaluate when it is a viable option. Additionally, to determine a relation between partial prestressing and additional reinforcement. The details of post-tensioning should be analyzed to optimize the tendon profile by minimizing losses and controlling the loading exerted by them.

1.9. Methodology and Approach

The first steps will be to identify a relation between the slenderness of the slab and reinforcement requirements. Using the final immersed stage, the required post-tensioning forces will be determined. This will indicate the amount of maximum prestressing force needed. Numerical models will be done using DIANA to analyze the cross-section at the dry dock stage after the final stage exhibits adequate capacity. The analysis will indicate the areas of concern and the amount of additional reinforcement required to compensate for excess prestressing loads. From there, modifications will have to be made to the two different scenarios to determine a balance between prestressing and additional reinforcement.

Modification and optimization of the following parameters will be tested:

- Span slenderness
- Prestressing force required/ percentage of force implemented
- Tendon profile- degree of curvature
- Amount of additional reinforcement required to control cracking due to post tensioned loading.
- Allowable depth of structure

2

Background Research

2.1. General Immersed Tunnel Construction

Immersed tunnels were predominantly made out of steel, and when concrete started to become an attractive option, they were primarily very large monolithic elements. Starting around the 1960s this started to change, as smaller segments of about 20-30m each were being constructed to form 100m elements once connected. This was done to avoid the early thermal shrinkage cracking that would appear when casting very long elements, which meant an external waterproof membrane was no longer necessary. With the advancement of technology, controlling temperatures during casting also avoids fast temperature changes that would cause cracking.

That is why nowadays, the casting of the segments is done faster and in a more controlled manner in casting basins. The segments are then connected to each other to form a larger element. The elements are also often joined by longitudinal post-tensioning; this allows for an increase in stability during the floating and immersion process. Temporary bulkheads are placed, which provides a seal for the element during the whole floating process. The basin is then flooded to match the water level of the body of water it will be travelling in. It is then transported by means of floating and the help of tugboats to its final destination, where it will be submerged.

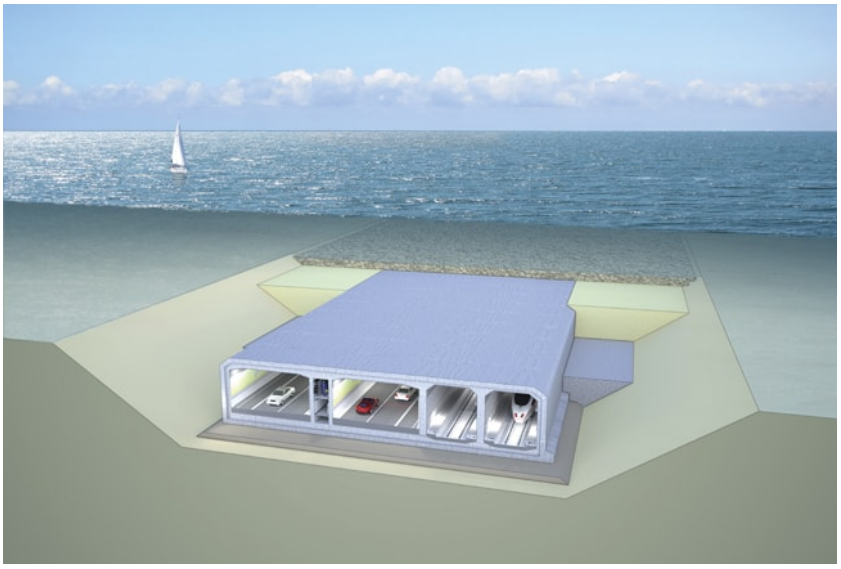

Figure 2.1: Placement of concrete tunnel and backfilling [3]

Meanwhile, dredging of the waterbed must take place, and a layer of gravel placed prior to the elements

being submerged. Once the element has reached the final location, it is lowered using the help of water ballast or tremie concrete. The next element is then placed, and the connection is done using omega and GINA gasket seals, which provide a watertight connection between the elements. Grout is inserted to make the joints between elements watertight. Longitudinal post-tensioning tendons are then cut, once the elements are in the final position. There are cases where it can be used permanently in the design to increase the tension and bending capacity of the vertical construction joints. This is mainly in areas where there is seismic activity[15]. Backfilling of the tunnel will then take place, which helps keep the element in place and minimize the movement that can take place due to the hydraulic loads. A protection stone later is then placed with its primary purpose of avoiding the damage that can occur from grounded ships or anchors colliding into the tunnel [1]. In Figure 2.1 above, the trench and then different layers of backfilling are visible, whereas Figure 2.2 illustrates a summary of the process.

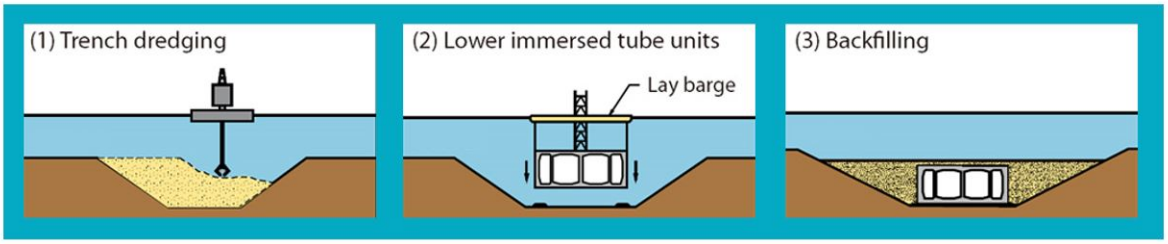

Figure 2.2: Process of immersing tunnel elements in a river or sea bed [4]

2.2. Tunnel Design

An immersed concrete tunnel experiences different internal and external loads throughout the initial stages, which include fabrication, floating, immersion and finally, the submerged stage. There are no external loads in the casting basin; then during the floating stage, buoyancy loads are acting on the element. To make sure there is the least possible risk of sinking in this stage, the element is designed to have a freeboard of 15-30cm. This means that the dimensioning of the tunnel is critical to optimize the use of the inner spaces and amount of concrete. The cross-section must have sufficient space for all the main services, either suspended from the roof or placed in the ballast layer. The cross-section must also be designed for the adequate size road and highway standards[16].

In the design stage, the weight of the concrete plays an important role; when the structure is very lightweight, it can have low stability when towing and a longer ballasting time. On the contrary, when it is heavyweight, then the buoyancy of the structure needs to be increased by making the internal clearance larger. Thus the cross-section size is increased, and more concrete is needed[16]. This might also mean that floating aiding measures would be required.

Having an adequate freeboard will influence the elements stability, and the time it takes for it to undergo immersion. For elements that have thick walls and are therefore heavier, the freeboard tends to be too low. The height or width of the structure has to increase in order to have an appropriate buoyancy force. With smaller freeboard values, the risk of the element sinking is high[16].

During the immersion stage, ballast water is added to create the necessary weight to sink the element to the proper location. In the final stage, the concrete structure experiences external loading from the hydraulic pressures, soil pressures, backfilling & rock protection, and the traffic loads requirements.

2.2.1. Structural design of immersed tunnels

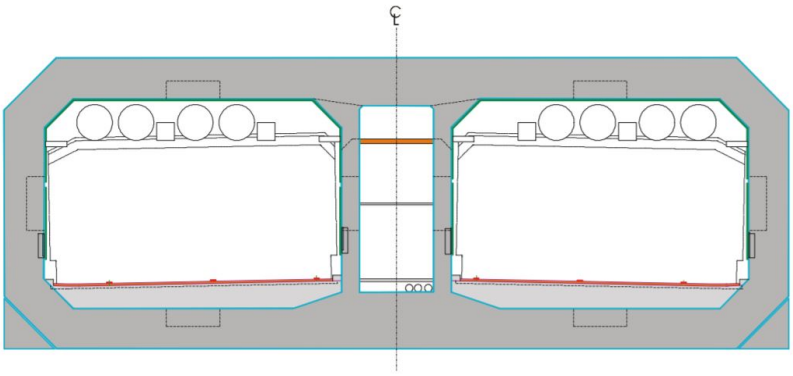

Figure 2.3: Typical cross-section of reinforced concrete immersed tunnel [5]

The typical cross-section of a concrete immersed tunnel is seen above in Figure 2.3. At the final water depth and highest sedimentation level is where the section is most critical due to the highest external loads, which should be the starting point of the transverse analysis[15].

Transverse dimensions are designed based on the following criteria:

- Large spans due to road design
- Water depth
- Ground cover of the tunnel
- Ground conditions
- Buoyancy requirements

The top and bottom slabs of the cross-section are subject to compression forces and bending tensile stresses. The sections require enough thickness so that the compression zones can avoid cracks from fully penetrating the slabs and leak through.

The dead load of the tunnel includes self-weight, ballast concrete, equipment load, hydrostatic pressure, vertical earth pressure, bilateral wall negative friction, concrete shrink and creep, and finally, foundation displacement impact. The list for live loads includes traffic load, water level variation, wave load, gradient temp and seismic load. There are also accidental loads to consider: sunken vessel, vessel impact, dropped anchor load, fire effect, extremely high water level and wave, explosion load, seismic load, and flooding.

Generally immersed concrete tunnel walls and slabs are 1m thick to accommodate hogging and sagging moment. A thick haunch is often required to increase resistance for the large shear forces. There is an axial compression that comes from the hydrostatic pressure in the final stage; this force increases the bending capacity of the section and is a benefit when it comes to the transverse design[17].

The shear transfer takes place in the intermediate joints. This can be achieved by using shear keys that are cast in-situ after immersion. Settlement discontinuities typically happen at the immersion joint; it is better not to have a fixed connection since significant moments and shear forces would result. Improvements for reduction of shear are:

- Ground improvement
- Delaying shear connection until some of the settlement has occurred

- Reinjection of bedding sand
- Preloading

A rubber gasket is fitted throughout the perimeter at the end of the elements, which forms the initial seal before removing the water held between the bulkheads. A second seal is then installed, which is the omega seal, on the inside of the rubber gasket.

When looking at longitudinal stresses, they are much lower when comparing them to transversal, but it is essential to look at the effect both have on each other. Transversal cracks caused by longitudinal action and longitudinal cracks caused by transverse bending. The subsoil ground pressure can cause uneven distributions, which vary with time, affecting the stresses significantly. Secondary effects like thermal shrinkage can also have an effect.

Instead of making the tunnel sections wider, the other option would be to make the cross-section taller, and then the need for a larger span would not be necessary. However, there are many more complications that arise. The constructability of the element in the casting bed would be more tedious and would require more steps. With an increase in height, the disadvantage comes with increased dredging, deeper basins and longer overall tunnel length.

2.3. Post-Tensioning

Using reinforced concrete, in general, has limitations when designing structures. The first is the limit of reinforcement ratio of 0.02 approximately. Once there is more reinforcement, the concrete compressive strength is governing, leading to brittle failures. The design bending moment increases at a rate of the span squared (l^2), deflection becomes an issue, and so does the ratio of variable load to permanent load that can be applied[6]. This means that the span length and slenderness of the span usually govern the design of the structure. Prestressing force is then required in these situations. In general, the benefits of prestressing allow for smaller section, smaller deflections, increased span length and increased durability. However, in the current industry, prestressed concrete has a higher risk associated with it due to the limited worldwide experience.

Due to the heavy water load on the structure, the bending moments to which it is subjected are very large, whereas the compressive stresses in the walls, roof, and bottom slab are relatively small. This requires large amounts of reinforcement, often larger diameter bars. Unfortunately, this affects the crack widths and the difficulty in limiting them[7]. Cracks will mainly occur in the construction dock on both the upper face at midspan and on the lower (inner) face near the centre support, as well as under service conditions on the lower face at midspan and on the upper face near the centre support. A simplified scheme is shown in Figure 2.4 showcasing the cracking due to the extreme camber. Therefore, it is essential to calculate the crack width taking into account the actual prestressing force that considers the losses.

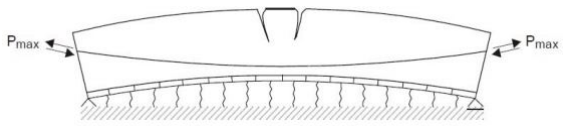

Figure 2.4: Flexural cracks at the opposite face due to high upward loads [6]

As mentioned in the Introduction, the loading in bridge structures, 70-80% of the total load is present when prestressed, which is self-weight and representing 90-95% of the permanent load. For immersed tunnels, the permanent load is 90% of the total load however, when the prestressing is happening, only 10-40% of that is present since the self-weight of the actual structure is not a significant component of it. For that reason, one of the key disadvantages of using post-tensioning in immersed concrete tunnels is having to mitigate the extra loads introduced by prestressing for the final stage.

Counteracting prestressing load

When it comes to counteracting the prestressing load at the dry dock, both permanent and temporary reinforcement can be used. Permanent would involve adding reinforcement to the critical areas in tension. Temporary reinforcement would mitigate the same critical stresses and avoiding cracking. Still, it would use a post-tensioned steel member that connects the bottom and top slabs to replicate the external loads. A study done for the HZMB Link showed a slight economic advantage to the temporary tie bar solution since there was less amount of rebar required. However, there is a significant disadvantage with this option, which is the constructability of the tunnel itself. These ties connect the bottom and top slabs in the centre of the span. This is where the ballast concrete tanks are placed, and therefore if the ties need to be placed there, the ballast tanks must be made into two separate tanks to allow a connection in the middle.

Detailing

The options for post-tensioning anchorage are to have a single end or multiple end anchorage. The single-end might require confinement reinforcement due to the sizeable concentrated force at one point. For multiple anchorages, it is possible to space them out as required, apply more compressive reinforcement, or even increase the concrete strength. When considering various anchors, it is improbable all will get overloaded with accidental loads. The scenario where one has to withstand a higher percentage of it is more probable[18].

The post-tensioning option would require complicated rebar detailing around the anchorages. This adds complexity and risk to the casting procedure[19]. This can be seen in Figure 2.5 below. Alternatively, in the Rupel tunnel, two anchors were used in the same cross-section.

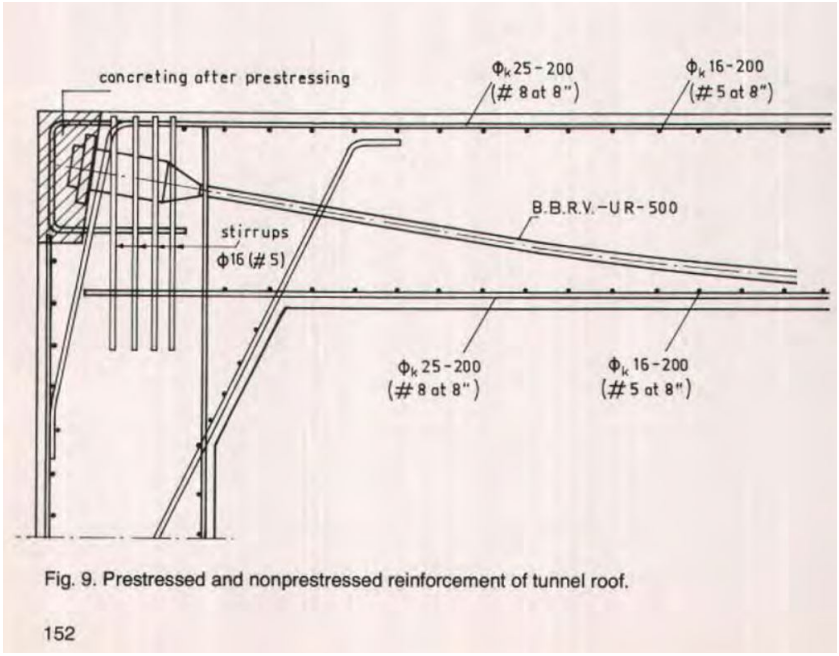

Figure 2.5: Post-tensioning anchor detail [7]

Post-tensioning losses

An essential factor to consider is all the prestressing losses that will occur, both immediately and over time. Thus, many factors come into play when optimizing the design of post-tensioning tendons. The first one is referred to as anchorage loss. The tendon is tensioned to its full strength, and when the jack is released, the force is transferred to the structure through the anchor. The loss occurs when the tendon slips before the wires are gripped by the wedge. The slip progresses until the force is fully developed and is typically between 5-15mm[6].

Friction loss occurs between the tendon and the duct that it is placed inside of. Due to the curvature typically laid out, friction between the tendon and the surrounding material is increased through curves and changes of direction. This depends on the material, length, and the amount of curvature. Friction losses cause variations in stresses along with the tendon of a beam. The following equation is used to calculate the friction losses along the tendon profile.

The friction losses are calculated based on the following equation. $P_m(x) = P_m \cdot e^{-\mu(\theta + kx)}$

where μ is the friction coefficient which corresponds to an internal strand wire and assumed as 0.19
k is the wobble effect equal to 0.01rad
θ is the angle in rad $\theta = \frac{x}{R}$
x is the distance from prestressing anchor

The coefficientμ depends on the type of duct and if it is lubricated, the latter has a lower coefficient of friction. The coefficient for unintended angular displacement or the wobble effect is based on the quality of the installation of the ducts, the distance that its acting over, the type of duct, and the vibrating technique used when placing the concrete around the duct. The values lie in the range of 0,005 < k < 0,01 according to the Eurocode EN 1992-1-1[20]. The wobble effect is introduced since the actual angular rotation in practice is typically larger. In addition, it considers unintended curvatures in the prestressing duct. The angle of the tendon is calculated using the radius of the tendon.

Elastic deformation of the concrete occurs when the prestressing force is transmitted to the concrete after each tendon is jacked. There is a sudden contracting of concrete which causes a slight strain change in the tendon. Elastic shortening is not considered since the assumption is that all cables are tensioned simultaneously.

Time Dependant Losses

Long term losses, which include concrete creep, shrinkage and tendon , are also significant. This is especially the case when considering crack width and the risk of them widening over time. If the prestressing load decreases, this gives way for larger cracks forming. Creep is the increased deformation of the concrete over time due to the prestressing force. The load is constantly sustained upon the concrete, which causes the strain to increase. The creep coefficient is determined assuming outside condition. This long-term effect modifies the modulus of elasticity of the concrete.

Drying shrinkage occurs when the concrete dries and results in strains because of the loss in moisture, which decreases the volume. Autogenous shrinkage is related to the hydration process and reaches its final value much quicker than drying shrinkage. Relaxation occurs when stress due to imposed deformation decreases in time in the prestressing steel. The effect is comparable to creep on concrete but depends on more variables.

Thermal changes

Thermal loading when using concrete is crucial during curing since the temperature changes can cause cracking. However, the concrete in its final stage also undergoes extensive temperature variations. Linear temperature variation will cause bending stress from -1.00 to + 1.00 MPA, more significant than the hydrostatic precompression stresses. Tension in the summer and compression in the winter will occur due to these temperature variations, outside the concrete walls and slabs. One important detail when considering post-tensioning ducts is the added risk when exposed to fire. This could cause localized damage to the concrete.

Underwater Post-tensioning

Post-tensioning the elements at the final stage would make it possible to avoid implementing the extra reinforcement required to counteract the final loads. This technique however, is not an option right now due to its lack of development. This would also mean that the additional labour would be taking place underwater, which ultimately might be as expensive as the additional reinforcement.

Unbonded post-tensioning tendons

Post-tensioning tendons have the option to be grouted after prestressing or left unbonded and protected. Studies have shown that the latter has a slightly lower ultimate strength[21]. Leaving unbonded tendons in a submerged state would also increase the chances of damage. The moment between prestressing the tendons and grouting, the structure follows the unbonded tendon behaviour at the dry dock.

Research into the finite element segments for post-tensioning was done by Van Greunen et al.[22], where they assumed that the tendon interacted with the concrete only at the element boundaries, and the force would be the average of the forces at the element boundaries. They also made the distinction that the stiffness of the unbonded tendons is ignored in the calculations contrary to bonded tendons. For the latter, the deformations could also be calculated directly since it is the same as concrete; however it is only calculated at the anchor points for unbonded tendons and affects the whole length of the tendon.

2.4. Montreal Louis-Hippolyte tunnel in Canada

The tunnel, briefly mentioned in the introduction, was completed in 1967. The tunnel carried 6 traffic lanes and was divided into elements, each of size 110m and a height of 7.62m. A single-span was approximately 12.8m long. The cross-section had to be calculated as a floating shell to reduce freeboard and towing risks. The designers found that the shear stresses exceeded the limits in the reinforced concrete and therefore introduced post-tensioning. By doing so, the height was reduced 1.5m and ended up shortening the length of the tunnel by almost 70m. In this design, the surcharge was 12 times the dead weight, and the designers investigated the option of prestressing the elements in their final position, however they found that the uncertainties and risks were too large[23].

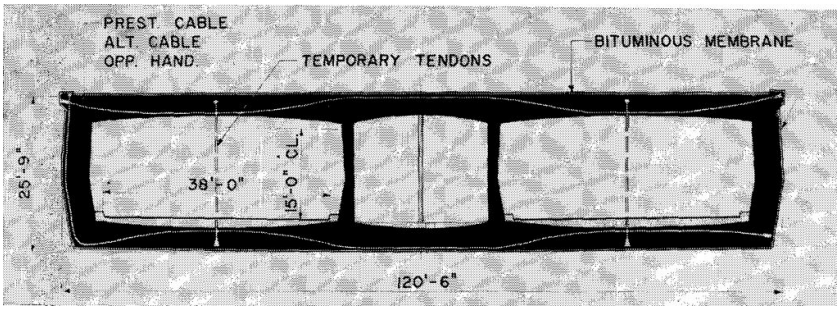

Figure 2.6: Montreal Louis Hippolyte tunnel post-tensioning layout[8]

The design solution to the absence of hydrostatic pressure in the dry dock was to add temporary prestressed steel tendons that connected both the top and bottom slabs together. It was also essential to ensure that there was no overstressing of the frame when implementing the temporary tendons, while the transverse post-tensioning was taking place. A sequence of prestressing was established between the temporary tendons and the transverse prestressing. The stresses in the tendons decreased as the elements are lowered into position since the water pressure causes slight deformations to the section. Simultaneously, the tendons were gradually relaxed.

As seen in Figure 2.6 the post-tensioning tendons from the bottom slab make a 90° bed to then go up to the top slab. The designers believed that placing the anchors at one end only would decrease the chances of water infiltrating into the ducts, which was a potential source of leaks. They then covered the corner with seal welded steel plates to provide extra protection to the anchors.

3

Base Case Reinforced Concrete

An initial base case consists of a concrete immersed tunnel with a 15m span. The goal is to perform design checks and evaluate the cross-section to identify critical parameters that govern the capacity. It also seeks to find what limits the traffic envelope width for concrete immersed tunnels. The internal height of the tunnel is decided based on the traffic tube standards and the ventilation requirements. The inner height of the tunnel plays an vital role in the buoyancy calculations since it will determine how much free space is available in the tunnel.

3.1. Dimensions of Base Case

For the dimensions of this model, a height is chosen to be 5.9m and the remaining tunnel dimensions are seen below in Table 3.1, and on the cross-section in Figure 3.1. The height and span were loosely based on some recent tunnelling projects, like the ShenzhenZhongshan Link Project.

Table 3.1: Dimensions for RC structure

Dimensions		
Width of tunnel spans	15	m
Width of Gallery	1.5	m
Height of tunnel	5.9	m
Thickness of bottom slab	1.2	m
Thickness of roof	1	m
Thickness of outer walls	1	m
Thickness of inner walls	0.9	m
Total width	35.3	m
Total height	10.1	m

Figure 3.1 shows the cross-section layout. The focus of the calculations will primarily be on the top span of the tunnel.

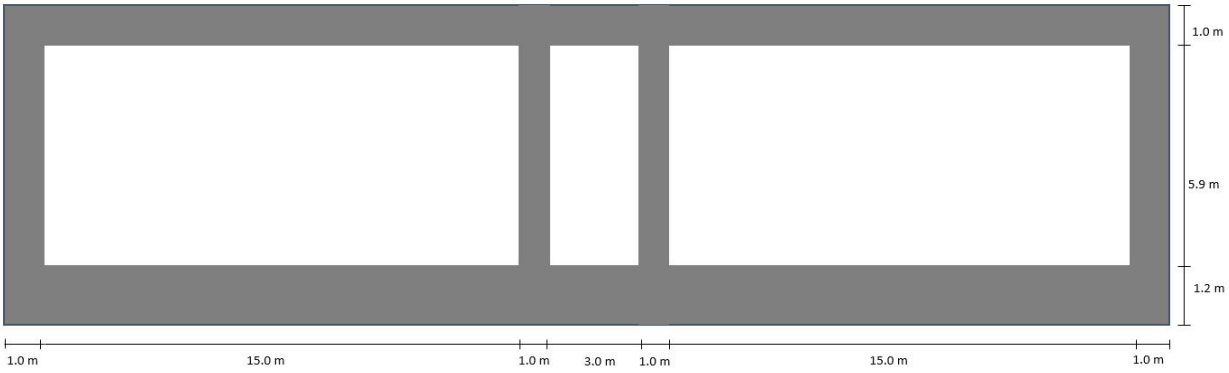

Figure 3.1: Cross-section for reinforced concrete immersed tunnel

The material densities and properties used in the calculations are shown in Tables 3.2 and 3.3 respectively.

Table 3.2: Material properties for RC cross-section

	Densities (kN/m^3)
Concrete	23.2
Ballast Concrete	23.2
Steel	77
γ_{water}	10.35
$\gamma_{Backfill}$	20
γ_{Rock}	22

Table 3.3: Steel and concrete caterial properties

Material Properties					
Steel			**Concrete**		
fy	500	N/mm^2	fck	40	N/mm^2
Ys	1.15		Yc	1.5	-
fyd	435	N/mm^2	fcd	26.67	N/mm^2
Elastic Modulus	200000	N/mm^2	fctd	1.64	N/mm^2
			Elastic Modulus	35220	N/mm^2

3.2. Buoyancy Calculation

Buoyancy calculations ensure that the elements are able can float during transportation; this is done by having a freeboard to avoid the element sinking, minimize the need for extra equipment or require too much ballast throughout the process. There should be a close balance between the weight of the concrete and the upward hydraulic force from the water, optimizing the design to ensure the least amount of materials are used in the process. The freeboard should be 0.15-0.3m [17]. The upward force is calculated using the following equation:

$$Fb = \text{Total Area} * \gamma_{water} \tag{3.1}$$

Table 3.4: Buoyancy calculation result summary table

	Area (m^2)	Density (kN/m^3)	Load (kN)
Buoyancy Force	299.70	10.35	3,101.90
Concrete Weight	105.00	23.2	2,436.00
Steel Weight	2.10	77	161.70
Water ballast	39	10.35	403.36
Freeboard (m)	**0.26**		

3.3. Immersion Safety calculations

The next step is to calculate the forces that will act during the immersion and ensure that the elements will not float up with the hydraulic load, when placed on the bedding. A safety factor of 7.5% is used against uplift, a standard value used in the design of immersed tunnels,varying between 5-10%, to ensure no uplift will occur[17]. Therefore, the weight of the element including the ballast material has to be 1.075 x buoyancy force that will push the element upwards.

Table 3.5: Immersion calculation results summary table

	Area (m^2)	Density (kN/m^3)	Load (kN)
Buoyancy Force	285.12	10.35	3,101.90
Concrete Weight	105.00	23.2	2,436.00.13
Downward Steel	2.10	77	161.70
Ballast Concrete	31.76	23.2	736.84
Safety Check	**1.075**		

3.4. Self-Weight & Hydraulic Calculation

Self-Weight

The concrete and steel self-weight loads are based on their unit weight. The distributed loads are calculated and shown in Table 3.6. The steel area is assumed as 2% of the concrete area for the self-weight calculations, which is an upper limit to the allowable reinforcement, and will be reduced when analyzing the structure capacities.

Table 3.6: Self-weight loads from concrete and steel

Roof	**Area(m^2)**	**Unit weight (kN/m^3)**	**Load(kN/m)**
Concrete	35.3	23.2	23.20
Steel	0.706	77	1.54
Floor	**Area(m^2)**	**Unit weight (kN/m^3)**	**Load(kN/m)**
Concrete	42.36	23.2	27.84
Steel	0.8472	77	1.85
Ballast	31.76	23.2	19.91

Hydraulic Loading

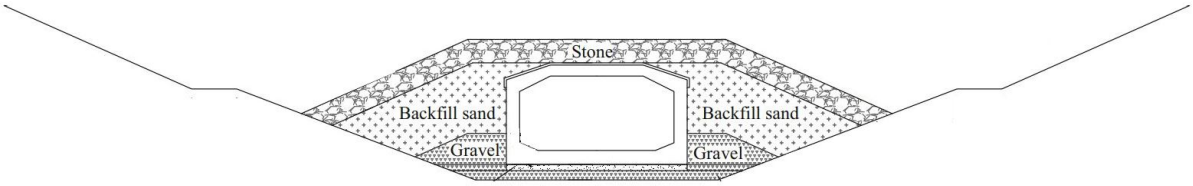

Figure 3.2: Backfilling of immersed tunnel. Modified from [9]

Table 3.7: Dimensions of water and rock layers for base case

Material	**Levels (m)**
Water Level	1
Top of Roof	-9
Protection Layer thickness	1

The hydraulic stresses will depend on the distance below the water level the structure is positioned at in its final immersed stage. Figure 3.3 represent the hydraulic loading and earth loading on the structure. The hydrostatic loads experienced on the bottom slab are greater by a factor equal to the height of the tunnel.

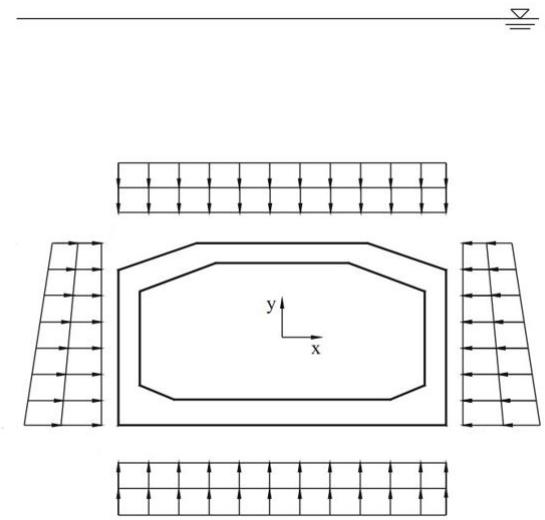

Figure 3.3: Loading on immersed tunnel. Modified from[9]

In this case, 10m below the sea/river level was chosen. The hydraulic stresses at each relevant point of the cross-section are shown in Table 3.8. These include the top and bottom of the roof and the top and bottom of the bottom slab. The stresses will form part of the vertical and horizontal loading on the structure. The internal angle of friction ϕ used is 30°. The $\boldsymbol{\sigma}_{\text{soil}}$ takes into account the unit weight of both rock protection and backfilling materials and the height above the point being analyzed that contains either of the materials. $\boldsymbol{\sigma}_{\text{eff}}$ is the difference between the hydraulic loading and vertical soil stress, this value is then used to calculate the horizontal force on the wall from the backfilling material using the following equations:

$$\boldsymbol{\sigma}_{\text{h}} = \sigma_{\text{kh}} + \sigma_{\text{hydraulic}} \tag{3.2}$$

where $\boldsymbol{\sigma}_{kh} = \sigma_{eff} * K_0$
$K_0 = 1 - \sin(\varphi) = 0.5$

The values are then used when identifying all the loads on the immersed tunnel's final immersed stage.

Table 3.8: Hydraulic and earth Pressures

	Height (m)	$\boldsymbol{\sigma}_{\mathbf{hydraulic}}$ **(kN/m^3)**	$\boldsymbol{\sigma}_{\mathbf{soil}}$ **(kN/m^3)**	$\boldsymbol{\sigma}_{\mathbf{eff}}$ **(kN/m^3)**	$\sigma_{\mathbf{kh}}$ **(kN/m^3)**	$\boldsymbol{\sigma}_{\mathbf{h}}$ **(kN/m^3)**
Water Level	0					
Ground Level	-10.00	103.50	103.50	0	0	103.50
Top Side Roof	-11.00	113.85	125.50	11.65	5.83	119.68
Bottom Side Roof	-12.00	124.20	145.50	21.30	10.65	134.85
Top Side Floor	-17.90	185.27	263.50	78.24	39.12	224.38
Bottom Side Floor	-19.10	197.69	287.50	89.82	44.91	242.59

Load Combinations

Table 3.9: Load combinations applied to model

Load	SLS	ULS	ULS(favourable)
Self-Weight	1	1.2	0.9
Hydrostatic Load	1	1.15	0.9
Backfill	1	1.2	0.9
Rock	1	1.2	0.9
Ballast	1	1.15	0.9
Traffic	1	1.5	0

Table 3.10: SLS and ULS Loading on all sides of structure

Total Loading					
Roof			**Floor**		
	SLS (kN/m)	**ULS (kN/m)**		**SLS (kN/m)**	**ULS (kN/m)**
Concrete	23.20	27.84	Concrete	27.84	26.45
Steel	1.54	1.85	Steel	1.85	1.76
Hydrostatic	113.85	130.93	Hydrostatic	-197.685	-227.34
Rock Protection	11.65	13.98	Ballast Concrete	19.91	18.92
			Traffic load	10	-
Total	**150.24**	**174.60**	Total	**-138.08**	**-180.22**

Wall (Roof)			**Wall (Floor)**		
Wall (roof)	**SLS (kN/m)**	**ULS (kN/m)**	**Wall (floor)**	**SLS (kN/m)**	**ULS (kN/m)**
Hydrostatic	119.68	137.63	Hydrostatic	242.59	278.98
Backfill	5.83	6.70	Backfill	44.91	51.64
Total	**125.5**	**144.33**	**Total**	**287.5**	**330.63**

Design forces

Using the ULS & SLS loading, the moment, shear and normal design forces are calculated.

M_{ED} is calculated by using rule of thumb for continuous beams $Med = \frac{1}{10}ql^2$, for the largest moment, located above the first inner wall, which acts as a support. Furthermore, the moment at the connection of the outer wall and beam, uses the following equation:

$$\frac{ql^2}{6(\beta e+2)} \tag{3.3}$$

where $\beta = \frac{I_h}{I_v}$
$e == \frac{h}{L}$

Table 3.11: SLS and ULS Design Loads for roof and floor

	SLS		**ULS**	
Med- roof	3,380.40	kNm	3,928.40	kNm
Med- floor	-3,106.86	kNm	-4,054.85	kNm
V- roof	1,126.80	kN	1,309.47	kN
V-floor	-1,035.62	kN	-1,351.62	kN
N-roof	628.25	kN	722.49	kN
N-floor	817.25	kN	939.84	kN

3.5. Section capacity

Moment Capacity

Basic reinforcement design is implemented, considering one layer of tensile reinforcement and one layer of compressive reinforcement. The cover is determined based on the exposure class related to the environmental conditions the concrete is subjected to, which is found in Table 4.1 of the EN 1992-1-1[20]. The tunnel is permanently submerged, assuming that the surroundings would be seawater, for the worst-case scenario, the concrete class is specified is XS2, which has a minimum cover of 50mm. With $C_{\text{dev}} = 10\text{mm}$

$$c_{\text{nom}} = c_{\text{min}} + \Delta C_{\text{dev}} = 60mm. \tag{3.4}$$

Table 3.12 , shows the details used to come up with the section capacity, which includes the beam properties.

Table 3.12: Section Details for RC roof design

Section details Roof					
Height	1	m	Cover	60	mm
I_{yy}	0.083	m^4	Stirrup	16	mm
W_{top}	0.167	m^3	A_c	1	m^2
W_{bot}	0.167	m^3	Width	1	m

The two unknowns are now the compression zone height x_u and the area of steel in the tensile zone A_s. With an iterative procedure using the equilibrium of forces and moments in ULS, both values are solved. The result is an x_u of 246.29mm and an A_s of $10,300mm^2$. This is divided into two layers and an increase in area to compensate for the slight loss in lever arm with the second layer. The following reinforcement is chosen for the section:

1st tensile Reinforcement	8 x 36 ∅
2nd tensile Reinforcement	8 x 32∅
Compressive Reinforcement	8 x 20∅

This corresponds to a compressive reinforcement area of $2,512mm^2$ and a tensile reinforcement area of $14,592mm^2$ .The moment resistance M_{rd} is determined in ULS by calculating the forces at each level of reinforcement, assuming yielding has been reached. M_{rd} is then the summation of all the forces multiplied by their respective lever arms. M_{ED} as seen in Table 3.11 with the addition of the normal force by an eccentricity of $\frac{h}{30}$.

M_{rd}	$6,714.86kNm$
M_{ED}	$3,956.27kNm$
Unity Check	0.59

Shear capacity

The shear capacity of the concrete is checked without taking into account any shear reinforcement. The axial loading from the hydraulic pressure also influences the resistance of the concrete struts and is taken into account when calculating σ_{cp} .

$$V_{Rd,c} = \left[C_{Rd,c^*} k \left(100.\rho_{l'} f_{ck}\right)^{\frac{1}{3}} + k_1 \cdot \sigma_{cp}\right] \cdot b_w \cdot d \tag{3.5}$$

where

σ_{cp}	$\frac{N_{ED}}{A_c} \leq 0.2 f cd$
$C_{Rd,c}$	0.12
ρ_l	$\frac{A_s}{d.b} = 0.008$
k_1	0.15
k	$1 + \sqrt{\frac{200}{d}}$
b_w	width of cross-section in tensile area
d	effective depth

$V_{rd,c}$	$758.19kN$
V_{ED}	$1,309.47kN$
Unity Check	1.73

This calculation concludes that the section requires shear reinforcement. The following calculations for shear capacity include shear reinforcement, an assumed 12∅ 4-legged stirrup.

$$V_{Rd,s} = \frac{Asw}{S} \cdot z \cdot f_{yd} \cdot \cot\theta \tag{3.6}$$

where

$A_s w$	area of stirrups $452mm^2$
s	stirrup spacing 100mm
θ	angle of inclined strut 45
z	0.9 d_s the effective depth of cross-section

$$V_{Rd,max} = \alpha_{\mathrm{cw}} \cdot b_{\mathrm{w}} \cdot z \cdot \upsilon_1 \cdot f_{cd} (\cot\theta + \tan\theta) \tag{3.7}$$

where

α_{cw}	coefficient of the compression chord= 1 for non-prestressed structures
b_w	width of cross-section= 1
υ_1	strength reduction factor for concrete in shear =0.6

$V_{Rd,s}$	$1,620.56kN$
Unity Check	0.81
$V_{Rd,max}$	$6,588.82kN$
Unity Check	0.20

Normal Capacity

The compressive stress of the concrete is checked with the following formula, taking into account the applied bending moment and normal force on the roof.

$$\sigma(c) = -\frac{N}{A_{ceff}} - \frac{M}{W_{top}} \tag{3.8}$$

where N is the Normal force applied to the roof in ULS
M is the moment applied to the roof in ULS
M is the moment applied to the roof in ULS

$\sigma(c)$ is equal to -24.68 N/mm^2 and fcd = 23.3N/mm^2. The stress is just over the allowable limit.

Crack width control

The last check is for the crack width, and it is calculated in SLS loading. This means finding x_e, the compressive height of the concrete at SLS. Similarly to ULS, this is done by balancing forces and moments; however, the steel area is known in this case. There is, however, another unknown, which is the concrete strain. By balancing the sum of forces and equating the moment to the SLS design moment, the values for x_e and e_c are 431.79mm and -1.07%, respectively.

From there, the following equation is used to determine the crack width.

$$W_{\mathrm{k}} = S_{\mathrm{r,max}} \left(\varepsilon_{\mathrm{sm}} - \varepsilon_{\mathrm{cm}}\right) \tag{3.9}$$

where W_{k} is crack width
$S_{\mathrm{r,max}}$ is crack spacing
$\varepsilon_{\mathrm{sm}}$ is the average steel strain
$\varepsilon_{\mathrm{cm}}$ is the average concrete strain

$$\varepsilon_{\mathrm{cr}} = \left(\varepsilon_{\mathrm{CS}} - \varepsilon_{\mathrm{cm}}\right) = \varepsilon_{\mathrm{cr}} = \left[\sigma_{\mathrm{s}} - k_{\mathrm{t}} \left(f_{\mathrm{ct,eff}} / \rho_{\mathrm{p,\,eff}}\right)\left(1 + \alpha_{\mathrm{e}} \rho_{\mathrm{p,eff}}\right]\right. / E_{\mathrm{s}} \geq 0.6 \left(\sigma_{\mathrm{s}}\right) / E_{\mathrm{s}} \tag{3.10}$$

where k_t is Eurocode 2 factor dependent on the duration of the load
$\rho_{\mathrm{p,eff}}$ is effective reinforcement percentage, ratio $\frac{As}{Ac,eff}$
α_{e} is the ratio Es/Ec

$$s_{r,\max} = k_3 c + k_1 k_2 k_4 \phi / \rho_{p,eff} \tag{3.11}$$

where k_1 is 1.6 for plain reinforcement bars
k_2 is 0.5 for flexure.
k_3 is 3.4
k_4 is 0.425
ϕ is the reinforcement bar diameter
c is the concrete cover

The $\rho_{p,eff}$ is the ratio between the efficient concrete area in tension $A_{c,eff}$ and the reinforcement that lies within it . h_{eff} is the depth of the effective area which is the minimum of the following:

$$h_{c,eff} = min[2.5(h-d), (h-x)/3, h/2]$$

The steel stress at SLS is required for the crack width calculation. Having the compression zone height and strain in SLS, the steel stress is then calculated in the outermost layer of reinforcement, which is most critical as it is the first to come into action during cracking.

$$\varepsilon_s = \left(\frac{d-x}{x}\right)\varepsilon_{\mathrm{c}} \tag{3.12}$$

$$\sigma_s = \varepsilon_s E_s \tag{3.13}$$

where $\varepsilon_s = 1.2\%$
$\sigma_s = 240.78MPa$

The crack width limit values are found in Table 7.1 of the Eurocode EN 1992-1-1 [24], based on which exposure class the concrete is XS2. In this case 0.3mm corresponds to the w_{max}.

Table 3.13: Crack width values for RC base case

Crack Width Values					
σ_s	240.78	N/mm^2	$\rho_{p,eff}$	0.077	
h_{eff}	189.4	mm	e_{cr}	0.0011	
$\emptyset$	36	mm	$S_{r,max}$	266.437	mm

The values listed in Table 3.13 lead to a crack width of 0.28mm, which is below the limit of 0.3mm.

3.6. Parameter analysis

To better understand the parameter influences of the reinforced concrete tunnel roof, a simplified model was created, where the cross-section capacity is calculated considering only one tensile layer of reinforcement. Starting with a 10m span and increasing in intervals up to 30m, the heights were modified to pass all the required checks mentioned in the 15m base case, including the moment, shear and normal capacities.

A reinforcement ratio of 2% was kept constant for each scenario, which dictated the steel area (As). Along with concrete strength (40Mpa), the height of the traffic envelope and thickness of walls and gallery, were also kept constant. As the span length increased, the height of the roof increased, primarily to accommodate the normal capacity requirement check, which governed most scenarios. Figure 3.4 shows this steadily increase, with a maximum height of 2.14m for the 30m span. Table C.1 has an overview of the vlaues from this paramter analysis.

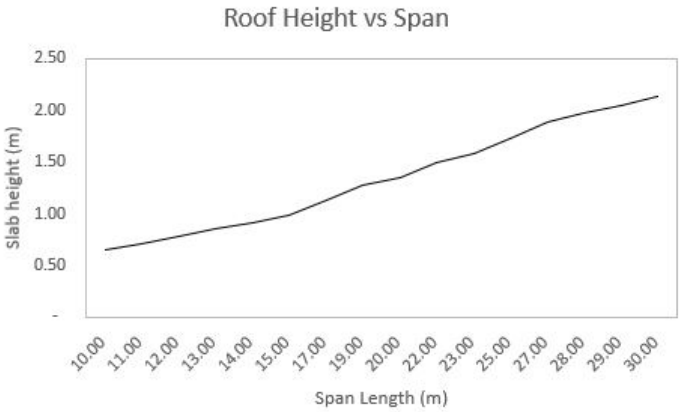

Figure 3.4: Roof height vs span

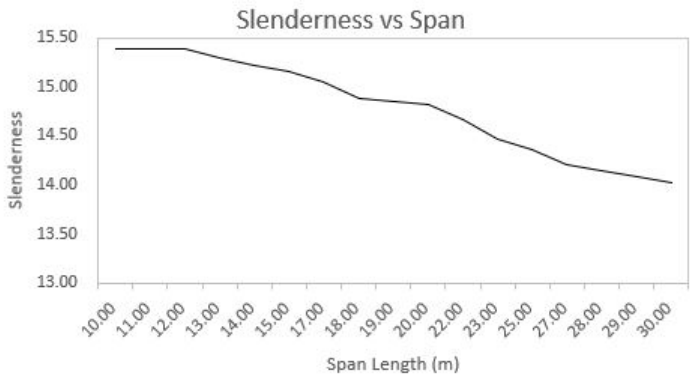

Figure 3.5: Slenderness vs span length for reinforced concrete element

The slenderness of the roof span, graphed in Figure 3.5 indicates that the changes in height increased by larger amounts, this is due to the fact that the design moment has a relation, which is the span length to the power of two. Finally, Figure 3.6 indicates that approximately after 18m span length, the buoyancy check fails, and an increase in the traffic envelope will be required.

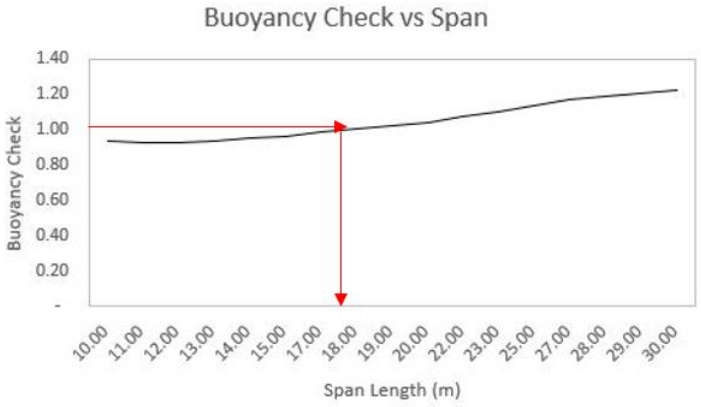

Figure 3.6: Buoyancy Check vs span length for reinforced concrete element

3.7. Conclusion

The analytical calculations of the reinforced concrete section checked the main criteria to establish the capacity of the top slab of the section. The buoyancy and immersion calculations are vital to ensure the dimensions chosen provide the required freeboard to be transported and to identify the amount of ballast needed in the final stages. Based on the self-weight and the external loads acting on the section, the design loads were checked against the capacity, for moment, shear force and normal stress. The normal stress was over the limit of the compressive stress for the chosen concrete strength. The crack width was the final check done, which was just below the limit set for a concrete class of XS2. Based on these findings, a simplified model was done, to analyze the influence of the parameters. The goal was to find the limitation of the concrete span length, and what parameters limited the slenderness. From the analysis, the normal stress check was governing the design. The moment increased at a rate of length of the span (l^2), which meant that the stress brought on by the moment was increasingly higher. The slenderness of the structure, therefore, decreases with increasing span length. At a span length of 17m, the buoyancy check then also failed. Thus, the governing check for the concrete immersed tunnels is the normal stress and buoyancy.

4

Post-tensioning

4.1. Base Case

The following chapter will go over the analytical calculations for the post-tensioning base case. The initial situation has not yet been optimized and therefore has a low slenderness value. Only the top slab of the tunnel element has post-tensioning applied and will be the focus in this chapter.

As discussed in the introduction, the tunnel element goes through stages that involve varying loading conditions. When implementing post-tensioning, the most critical stage is when the element is in the dry dock after it has been cast. This is a big contrast from the reinforced concrete element, where only self-weight is present. When post-tensioning force is added, this acts as an external load to the structure. When the strands undergo jacking, the prestressing force exerted is at its highest, before any of time dependant losses are present. At this moment, the dry dock stage is at its most critical. However,the prestressing force is designed according to the final immersed loading consitions, since it will have to endure these for the majority of its life span. The following chapter will go through the calculations and capacity checks of the roof slab of the tunnel when applying the transverse post-tensioning forces.

4.2. Dimensions

A span of 20m was chosen roughly based on the observations in the parameter analysis in the previous chapter, considering a thickness of 1.3m. The remaining dimensions shown in Table 4.1 were chosen for the model after ensuring both immersion and buoyancy checks were sufficient.

Table 4.1: Post-tensioned base base tunnel cross-section dimensions

Dimensions		
Width of tunnel spans	20	m
Width of Gallery	3	m
Height of tunnel	5.7	m
Thickness of bottom slab	1.4	m
Thickness of roof	1.3	m
Thickness of outer walls	1.2	m
Thickness of inner walls	1.0	m
Total width	47.4	m
Total height	8.4	m

Material Properties

Table 4.2 shows the material properties used for the tunnel element.

Table 4.2: Post-tensioning steel, regular steel and concrete material properties

Post-Tensioning Steel		
Strength Class	Y1860S7	
f_{pk}	1860	N/mm^2
f_{pk}/Υ_s	1691	N/mm^2
e_{pu}	35	%
σ_{pm0}	1395	N/mm^2
Elastic Modulus	195000	N/mm^2

Steel & Concrete		
Steel		
f_{yd}	435	N/mm^2
Elastic Modulus	200000	N/mm^2
Concrete		
f_{ck}	50	N/mm^2
Elastic Modulus	37278	N/mm^2

4.3. Loads

Self-weight and the hydraulic load are calculated similarly to the reinforced concrete cross-section. With a larger span, the loads differ from the ones in the base case for reinforced concrete. Tables 4.3 and 4.4 show the updated values.

Table 4.3: Hydraulic and earth pressures for PT base case

	Height (m)	$\sigma_{\text{hydraulic}}$ **(kN/m^3)**	σ_{soil} **(kN/m^3)**	σ_{eff} **(kN/m^3)**	σ_{kh} **(kN/m^3)**	σ_{h} **(kN/m^3)**
Water Level	0					
Ground Level	-10.00	103.50	103.50	-	-	103.50
Top side roof	-11.00	113.85	125.50	11.65	5.83	119.68
Bottom side roof	-12.30	127.31	151.50	24.20	12.10	139.40
Top side floor	-18.20	188.37	269.50	81.13	40.57	228.94
Bottom side floor	-19.60	202.86	297.50	94.64	47.32	250.18

Table 4.4: SLS and ULS loads on element

Total Loading		
Roof		
	SLS (kN/m)	**ULS (kN/m)**
Concrete	30.16	36.19
Steel	2.00	2.40
Hydrostatic	113.85	130.93
Rock Protection	11.65	13.98
Total	**157.66**	**183.50**

Floor		
	SLS (kN/m)	**ULS (kN/m)**
Concrete	32.48	29.23
Steel	2.16	1.94
Hydrostatic	-200.79	-230.91
Ballast Concrete	13.57	12.21
Traffic load	10	-
Total	**-142.89**	**-187.52**

Wall (Roof)		
Wall (roof)	**SLS (kN/m)**	**ULS (kN/m)**
Hydrostatic	119.68	137.63
Backfill	5.83	6.70
Total	**125.50**	**144.33**

Wall (Floor)		
Wall (floor)	**SLS (kN/m)**	**ULS (kN/m)**
Hydrostatic	247.15	284.22
Backfill	46.36	53.31
Total	**293.50**	**337.525**

Prestressing Load

The principle moment distribution caused by the prestressing load are illustrated in Figure 4.1, where the moment due to the distributed load and eccentricity at the support are shown. There is no eccentricity at the edge of the structure in this case, however since it is not a simply supported beam, the moments caused at the beam to wall connection will have to be taken into account similarly to the eccentricity.

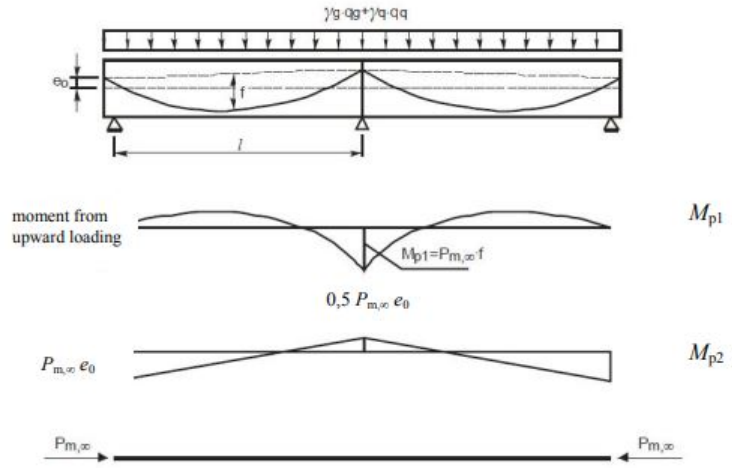

Figure 4.1: Moments due to Pretressing Load [6]

The tendon will be designed to begin at the centre of the roof cross-section and drape the lowest possible at midspan, taking into account cover and reinforcement. A smooth transition over the gallery is essential, and thus a smaller drape for the centre parabola is required as seen in Figure 4.2. This is the assumption for the tendon profile in this particular case. Modifications of the eccentricity at midspan have a an impact over the prestressing load required to obtain the desired concrete stress for the section, which will be further investigated in Chapter 6. The tendon profile curvature dictates what distributed load will be generated. Higher curvature due to higher eccentricities will have a larger load associated to it as seen in Figure 4.1.

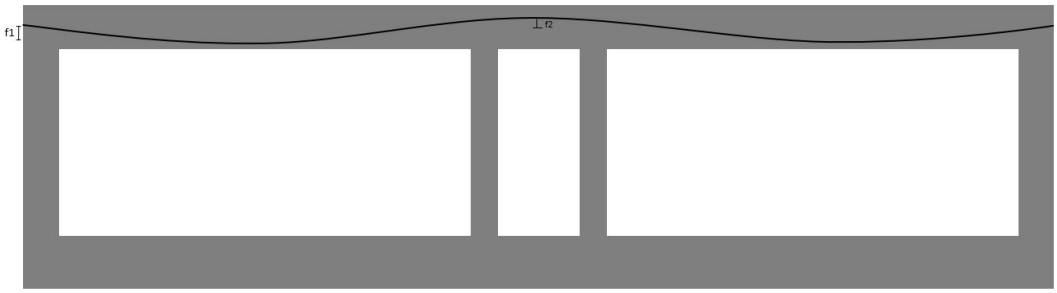

Figure 4.2: Layout of PT tendon profile in roof slab

The maximum drape at midspan, taking into account cover, stirrups reinforcement and the duct diameter of 45mm, is 386.5mm. To calculate the radius of the tendon profiles, the following relation is used:

$$R = \frac{l^2}{8f} \tag{4.1}$$

where R is the radius of curvature
l distance between two points used to define the drape
f drape of the tendon

And, the uniform distributed load due to the tendon curvature is therefore:

$$q_p = \frac{P_{m_o}}{R} \tag{4.2}$$

where q_p is the prestressing distributed load
P_{m_o} is the initial prestressing force

Equation 4.2 shows the inverse correlation that the distributed prestressing force has with the radius of the tendon profile. There is no eccentricity at the ends however, the moment at the wall-slab connection is also accounted for.

Table 4.5 summarises the tendon profile measurements used.

Table 4.5: Post-tensioned tendon dimensions

Dimensions		
f1	0.54	m
f2	0.10	m
R1	103.37	m
R2	36.45	m
q1	0.01	1/m
q2	0.03	1/m

Different stages have to be taken into account, these are the initial moment of tensioning, therefore self-weight and prestressing force, and then including the variable loads. Both scenarios will be analysed to find P_{mo}. Without knowing the value of P_{m0}, the bending moments for the post-tensioning can still be calculated using q_p as $1/R$ and can be seen in Table 4.6.

Table 4.6: Moments in ULS and SLS of roof slab

	Midspan		Left Edge		Right Edge	
	SLS	ULS	SLS	ULS	SLS	ULS
M self-weight (M_{sw}) (kNm)	705.33	846.40	-902.77	-1,083.32	-1,286.48	-1,286.48
M total (kNm)	**3,888.78**	**4,680.26**	**-3,387.93**	**-4,219.21**	**-6,306.48**	**-6,427.40**
Prestressing Moment (M_p)	-0.21P_{m0}	-0.21P_{m0}	0.27P_{m0}	0.27P_{m0}	0.39P_{m0}	0.39P_{m0}

Prestressing Losses

The friction losses are calculated based on the following equation:

$$P_m(x) = P_m \cdot e^{-\mu(\theta + kx)} \tag{4.3}$$

where μ is the friction coefficient which corresponds to an internal strand wire and assumed as 0.19
k is the wobble effect equal to 0.01rad
θ is the angle in rad $\theta = \frac{x}{R}$
x is the distance from prestressing anchor

The two points of interest are at midspan and the beginning of the inner wall. Table 4.7 shows the values corresponding to each of these locations, with a loss of 7% at midspan and 10% at the gallery.

Table 4.7: Friction loss results summary

Friction Losses			
$\sum\theta_1$	0.1392	$\sum\theta_2$	0.2784
x	11.2m	x	21.2m
Pm(x)	0.93	Pm(x)	0.90

Time Dependant Losses

The following phenomena all contribute when calculating the losses:

Creep

The creep coefficient $\varphi(\infty, t_0)$=1.4 is determined assuming outside condition with a relative humidity of 80% according to Eurocode EN 1992-1-1[20].

$$\varepsilon_{cc} = \frac{\sigma_{c,p0}}{E_c} \cdot \varphi(\infty, t_0) \tag{4.4}$$

$$\Delta P_{creep} = \varepsilon_{cc} E_p A_{p,total} \tag{4.5}$$

Drying Shrinkage

$$\varepsilon_{\mathrm{cd},\infty} = \varepsilon_{\mathrm{cd},0} k_h \tag{4.6}$$

where $\varepsilon_{\mathrm{cd},0}$ from Table 3.2 in Eurocode with a relative humidity of 80% = 0.19x10^{-3}
k_h is obtained by interpolating the h_0 values from table EN 3.1.4.6.
h_0 $= \frac{2A_c}{\mu}$

Autogenous Shrinkage

$$\varepsilon_{\mathrm{ca}}(t) = \beta_{\mathrm{as}}(t)\varepsilon_{\mathrm{ca}}(\infty) \tag{4.7}$$

where $\varepsilon_{\mathrm{ca}}(\infty)$ is the final autogenous shrinkage = $2{,}5 \cdot \left(f_{\mathrm{ck}} - 10\right) \cdot 10^{-6}$
$\beta_{\mathrm{as}}(t)$ is the influence of the age of the concrete = $1 - e^{-0{,}2\sqrt{t}}$
t is the age of concrete in days

Relaxation

$$\Delta\sigma_{pr} = \sigma_{pm,0} * 0.66 * \rho_{1000} * e^{9.1\mu_{relax}} * (\frac{t_{relax}}{1000})^{0.75(1-\mu_{relax})} \tag{4.8}$$

where μ is defined as $\frac{\sigma_{pm,0}}{f_{pk}}$ = 0.75
ρ_{1000} is relaxation from Eurocode and equals to 2.5%
t_{relax} equals to 500,000 hrs

As the losses are combination of shrinkage and creep, a combination factor ψ = 0.8 is used. The total time dependandt losses then become:

$$\Delta P_s = \varepsilon_{\mathrm{cd},\infty} E_p A_p \tag{4.9}$$

$$\Delta P_r = \Delta\sigma_{pr} A_p \tag{4.10}$$

$$\Delta P_{tot} = \Delta P_{creep} + \Delta P_s + \Delta P_r \tag{4.11}$$

Table 4.8: Time-dependent losses summary

Time Dependant Losses										
Creep			**Drying Shrinkage**			**Autogenous Shrinkage**			**Relaxation**		
$\varphi(\infty, t_0)$	1.4		$\varepsilon_{cd,\infty}$	0.000173		$\varepsilon_{ca}(t)$	0.0001		$\sigma_{pm,0}$	7.61	MPa
$\sigma_{c,p0}$	7.61	MPa	k_h	0.72		Bas	1		$\Delta\sigma_{pr}$	67.94	MPa
ε_{cc}	0.00028										
ΔP_{creep}	**546.50**	**kN**	$\Delta P_{dryshrinkage}$	**283.05**	**kN**	$\Delta P_{auto.shrinkage}$	**163.80**	**kN**	ΔP_{relax}	**570.76**	kN

The time-dependent losses that are summarized in Table 4.3, add up to 1,564.11kN and correspond to a 13.5%, however, a 15% will be assumed moving forward, the working prestressing force is calculated as $P_{m\infty} = 0.85Pm0$.

4.3.1. Prestressing Force Calculation

At the dry dock, which is at t=0, the prestressing force and self-weight are the only loads present. At this stage there is a camber that results from the deflections of the effective post-tensioned forces and the counteracting deflection of the self-weight [25]. At $t = \infty$, which is at the final immersed stage, the variable external loads are also present. The prestressing load is multiplied by a factor of 0.85 to compensate for the time-dependent losses as seen in section 4.3. The allowable concrete tensile stress is noted as σ_c = + 1,0 MPa, even though the material limits for C50/45 allow a larger tensile stress. The following equations are used, to identify the prestressing force required, both dry dock and final stage are used as well as the midspan and wall support. The top and bottom fibres are checked and results are shown in Table 4.9. Normal force N is added in the equation of $t = \infty$, where the hydrostatic horizontal force plays a part in the final calculation.

At t=0:

Midspan Bottom: $-\frac{P_{m0}}{A_c} - \frac{M_p}{W} + \frac{M_{sw}}{W} \leq 1$ MPa

Top: $-\frac{P_{m0}}{A_c} + \frac{M_p}{W} - \frac{M_{sw}}{W} \leq 1$ MPa

Edge: Bottom: $-\frac{P_{m0}}{A_c} + \frac{M_p}{W} - \frac{M_{sw}}{W} \leq 1$MPa

Top: $-\frac{P_{m0}}{A_c} - \frac{M_p}{W} + \frac{M_{sw}}{W} \leq 1$ MPa

At t= ∞:

Midspan Bottom: $-\frac{0.85P_{m0}+N}{A_c} - \frac{0.85M_p}{W} + \frac{M_{total}}{W} \leq 1$ MPa

Top: $-\frac{0.85P_{m0}+N}{A_c} + \frac{0.85M_p}{W} - \frac{M_{total}}{W} \leq 1$ MPa

Edge: Bottom: $-\frac{0.85P_{m0}+N}{A_c} + \frac{0.85M_p+N}{W} - \frac{M_{total}}{W} \leq 1$ MPa

Top: $-\frac{0.85P_{m0}+N}{A_c} - \frac{0.85M_p}{W} + \frac{M_{total}}{W} \leq 1$ MPa

Table 4.9: Prestressing Load Values

Prestressing Force (kN)					
t=0			**t=∞**		
Midspan			Midspan		
P_{m0}	>	992.89	P_{m0}	>	9,943.93
P_{m0}	>	-169,210.00	P_{m0}	>	-735,823.52
Edge			Edge		
P_{m0}	<	21,377.27	P_{m0}	<	88,829.
P_{m0}	>	1,982.24	P_{m0}	>	11,002.10

The governing P_{m0} is therefore 11,002.10kN and with a prestressing initial stress of σ_{pm0} = 1395 MPa the

required total area of strands can be calculated.

$$A_p = \frac{P_{m0}}{\sigma_{pm0}} \tag{4.12}$$

The size of the strands chosen is 15.7mm diameter, an area of 150mm^2, and would therefore require 53 strands. According to the VSL brochure [26], the maximum offered number of strands for one anchor is 55. The chosen unit is 6-55, and for the corresponding concrete strength of 50Mpa, the outer diameter of the anchor is 460mm. There is also a minimum spacing between anchorages of 520mm specified. Considering a roof height of 1.3m, if there are more strands required, this could be a limitation in the design. One option would be to place them side by side, however the assumed width of 1m, would have to be reconsidered.

The 53 strands with an area of $7,950 mm^2$ correspond to a force of 11,090.25kN.

4.4. Design capacity

In this section, less steel reinforcement is used considering the high prestressing force present. Only one row of reinforcement is therefore assumed in the tensile and compressive areas, the section details are seen in Table 4.10.

Table 4.10: Section Details for PT cross-section

Section details					
Height	1.3	m	Cover	60	mm
I_{yy}	0.183	m^4	Stirrup	16	mm
W_{top}	0.281	m^3	Compressive Reinforcement	20	mm
W_{bot}	0.281	m^3	Tensile Reinforcement	34	mm
Width	1	m			
A_c	1.3	m^2			

Moment Capacity

Finding x_u initially through horizontal equilibrium using the following equation,

$$\mathrm{x_u} = \frac{\mathrm{A_s f_{yd}} + \mathrm{A_p} 0,95 \cdot \frac{\mathrm{f_{pk}}}{1,1}}{\alpha \mathrm{b f_{cd}} + \mathrm{A_{s2} f_{yd}}} \tag{4.13}$$

where α the sectional area factor is 0.75
A_s is $2,568 mm^2$, with a ds=1,212mm
A_{s2} assumed to be $1,256 mm^2$ with a ds=86mm

The tensile reinforcement A_s, was calculated to be the lowest admissible tensile reinforcement using EN 1992-1-1 requirements. The assumed prestressing stress σ_p =1,606 MPa is then checked by using the calculated value of the compressive zone height, x_u, to find the actual prestressing strain. This value is lowered to $1534 N/mm^2$ and the final value of x_u is 512mm. The rotational capacity of the structure is checked by the following equations. This is done by ensuring the compressive height meets the following requirements.

$$\frac{x_\mathrm{u}}{d} \leq \frac{500}{500 + f} \quad \text{for} \quad f_\mathrm{ck} \leq 50 \ \mathrm{N/mm^2} \tag{4.14}$$

$$\text{where,} \quad f = \frac{\left(\frac{f_\mathrm{pk}}{\gamma_\mathrm{s}} - \sigma_{\mathrm{pm},\infty}\right) A_\mathrm{p} + f_\mathrm{yd} A_\mathrm{s}}{A_\mathrm{p} + A_\mathrm{s}} \tag{4.15}$$

Which results in a value that xu< 553mm, which has been satisfied. Then finally, the bending moment resistance is calculated:

$$M_{Rd} = P_{m\infty}(h/2 - y) + N_s\left(d_{s1} - y\right) + N_{s2}\left(y - d_{s2}\right) + \Delta N_p(d_p - y) \tag{4.16}$$

where y is $\beta x_u = 0.39 x_u$
N_s $A_s f_y$
N_{s2} $A_{s2} f_y$
ΔN_p $A_p(\sigma_p - \sigma_{pm\infty})$
$\sigma_{pm\infty}$ $\frac{P_{m\infty}}{A_p}$

M_{Rd} $8,829.18kN$
M_{ED} $2,763.82kN$
Unity Check 0.31

Normal Force

$$\sigma(c) = -\frac{N}{A_{ceff}} - \frac{M}{W_{top}} \tag{4.17}$$

where N consists of both the axial load from the hydraulic loading, as well as prestressing force. M, the design moment, includes self-weight, variable loads and prestressing moments.

where $\sigma(c)$ -24.69 N/mm^2
fcd -33.33 N/mm^2
Unity Check 0.74

Shear Capacity

Similarly to the procedure for reinforced concrete, the following equation is used to calculate the shear capacity of concrete without shear reinforcement.

$$v_{Rd,c} = \left[C_{Rd,c^*} k \left(100.\rho_{l'} f_{ck}\right)^{\frac{1}{3}} + k_1 \cdot \sigma_{cp}\right] \cdot b_w \cdot d \tag{4.18}$$

However, in this scenario the prestressing force is taken into account within the concrete compressive stress due to axial loading $\sigma_{cp} = \frac{P_{m\infty}+N_{ED}}{A_c} \leq 0.2fcd$, where $0.2fcd$ is actually governing due to the high prestressing force.

$V_{rd,c}$ $1,663.74kN$
V_{ED} $1,835.02kN$ $V_{Rd,s} = \frac{Asw}{S} z f y d \cot\theta$
Unity Check 1.10

$V_{Rd,s} = \frac{Asw}{S} z f y d \cot\theta$

With the same Asw of $452mm^2$ and a spacing of 100mm:

$$V_{Rd,max} = \alpha_{cw} \cdot b_w \cdot z \cdot v_1 \cdot f_{cd}(\cot\theta + \tan\theta) \tag{4.19}$$

The difference is in the coefficient α_{cw}, for prestressing structures the following applies $\left(1 + \sigma_{cp}/f_{cd}\right)$ for $0 < \sigma_{cp} \leq 0,25 f_{cd}$ With $\left(1 + \sigma_{cp}/f_{cd}\right)$ $= 1.25$

$V_{Rd,s}$	$2,146.58kN$
Unity Check	0.85
$V_{Rd,max}$	$13,606.65kN$
Unity Check	0.13

Crack Width

The allowable crack width is modified since the use of prestressing steel is present. According to Eurocode EN 1992-1-1 Table 7.1[20], when using prestressing the w_{max} for the particular class of concrete, the decompression limit requires that all parts of the bonded tendons or duct lie at least 25 mm within concrete in compression. This is followed with the ducts that are closer to the external faces of the perimeter structure, however, it is assumed that since internal faces are not in contact with the seawater, the allowable width is 0.2mm, which applied to general members with bonded tendons. According to [17] however, a conservative value of 0.15mm can be taken, especially in the external faces of perimeter structure. Therefore for this study, when using post-tensioning, an allowable crack width of 0.15mm will be followed. Crack width calculations are part of the SLS loading requirement, in this case, both the dry dock and final stage will be checked for cracks in SLS at the locations shown in Figure 4.3.

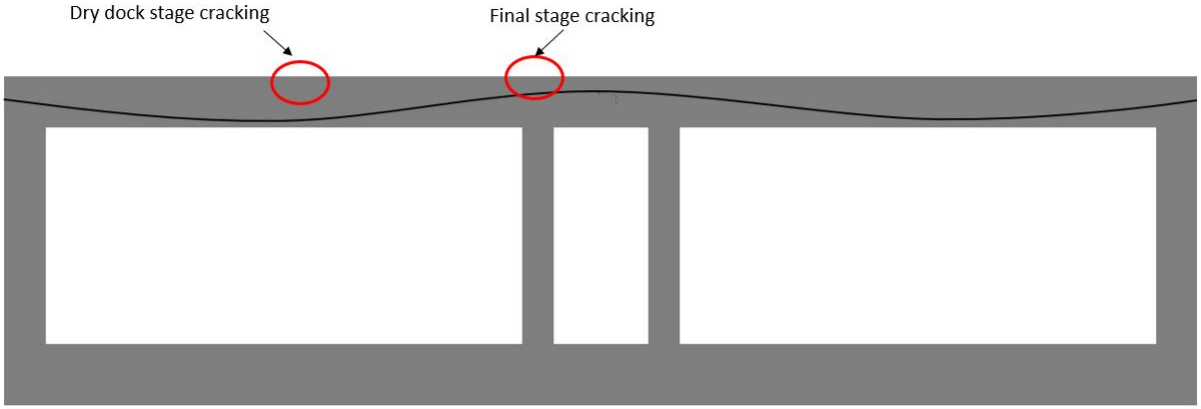

Figure 4.3: Locations to be checked for cracking

Dry Dock

Cracking during the dry dock stage is checked at the top section of midspan, where tensile forces might occur under the given loads. x_e and e_c are calculated through moment and force equilibrium. The maximum prestressing force occurs at the moment the tendons are stressed, prior to any time dependant losses. At this initial time frame, there has also not been any grout inserted in the ducts, thus the first analysis for cracking stage at the dry dock, the tendons are assumed to be unbonded. The bond strength ratio $\xi_1 = 0$ in the equation below, and therefore ΔN_p does not contribute in the calculations to determine x_e and e_c.

The application of prestressing at the initial stages when it is ungrouted, there is assumed to be no time dependant losses, only friction and anchor losses present. The assumption that the grout is injected at the earliest instance to avoid damage to the cables, is made. The implication is therefore that a minimum amount of time dependant losses is then assumed for the analysis of the crack width with subsequent bonded tendons. Grouting the tendons provides protection to the steel cables and allows there to be a bond between the concrete and the steel. If the grout is not implemented within the first few weeks of tensioning the cables, an alternative method to protect the cables must be used. After the grout has hardened, prestressing steel and concrete work together in unison to resist the forces. The difference between the grouted and ungrouted scenario are small for the analytical calculations in the dry dock stage. They resulted in less than a 2% difference in the force equilibrium calculation. This is due to the lever arm of the change in prestressing force being small, as the compressive zone is on the bottom of the cross-section in the dry dock stage.

Due to friction the prestressing force will be 93% of the initial Pm0. ξ_1 is 0 for ungrouted tendons and 0.5

for grouted.

$$\sum F = 0 : N_s + \Delta N_p + N_s - N_c + P_{m0} = 0 \tag{4.20}$$

where

$$\Lambda N_p = \left(\frac{d_p - x}{x}\right) E_p \varepsilon_{c,top} \xi_1 A_p \tag{4.21}$$

x_e and e_c are 818.16mm and 0.82% respectively with the distinction that the compressive zone is positioned at the bottom of the beam. The effective concrete height is taken around the upper reinforcement where cracking is expected, thus the prestressing and lower reinforcement do not lie within the area of $A_{c,eff}$. Using the following equation, the crack width is calculated with the parameters in Table 4.11.

$$W_\mathrm{k} = S_\mathrm{r,max} \left(\varepsilon_\mathrm{sm} - \varepsilon_\mathrm{cm}\right) \tag{4.22}$$

where $\varepsilon_\mathrm{cr} = \varepsilon_\mathrm{cr} = \left[\sigma_\mathrm{s} - k_\mathrm{t}\left(f_\mathrm{ct,eff}/\rho_\mathrm{p,\,eff}\right)\left(1 + \alpha_\mathrm{e}\rho_\mathrm{p,eff}\right]/E_\mathrm{s} \geq 0.6\left(\sigma_\mathrm{s}\right)/E_\mathrm{s}$
$s_{r,\max} = k_3 c + k_1 k_2 k_4 \phi / \rho_{p,eff}$

Table 4.11: Dry dock crack width values

Crack Width Values - Dry Dock					
σ_s	146.70	MPa	$\rho_{p,eff}$	0.0078	
h_{eff}	160.61	mm	e_{cr}	0.00044	
$\emptyset$	20	mm	$S_{r,max}$	638.78	mm

Taking into account the values in Table 4.11, the crack width is 0.28mm, which is over the allowable limit of 0.15mm.

Final Stage

In the final stage at SLS, the crack width is analyzed at the maximum moment in SLS, which corresponds to the top of gallery wall . In this case the tensile reinforcement and prestressing reinforcement are considered in the $p_{p,eff}$ ratio along with the corresponding effective concrete.

$$\rho_\mathrm{p,eff} = \left(A_\mathrm{s} + \xi_1 \quad A'_\mathrm{p}\right) / A_\mathrm{c,eff} \tag{4.23}$$

Due to friction losses, 90% of the prestressing force at the final conditions is considered, which is in addition to the 15% loss from the time dependant losses.

To calculate x_e and e_c for this section, ΔN_p is taken into account in the equilibrium equations, since the tendons are assumed to be grouted at this point. The values are 956.5mm and 0.97% respectively.

Table 4.12: Final stage crack width values

Crack Width Values - Final Stage					
σ_s	58.77	MPa	$\rho_{p,eff}$	0.0485	
h_{eff}	114.5	mm	e_{cr}	0.00018	
$\emptyset$	24	mm	$S_{r,max}$	288.08	mm

Taking into account the values in Table 4.12, the crack width is 0.05mm, which is under the allowable limit.

4.5. Conclusion

The post-tensioning base case, similarly to the reinforced concrete one in Chapter 3 was done to understand the capacity requirements and the governing parameters that influenced the design. A larger span was chosen and again the buoyancy and immersion requirements had to be met. Adding a level of complexity from the reinforced concrete section, the prestressing force is first determined based on the stress requirements set. From there, the capacity of the section is determined, again with the moment, shear force and normal stress capacity checks. The final check for crack width, is done in two locations for the critical stages: dry dock and final immersed stage. As expected, the dry dock crack width exceeded the limit, whereas the final stage did not.

5

Finite Element Model Analysis

5.1. DIANA

Finite element modeling is a numerical method that will be used to simulate the behaviour of the immersed tunnel and analyze the weakest areas, where additional reinforcement may be required. The finite element modelling for this project was done using DIANA, a program developed in the Netherlands by TNO. This program allows nonlinear analysis which is advantageous when considering a structure with nonlinear relations due to geometrical, material, and contact origins.

The model will be used to assess and evaluate the behaviour of the structure in response to the application of transverse post-tensioning forces. Since the analytical calculations are a simplification, they do not account for the exact boundary conditions or accurate material interactions. The numerical model will have to be chosen in such a way that realistically depicts the cross section of a tunnel element and yet is simplified to reduce computational time. With DIANA, the load cases can be added to the structure separately, this is beneficial when analyzing the different stages that a tunnel element undergoes. The post tensioning force will be established analytically, along with self weight, hydraulic pressure, and backfilling/rock pressure.

An analysis of the structure at its final stage will validate that the prestressing forces are not resulting in any failures and that the stresses are below limits. The dry dock stage, which includes only the self weight and post tensioning forces will also be analyzed. This stage is critical in observing the response of the structure to the extreme camber and to identify the consequential tensile stresses. The FEM results will be compared with respect to the analytical calculations to identify the main differences and validate the design.

5.2. Model Parameters

Shape and reinforcement

The plane strain model was used for the tunnel cross section elements, as it is part of an infinitely long tunnel, the strain e_{zz} should be 0. The only strains in the model should be in plane, this will allow for more precise stress and strain distributions over the height of the structure.

5.3. Material Models

Concrete

Cracking of the structure plays a role when analyzing the effects of the application of post tension loading to the main structure. The rotating crack model is used in this thesis, which uses the smeared cracking concept. It follows the distributed effect of cracking, as opposed to the other option, discrete cracking model, that fo-

cuses on specific cracks that are modelled prior. Smeared cracking is a total strain crack model, a constitutive model that uses one stress-strain relationship . Rotating refers to the crack direction, which is continuously rotating according to the strain vector's principal direction. The strain increments are calculated in each iteration based on the direction given by the crack. [10]

Within the total strain cracking model the Hordijk tension softening model was chosen, which is a non-linear model that results in the stresses in the crack equal to 0 at a certain crack width. For the compressive behaviour, the parabolic curve was used, which considers the element size and crack-band width as it dictates the softening path.

Reinforcement

Von Mises plasticity was used for the reinforcement, both regular steel and prestressing. The relationship diagrams can be seen in the corresponding Figures 5.1 and 5.2.

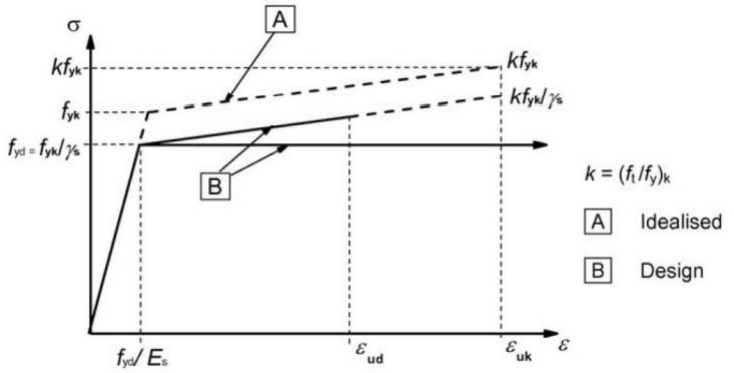

Figure 5.1: Regular steel stress-strain relationship in ULS [6]

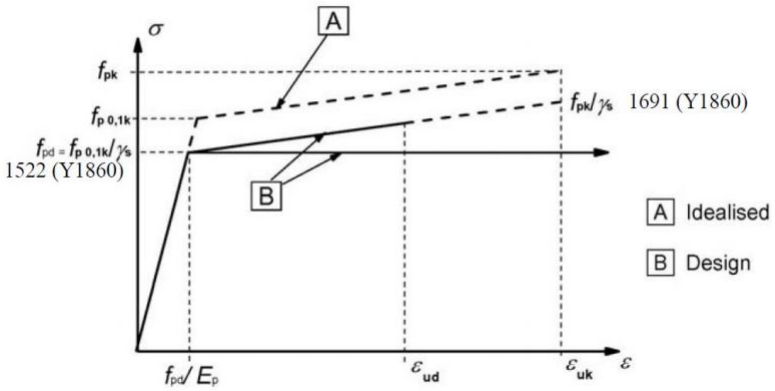

Figure 5.2: Prestressing steel stress-strain relationship in ULS [6]

5.4. Elements

Concrete

For this model standard plane strain elements were used, known to have a strain perpendicular to the element face of zero. CQ16E Quadrilateral plane strain with 8 nodes and quadratic interpolation and Gauss integration are depicted in Figure 5.3.

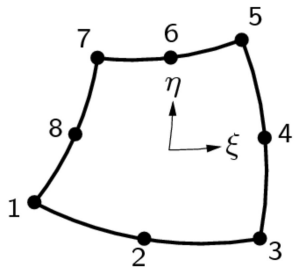

Figure 5.3: CQ16E Element in DIANA [10]

Reinforcement

Embedded reinforcement is used for the steel, which means the reinforcement is part of the structural elements and the computations are taken from the displacement field of the mother element. A perfect bond is assumed between the steel and concrete. The post tensioned tendon is also modelled as reinforcement.

Bedding

The bedding below the structure is modelled as a boundary interface element, which included the soil stiffness, however the interface itself does not have any physical properties. The boundary conditions are placed at this interface, restricting the vertical movements. A soil modulus of 50,000kN/m^3 was used.

Composed Elements

Composed elements are implemented only to calculate the cross section forces and bending moments. The stresses or internal forces are integrated over the specified area which covers the elements, which include all elements and embedded reinforcement.

5.5. Initial Case

Two scenarios were modelled in SLS: the dry dock stage and the final stage. The final stage was modelled to validate that all the loads acting simultaneously exhibited no high stresses above the specified limits. The moments extracted using the composed line were also compared to the analytical calculations. The initial model consists of prestressing forces implemented in the top slab only. Table 5.1 shows the dimensions used for the model implemented in DIANA. The dimensions of the cross section and the loading are the same as the post tensioning base case in Chapter 4.

Table 5.1: Post-tensioned base case dimensions used in the numerical model

Dimensions		
Width of tunnel spans	20	m
Width of Gallery	3	m
Height of tunnel	5.7	m
Thickness of bottom slab	1.4	m
Thickness of roof	1.3	m
Thickness of outer walls	1.2	m
Thickness of inner walls	1.0	m
Total width	47.4	m
Total height	8.4	m

Loads

Within DIANA, the self weight does not have to be manually added, since the program calculates the volume of the elements and the load based on the mass density specified. The earth and hydraulic pressures were

implemented as distributed loads on the cross section sides. By specifying the hydraulic head, DIANA calculates the pressures acting on the structure. The post tensioning force itself, is imposed in the tendon via the anchor, and the distributed loads generated by the curvature of the tendon are added independently.

Post-Tensioning

The option of adding a post tensioning load is available in DIANA, allowing for wedge set losses and friction losses to be included. The force is implemented along the modelled tendons at the elements and includes the losses and stress reduction. Even though DIANA can incorporate the friction and anchor losses, the time dependant losses are implemented manually, in a separate analysis when considering the later stages of the element lifespan.

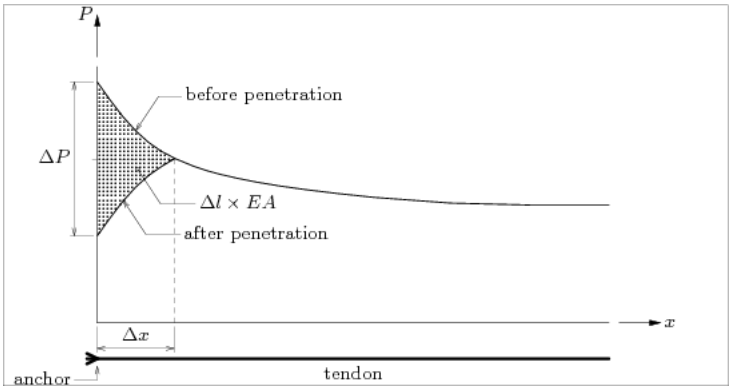

Figure 5.4: Graph showing anchorage losses in DIANA [10]

DIANA uses the following condition to calculate the influence length. $\int_L \Delta P(x)\mathrm{d}r \geq \Delta lEA$, which is depicted in Figure 5.4. However, it is stated in the manual that determining the influence length might be more inaccurate in nonlinear analysis due to the assumption of linear distribution over the integration. The initial model uses the same parameters as the analytical calculations, which are the following: $k = 0.19$, $\mu = 0.01$ and wedge set= $6mm$ [10]. DIANA has the option to use unbonded tendons, a brief look into this material property can be found in Appendix A.

The geometry of the cross section is shown in Figure 5.5 where the draped tendon on the top slab is visible in red, and the regular reinforcement in blue. The reinforcement is taken from the base case model in Chapter 4 for the roof. The floor and wall reinforcement is found in Appendix B. The intention is to first observe the effects of the post-tensioning on the top slab, and the implementation of bottom post-tensioning will be analyzed in section 5.7. The initial assumption being that the top and bottom slab post-tensioning do not have a significant effect on one another.

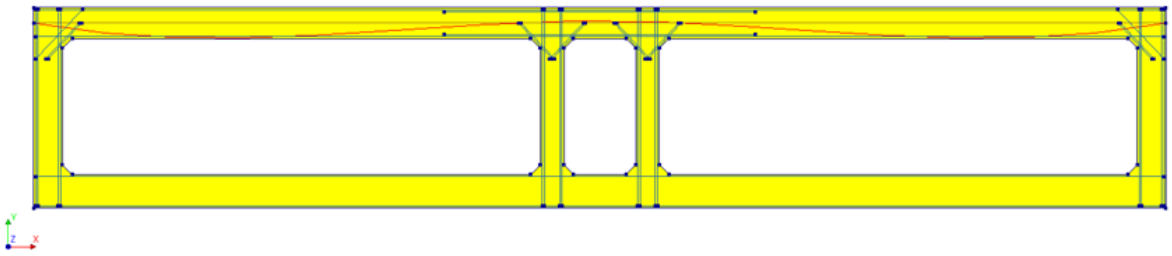

Figure 5.5: General geometry for initial numerical model

5.6. Linear Analysis Results

The initial step was to run a linear analysis, which is often a good representation of the structure behaviour, although the model depends on non linear relations for greater accuracy. A linear analysis is a simplified version of the model in which all the algebraic equations that the program uses are in a linear form and where the stress is proportional to the strain.

The different load cases were separated and compared to the analytical values. A composed line was used to identify the general moment distribution in the top slab. Using this method of extracting the structure results, the post-tensioning force was taken into account through the integration of stresses, as well as the force in the tendon by DIANA. This gave an inaccurate moment distribution, and therefore when extracting this data, the post-tensioning tendon must be deselected from the reinforcements when using a composed line. The line does not deform with the structure, therefore is visible in the following figures, as a straight line along the top of the beam. The following figures show the different moment distributions corresponding to the different load combinations that take place. The moment distributions shown in the DIANA model have the opposite sign compared to the analytical values used throughout this study. The tables will depict the actual values being compared, that will differ from the legend shown.

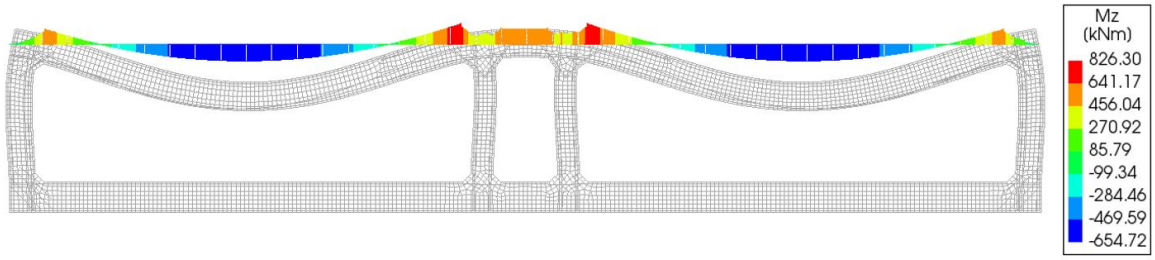

Figure 5.6: Self Weight- Linear Analysis

The self-weight of the section acts as a distributed load on the top of the section, which creates a sagging moment at the midspan and hogging moment at the beam to wall connections that are acting as the supports.

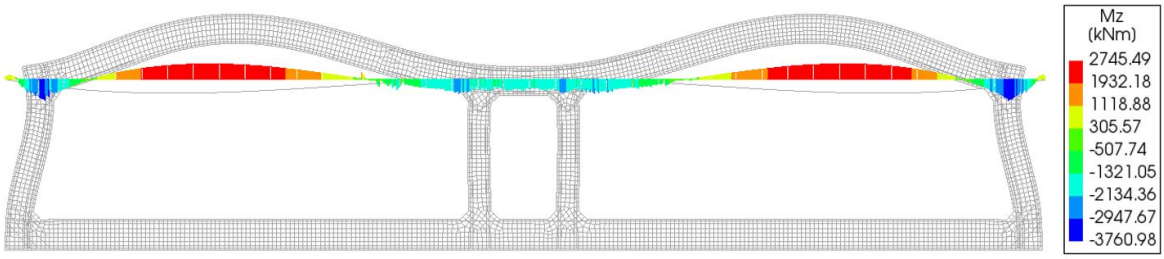

Figure 5.7: Post tensioning Loads- Linear Analysis

The post-tensioning load generates a large moment at the outer wall connection seen in Figure 5.7. The moment induced by the distributed load from the draped tendons has the opposite distribution to the self-weight seen in figure 5.6. As the loads follow the direction of the radius of the tendons, the distributed load over the midspan is acting in the opposite direction to the distributed load above the gallery. These loads generate a high negative moment at the midspan of -2,745.49kNm. Whereas, above the gallery the moments generated from the opposing distributed load counteract each other and there is a smaller moment of 2,134.36kNm.

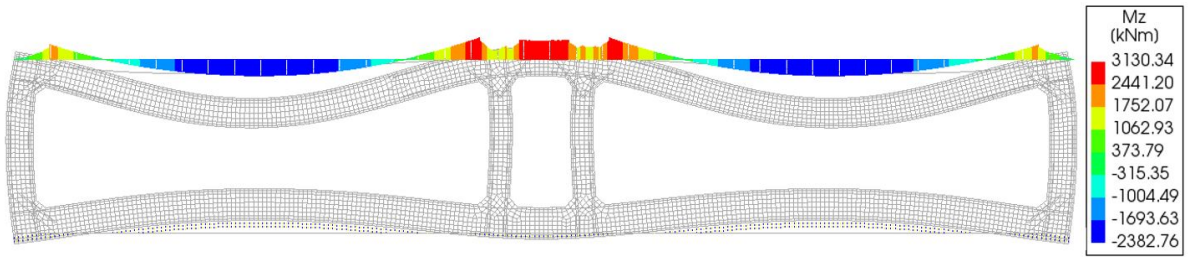

Figure 5.8: External loading- Linear Analysis

The moment distribution shown in Figure 5.8 consists of the additional loads that are present at the final stage. These include the hydraulic loading, backfill and rock pressures, and the traffic and ballast load. Although the top slab has a similar moment distribution to the self weight, the actions of the lateral pressures are visible from the slight wall deformation. The deformation of the bottom slab due to the upward distributed loads is also present, with settling of the bedding, marked with the dotted lines.

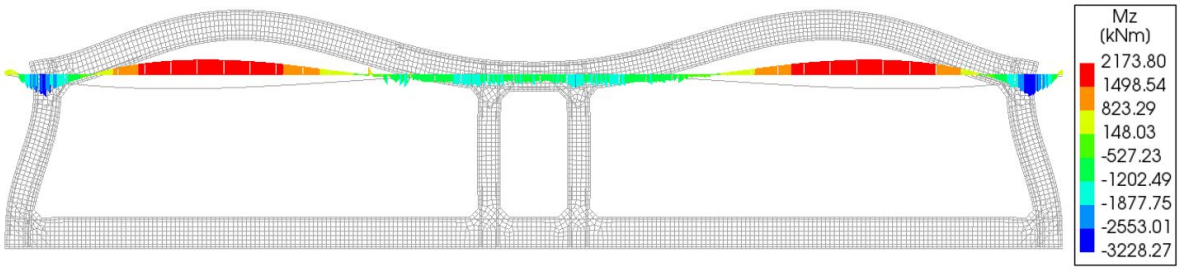

Figure 5.9: Dry dock loading- Linear Analysis

The dry dock loading is composed of the prestressing load and the self-weight; the two loads present at the dry dock stage, right after jacking of the strands. The prestressing load is considered to be 100% with no time dependant losses taken into account at this stage, to obtain the worst case scenario for the structure. The moment distribution is seen in Figure 5.9.

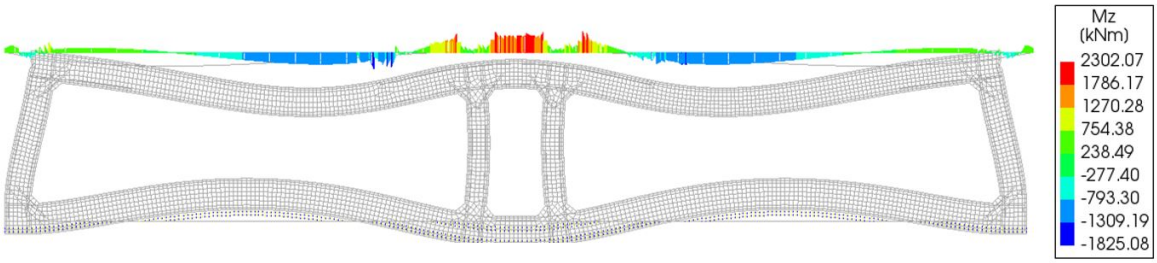

Figure 5.10: Final immerse state- Linear Analysis

The final immersed stage in Figure 5.10, where all loads are present, has the prestressing load at 85% to account for the time dependant losses. The distribution shows high negative moments above the gallery, beside the wall and slab connection. The moment tapers off, with a positive bending moment at midspan which causes the deflection of the beam downwards. At the outside corners, the moment is only 754.38kNm.

As mentioned above, the moments in Table 5.2 follow the opposite sign for the DIANA values as displayed in the legends.

Table 5.2: Summary of Analytical vs Numerical moments

	Moments											
	Left Edge				Midspan				Right Edge			
	Analytical		DIANA		Analytical		DIANA		Analytical		DIANA	
M_{sw}	-907.63	kNm	-641.17	kNm	700.47	kNm	654.72	kNm	-1,286.48	kNm	-826.30	kNm
$M_{Prestressing}$	4,138.44	kNm	3760.98	kNm	-2,525.10	kNm	-2,745.49	kNm	4,018.89	kNm	2,947.67	kNm
$M_{External}$	-3,541.67	kNm	-2,441.20	kNm	2,733.33	kNm	2,382.76	kNm	-5,020.00	kNm	-3,130.34	kNm
$M_{DryDock}$	3,230.82	kNm	3,228.27	kNm	-1,824.63	kNm	-2173.8	kNm	2,732.41	kNm	1,877.75	kNm
M_{Final}	-931.62	kNm	-754.38	kNm	1,287.47	kNm	1,309.19	kNm	-2,890.42	kNm	-2,302.07	kNm

Observing the moments from the numerical analysis with respect to the analytical calculation, a few distinct differences are noted in Table 5.2. To better visualize the differences, Figure 5.11 shows both numerical and analytical moment distributions for self-weight loading conditions. From this, the assumptions made for the analytical calculations can be checked if they are applicable to this scenario and if they can be made more accurate to represent the true behaviour of the structure.

The most visible difference occurs at both the outer and inner wall-slab connections. in both , there is an increase in the analytical calculations of less than 30%. This is also true when looking at the values for the external loading. This is due to the less rigid connection that can be seen in the numerical analysis, since the wall is not as rigid, as the assumptions made. The initial calculation was based on Equation 3.3, which forms a relation between the length of the wall and slab to determine the moment at the connection.

A reduction of 20% is used moving forwards to account for the slight decrease in rigidity from the analytical calculations in the outside corner. A full 30% is not used since other influences for the difference are possible and have not been identified. For the inner corner, instead of using the approximation of $\frac{1}{10}ql^2$, used for frame design, a $\frac{1}{12}ql^2$ resulted in a closer interpretation of the distribution over the gallery.

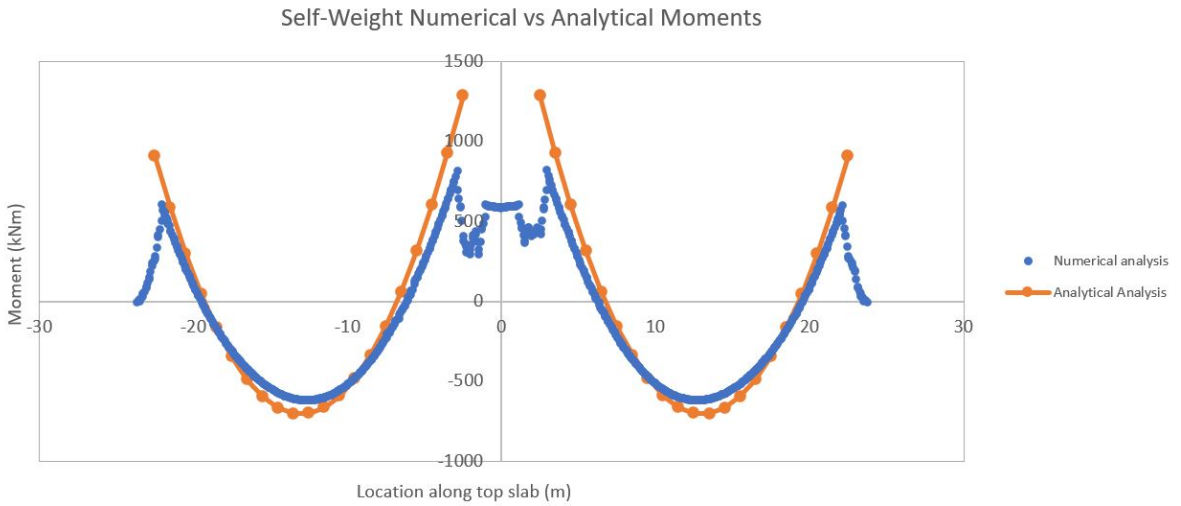

Figure 5.11: Self-weight numerical vs analytical moment

The second largest difference is in the prestressing moments, where the moment above the gallery is 36% larger in the analytical calculation. This is due to the influence of the tendon above the gallery, that has a downward distributed force. The simplification in the analytical analysis did not account for this subtraction from the moment. The difference in prestressing, taking into account the effect of the opposite tendon distribution, lowers the moment above the gallery.

Moving forward in the following sections and chapters of this study, the analytical calculations will take into effect the changes described. The updated values can be seen in Table 5.3.

Table 5.3: Updated values of Analytical vs Numerical moments

	Moments											
	Left Edge				Midspan				Right Edge			
	Analytical		DIANA		Analytical		DIANA		Analytical		DIANA	
M_{sw}	-726.10	kNm	-641.17	kNm	709.02	kNm	654.72	kNm	-1,072.07	kNm	-826.30	kNm
$M_{Prestressing}$	3,310.75	kNm	3,760.98	kNm	-2,968.35	kNm	-2,745.49	kNm	3,676.90	kNm	2,947.67	kNm
$M_{External}$	-2,833.33	kNm	-2,441.2	kNm	2,766.67	kNm	2,382.76	kNm	-4,183.33	kNm	-3,130.34	kNm
$M_{DryDock}$	2,584.65	kNm	3,228.27	kNm	-2,259.33	kNm	-2,173.8	kNm	2,604.84	kNm	1,877.75	kNm
M_{Final}	-745.29	kNm	-754.38	kNm	952.59	kNm	1,309.19	kNm	-2,130.03	kNm	-2,302.07	kNm

Stress Distribution

Figure 5.12 shows the stress distribution in the final immersed stage, with 85% of prestressing force included in the model to account for time dependant losses. The high compressive and tensile stresses are concentrated in the top corners, with both exceeding the allowable limits. A close up can be seen in Figure 5.14.

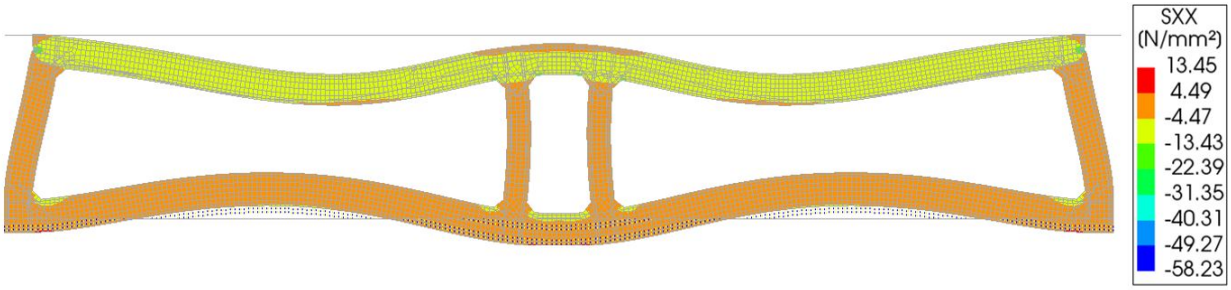

Figure 5.12: Stress distribution at the final stage

The goal is to observe the behaviour when implementing the post tensioning forces and to determine if the section behaves as predicted. The post-tensioning is designed according to the final stage loading conditions and therefore is important that the section comply with the limits. The stress at the top of gallery in the area marked in orange is -1.32 Mpa, which means that section is still in compression.

The midspan of top slab stresses are seen in Table 5.4, and indicate that the section is fully in compression. Now observing the rest of the structure, when looking at the bottom slab the area below the gallery and below each outside corner, exhibit tensile stresses of 5.04Mpa and 5.36Mpa respectively, where the sections are displayed in red. This is above the concrete design tensile limit of 1.93MPa set out by the material properties, and therefore requires additional reinforcement, or post-tensioning tendons. In Section 5.7, the effect of bottom post-tensioning is analyzed.

The analytical values seen in Table 5.4 have been carried out using the revised moments seen in Table 5.3. When comparing the numerical model values to the analytical, the top stresses at midspan are similar, however the bottom has a larger difference. The numerical model exhibits a greater distribution throughout the slab cross-section and a bottom stress of -3.33Mpa, 2.3 times smaller than the value calculated analytically. When observing the final moment at that location in Table 5.3, the numerical value is 40% higher, and is therefore having a larger effect on the tensile area of the slab.

Table 5.4: Stresses at top slab

Stresses									
Final					**Dry Dock**				
	Analytical		DIANA			Analytical		DIANA	
Top	-11.24	MPa	-12.38	MPa	Top	-1.03	MPa	-0.63	MPa
Bottom	-7.65	MPa	-3.33	MPa	Bottom	-17.06	MPa	-15.01	MPa

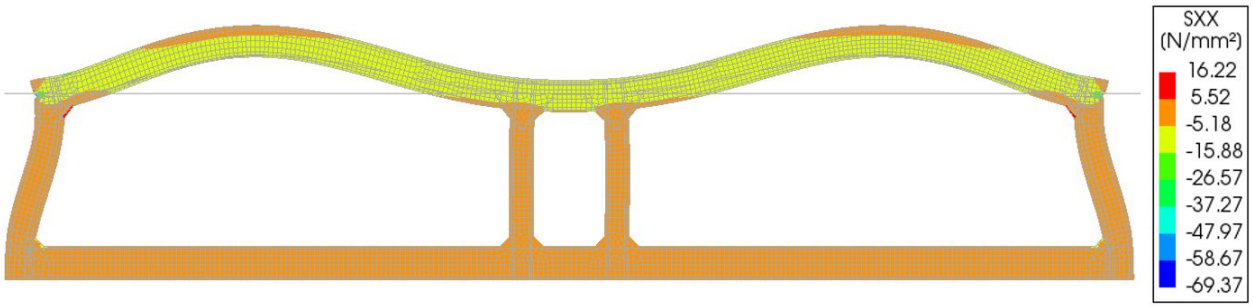

Figure 5.13: Stress distribution at the dry dock stage

The stress distribution at the dry dock stage can be seen in Figure 5.13 with an opposite deformation occurring at the top span, and a constant stress distribution at the bottom. Similarly to the final stage, the corner exhibits very high compressive and tensile stresses. In this stage due to the upward direction of the post-tensioning loads, there is a camber of the top slab, with the compressive zone at the bottom. The stresses at the top of the beam must be checked for tensile stresses. In this model, the maximum stress at the top slab is -0.63Mpa which is still in compression and within the limits. When taking into account the effects of prestressing only, without the self weight, the stress reached in the top slab is 1.51MPa. A second area of concern due to the upward camber, are the inner corners, which reach a tensile stress of 9.70Mpa, well above the structure's limits. In the left inner corner, slight tensile stresses are exhibited, especially in the inside corners between the top slab and the wall, with stresses reaching 0.77Mpa. Since the element is sitting on the dry dock, there is no bedding, and loads on the bottom slab are not present.

A close up of the corner is seen in Figure 5.14. Surrounding the anchor there are high tensile stresses, and at the point of entrance, the highest compressive stress is observed. This is due to the high force being implemented directly at the element, which requires additional reinforcement. The stresses in the corners, exceed both tensile and compressive design limits of the concrete, which are 1.93MPa and 28.33MPa respectively. In practice, spiral reinforcements are installed to avoid cracking in these particular areas. The other point of concern is at the corner of the inner traffic envelope where high tensile stresses are seen and the top, where again, an increase in reinforcement or larger hunch can be easily implemented.

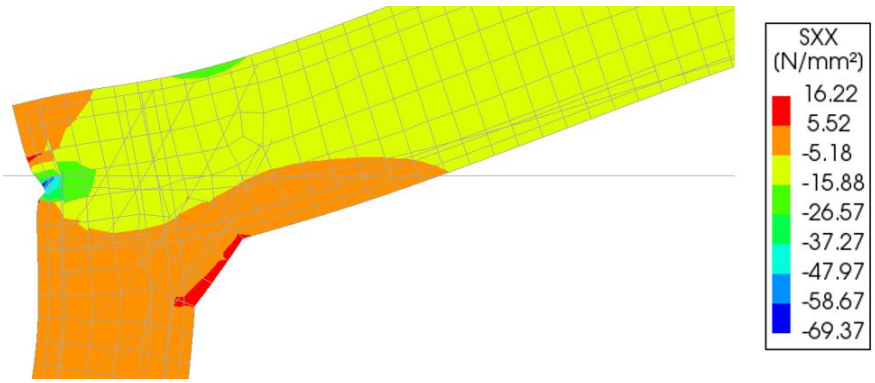

Figure 5.14: Close up of dry dock corner with stress distribution

5.7. Bottom Slab Prestressing

In all projects up to date where transverse post-tensioning has been used, the bottom slab has also had post-tensioning tendons implemented. This allowed for a slight reduction in height, and improved the overall stresses at the final stage. A model following the scenario that allows both top and bottom slab post-tensioned was carried out to analyze the effects. The analytical calculations in the previous chapters focused on the top slab and the effect the post-tensioning force had on the capacity of it.

The same procedure to calculate the amount of prestressing required for the top slab was used for the bottom slab. Based on the loading in Table 4.4 in Chaper 4, the moments, seen in Appendix B, and the required prestressing were calculated. The amount of prestressing implemented in the bottom tendon is 10,600kN. For the final stage, a 15% reduction is taken into account for the time dependant losses.

Figure 5.15 indicates the shape of both tendons which are draped in opposing directions, to account for the loading scheme acting on both slabs. In this case the hydraulic loading acting upwards needs to be counteracted, and therefore the tendons have the parabola shaped towards the top, so the distributed load of the tendons acts downwards.

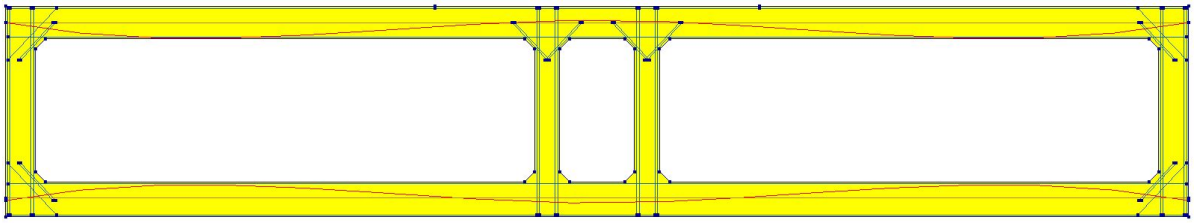

Figure 5.15: General geometry with both top and bottom slabs post tensioned

The final immersed stage stress distribution displayed in Figure 5.16 shows a similar behaviour to Figure 5.12 without floor tendons. When looking at the bottom slab, there is visibly less deformation upwards at midspan, and less downward settlement of the centre gallery section. No visible differences are seen in the top slab. The walls are slightly more upright with less rotation inwards.

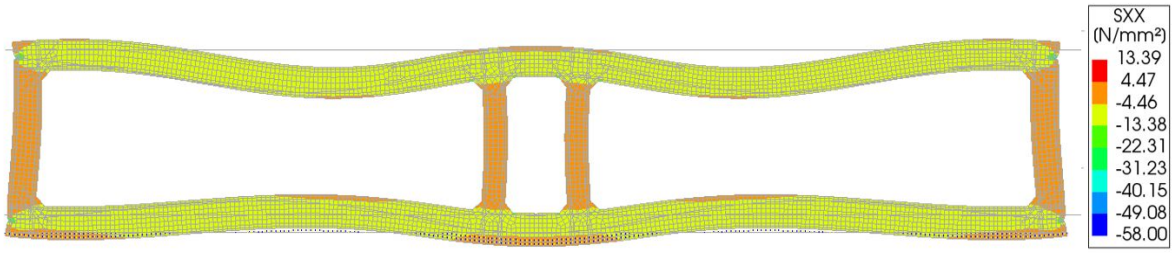

Figure 5.16: Stress distribution final stage immersed stage with floor and top post-tensioned

Table 5.5: Stress comparison from model with bottom slab post-tensioning and without

Stresses - Dry Dock									
Top Slab					**Bottom Slab**				
	Bottom PT		No Bottom PT			Bottom PT		No Bottom PT	
Top	0.20	MPa	-0.63	MPa	Top	-7.32	MPa	-1.05	MPa
Bottom	-16.25	MPa	-15.01	MPa	Bottom	-7.34	MPa	-1.06	MPa

Stresses- Final									
Top Slab					**Bottom Slab**				
	Bottom PT		No Bottom PT			Bottom PT		No Bottom PT	
Top	-12.49	MPa	-12.38	MPa	Top	-4.13	MPa	2.62	MPa
Bottom	-3.85	MPa	-3.33	MPa	Bottom	-8.51	MPa	-4.71	MPa

Table 5.5 indicates the stresses from the numerical models, both with and without floor post-tensioning. The values were taken from the same nodes, at midspan of the top and bottom slabs. A few observations can be made from them. First, is the effect that the bottom prestressing has on the top slab, a very minor increase in stresses can be seen in the dry dock stage, with the top having a slightly higher tensile force and the bottom a compressive, however neither goes above the limits. Figure 5.18 shows the stress distribution at the dry dock.

The increased stiffness in the bottom slab subsequently decreases the moment at the top outside corner. The moment distribution of the top slab thus, sees an increase at midspan which leads to the higher compressive and tensile stresses in the top slab when using bottom post-tensioning. Figure 5.17 shows the top slab moment distribution at the dry dock. Comparing Figure 5.9, which only has top post-tensioning and a midspan moment of 2,173.80 kNm, Figure 5.17 exhibits an increase in moment with a value of 2,504.93kNm. This behaviour is present in both dry dock and final stages. However, in the final stage, the slab is fully in compression.

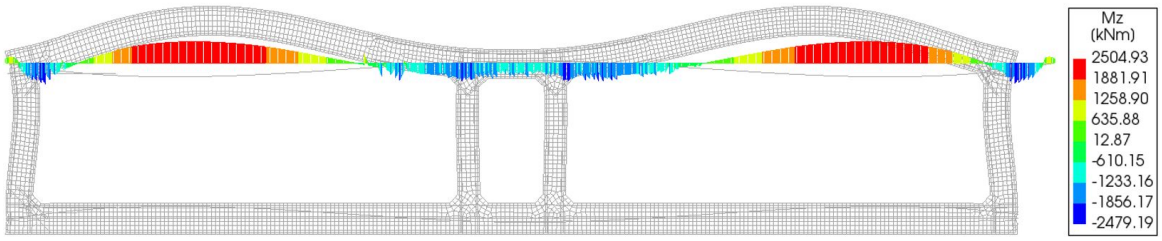

Figure 5.17: Dry dock moment distribution with floor and top post tensioning

When looking at the bottom slab, the post-tensioning forces have a clear effect in increasing the overall compressive state of the midspan section as is intended. In the dry dock stage all stresses are constant throughout the height of the section. The stresses in the top inside corners have a tensile stress of 7.48Mpa, a 30% reduction from the dry dock stress distribution seen in Figure 5.13, without bottom post-tensioning. Overall, the final immersed stage shows favourable results when using bottom post-tensioning. The dry dock requires close attention at the top slab for increased tensile stresses.

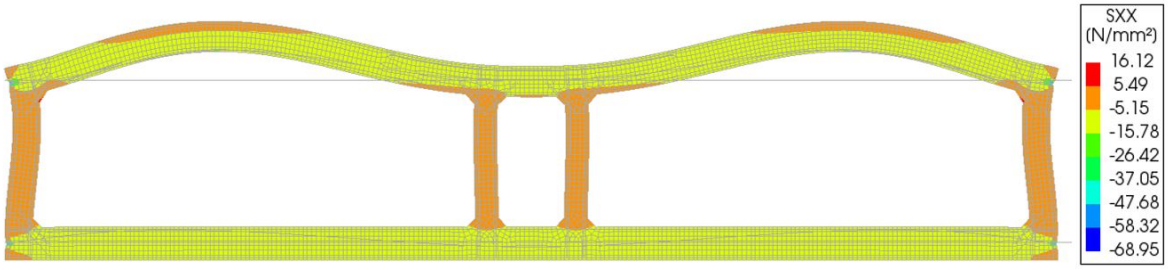

Figure 5.18: Stress Distribution Dry dock Immersed Stage with Floor and Top Post-Tensioned

5.8. Nonlinear analysis

A nonlinear analysis is used when there are non-linearities present in the stiffness matrix of the structure and a more accurate material behaviour needs to be simulated. As the load or displacement is increased in increments in a model, DIANA recalculates the stiffness matrix to more accurately determine the nodal displacements.

It is important to understand the development of the loading conditions on the structure at both the dry dock stage as well as the final stage. A better understanding of the limitations of each stage considering the loads applied can be seen by analyzing the global behaviour until failure is reached. When running a nonlinear analysis, there is more results available on the loading stages and post peak behaviour, since cracking of concrete and yielding of steel are taken into account.

Iterative Procedure

There are different iterative solution methods, which define how the subsequent iteration will increment the load. In DIANA it is possible to choose between Full Newton Raphson, Modified Newton Raphson, secant method and linear stiffness. The main difference between them is how the stiffness is recalculated, with the Newton Raphson method updating it in every iteration, whereas the tangent stiffness uses the initial stiffness for every iteration of every load increment. The amount of computational time for Newton Raphson is noticeably longer, but it requires less iterations and is more stable. The Full Newton Raphson method was chosen for the initial model. The iterations per load step was placed at a maximum of 30.

Convergence Criteria

In DIANA there are three ways to control the convergence; force norm, displacement norm or energy norm. This is how the program determines that the results are adequate enough to stop the iterations, unless it reaches the maximum number, then the results will diverge. A ratio is calculated between the current norms against the norm of the increments in the first predication of the increment. In this analysis, a combination of force and energy norm was used.

Incremental Procedures

Force control and displacement control are both methods used to increment the load, and they depend on the shape of the structures response. Force control is optimal when loads are being incremented continuously. If there is softening of the material however, force control is not the best option, as seen in Figure 5.19. The force exerted would keep increasing following the failure of the model even though the internal forces are decreasing. Displacement control in this case would increment a prescribed displacement.

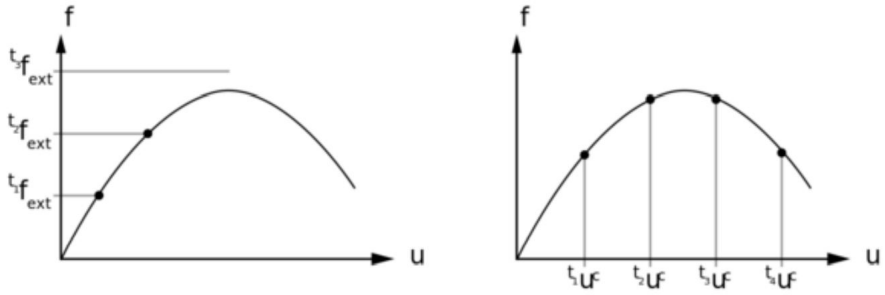

Figure 5.19: Load and displacement control [10]

Type of Nonlinear Analysis

Two types of nonlinear analyses are geometrical and physical. The geometrical non linearity method works when equilibrium equations must take into account the deformed structural geometry due to large deformations. Physical nonlinearity however, mainly depends on the changes in the material properties and are typically a function of the stress/ strain states. Due to the cracking of the structure and importance of steel yielding, physical nonlinearity was used for the model. Within this method, a Total Langrange nonlinear analysis was chosen for this model, since it is applicable for large rotations and displacements.

Post-tensioning load had to be evaluated as an initial state, since the load is applied as a stress in the numerical model. If it is implemented as a load the program will not take it into account as it does the other external loads. in DIANA, the initial state application is referred to as a start step, instead of a load step. The start step allows for the initial conditions of a structure to be set prior to implementing the loads in increments. For this study, this means the model will already have the effects of the post-tensioned loads before the self-weight for the dry dock stage and the remaining external loads for the final immersed stage. Even though in reality the self-weight is present before the strands are post-tensioned, the numerical model will follow the opposite order, similar to pre-tensioning of the structure, which is commonly used for bridge beams.

5.9. Results Nonlinear Analysis

Final Stage

More result options are available when running a nonlinear analysis, in addition to the moment and stress distributions seen in the section 5.6, a look into the crack strains, crack widths and reinforcement stresses can also be observed.

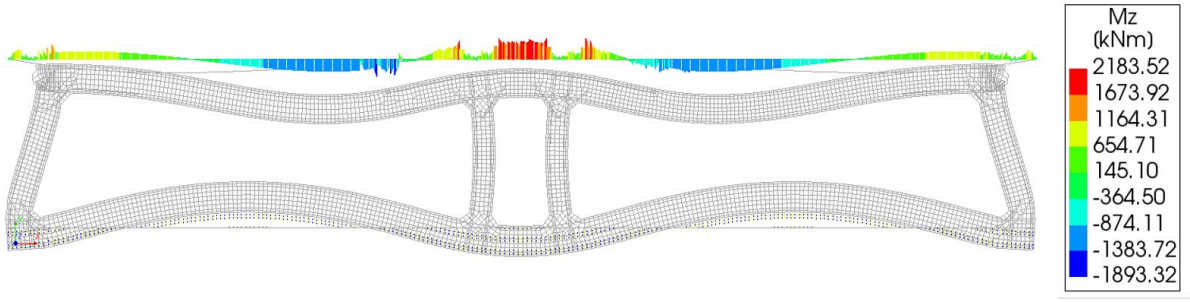

Figure 5.20: Moment Distribution at final stage

The moment distribution of the top slab in the final stage is seen in Figure 5.20. With an overall similar deformation, which is in line with the linear analysis and analytical calculation assumptions. In Figure 5.21,

both linear and nonlinear moment distributions are graphed. There is a slight reduction in the maximum moment, which is -2,183kNm at the wall-slab connections, compared to the -2,302.07kNm using linear analysis. The moments above the outside corner also have a slight difference, but overall the distributions are aligned and follow the same pattern.

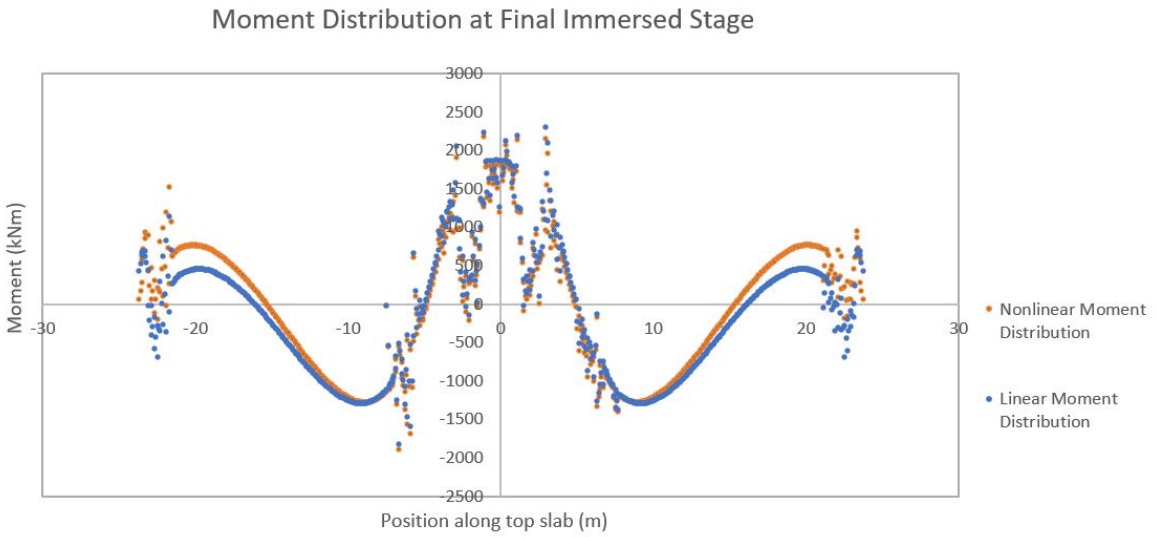

Figure 5.21: Nonlinear and linear moment distribution at final stage

Looking at the final stresses in Figure 5.22 a very similar shape and stress distribution can be seen to the linear analysis in Figure 5.12. There is an overall reduction of stresses at the corner, due to the redistribution that is happening in the nonlinear analysis, also prominent in the moment diagram.

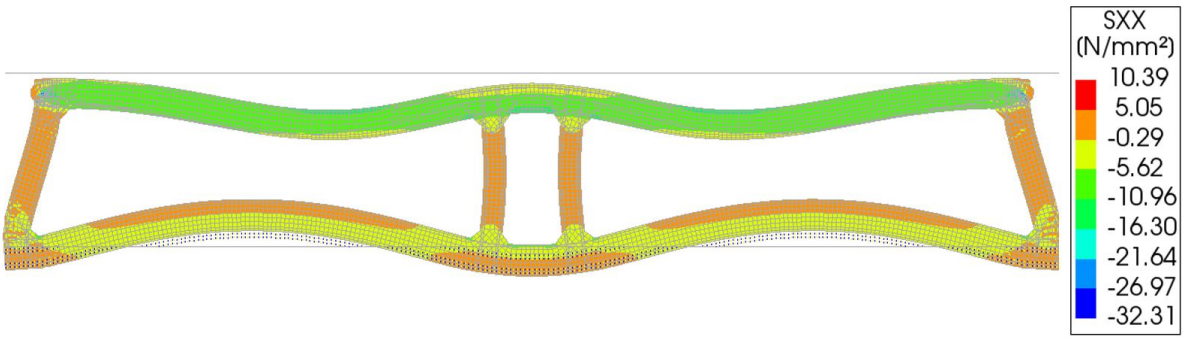

Figure 5.22: Stress at final stage using nonlinear analysis

Figure 5.23 represents the stress distribution down the top slab cross section for both linear and nonlinear analysis. The top value of -12.38 MPa is shared by both analysis, and the bottom of the slab has a difference of 6%. The stress distributions are therefore very similar, which leads to the assumption that the loading conditions for the final stage is in the linear elastic stage.

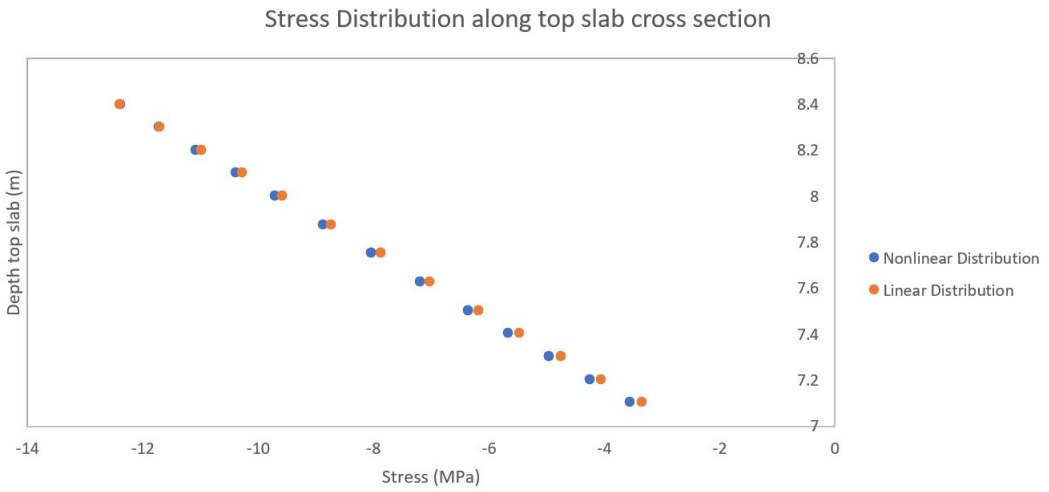

Figure 5.23: Stress at final stage along top slab section

A load displacement curve shows the overall global behaviour of the model. The analysis was done by keeping the self-weight and prestressing forces constant, while increasing the external loads in increments of 5%. The loads are increased to 200% where there is a subsequent failure of the structure, visible in the large displacement in Figure 5.24, in the last step. The positive displacement shown in the graph corresponds to the downward y direction. The prestressing start step is visible below the 50% load percentage, since the deflection starts at -22mm instead of 0mm. The deflection is taken at midspan, where the absolute displacement at that point is closely related to the relative displacement due to the two corners having negligible displacement throughout the loading increments.

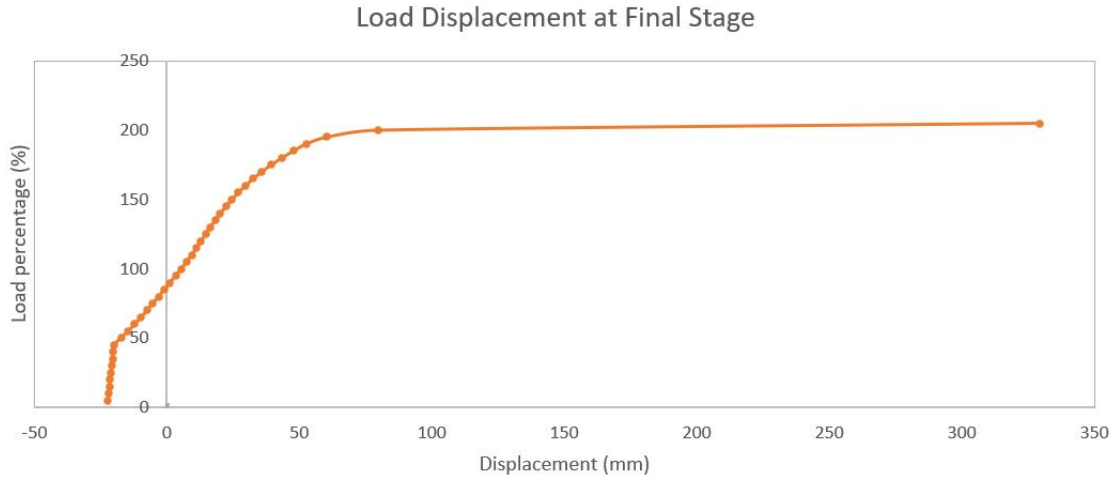

Figure 5.24: Load displacement curve for final immersed stage

To identify at what stage the current loading condition is in, a local stress strain curve is shown in Figure 5.25, taken at the top of midspan. The current loading conditions, considered as 100% loading, are pointed out by the red arrow, which aligns with the stress value seen at the top of the beam, at 8.4m in Figure 5.23, with a value of -12.38 MPa. The stress strain curve of the nonlinear analysis follows a linear elastic behaviour up until -16 MPa, which corresponds to a total load of 150%. Thus, this validates the assumption that the stress distribution of the top slab is in fact still following a linear elastic behaviour.

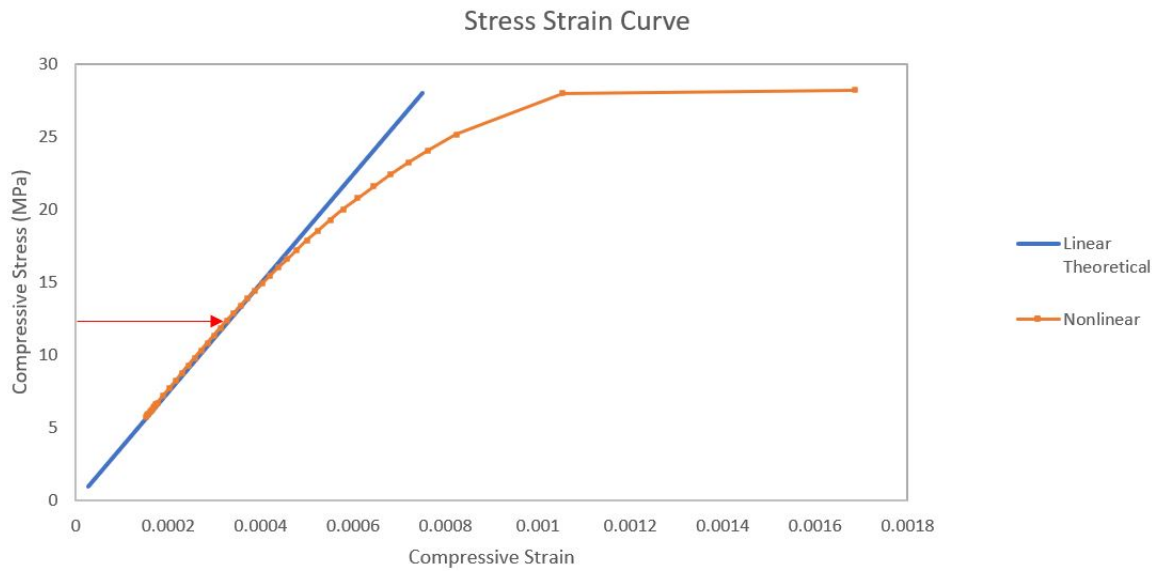

Figure 5.25: Stress strain curve for final immersed stage

Due to the use of the start steps, where the post-tensioning load is evaluated as an initial state prior to all other loads,as an initial state, the cracking is already present from the first load step. Even though the loading conditions for the final stage are in line with a linear behaviour, cracking will be present in this numerical model. A visual representation of the cracking locations can be seen in Figure 5.26 for load percentage 150%, where the linear elastic stage ends. The highest strains are seen in the top corners, which is in line with the high stresses due to the post-tensioning anchors. In addition, the bottom slab exhibits strains in the top of the midspan and bottom of the gallery. This is in accordance with the areas that would be improved by the addition of bottom post-tensioning seen in Section 5.7.

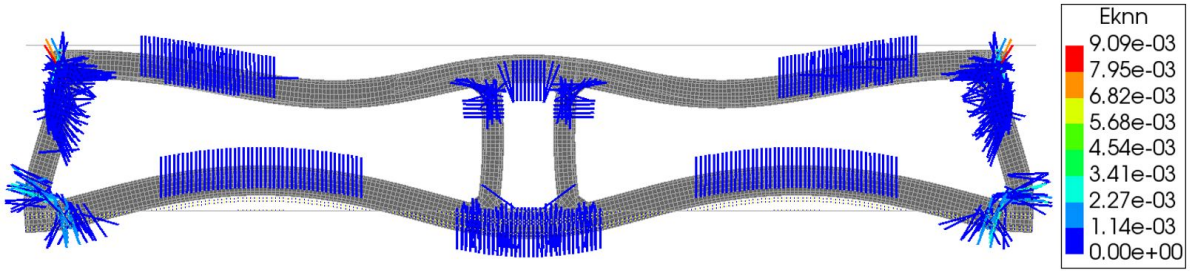

Figure 5.26: Crack strain at final immersed stage 150% loading

Dry Dock Stage

For the dry dock stage, the post-tensioning force is applied as an initial stress, similarly to the final stage, and then the self-weight is added in increasing incremental loads. Figure 5.27 illustrates the moment distribution with a nonlinear analysis. A similar shape to the linear analysis is seen from Figure 5.9, however the walls have a slight increase in deformation.

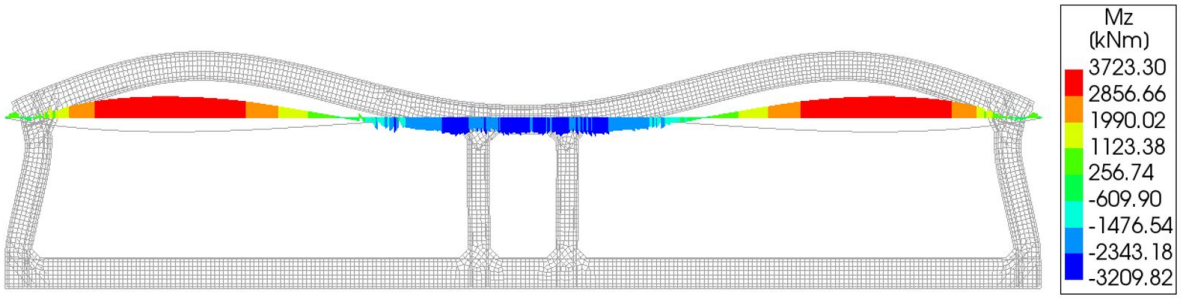

Figure 5.27: Moment distribution at dry dock stage

When looking at the comparison between nonlinear and linear moment distributions as shown in Figure 5.28, the most significant difference is in the outside corners, where the nonlinear moment is close to 0 kNm, whereas the linear moment reaches over 3,000kNm. Nonlinear analyses however, reaches overall larger moments throughout the slab. The shape of the distribution matches the linear analysis, however due to the redistribution of stresses in the nonlinear analysis, the corner sees a large reduction, which is seen distributed towards the slab. Since the moment distribution is obtained by the integration of stresses over the beam, this inherently means that the nonlinear stress distribution is slightly higher, which is further investigated in Figure 5.30.

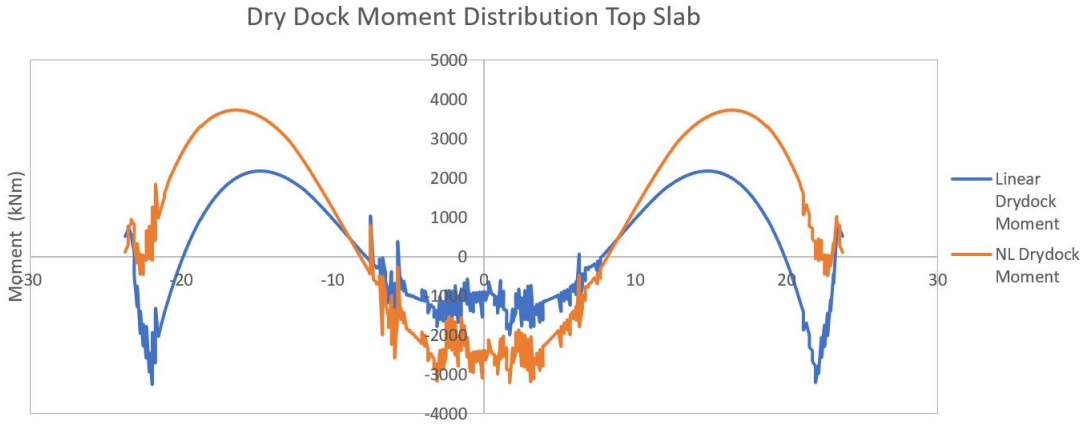

Figure 5.28: Moment distribution at dry dock stage Linear vs Nonlinear

The stress distribution from the nonlinear model is seen in Figure 5.29, which overall has a similar distribution to the linear analysis seen in Figure 5.13. In comparison to the linear analysis, however, Figure 5.29 shows a decrease in stress visible in the legend, which can be due to the redistibution of high stresses present in the corners. In addition, more stress changes are visible in the wall right under the top corners.

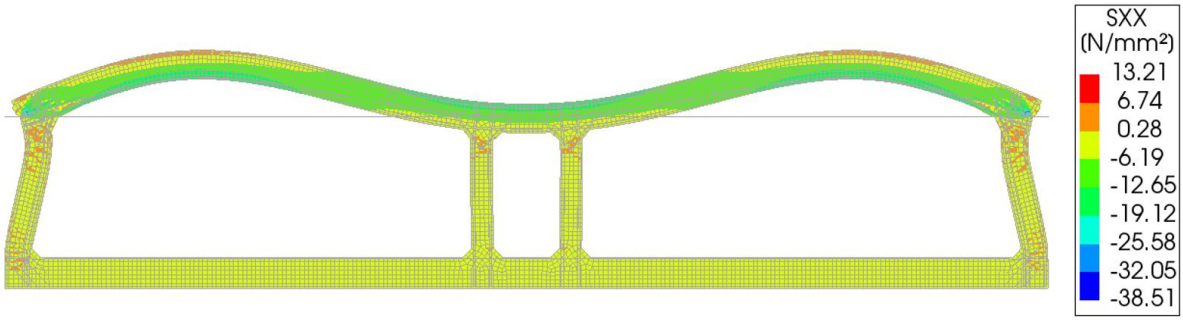

Figure 5.29: Stress distribution at dry dock stage

When focusing on the top midspan, Figure 5.30 shows the distribution down the top slab cross section. Unlike the distribution in the final stage, the dry dock has differences between the linear and nonlinear analyses. The values at the bottom of the slab, -18.87MPa for nonlinear and 20% reduction to -15.01MPa for the linear. At the top of the beam, the linear analysis remains in compression, whereas the nonlinear analysis has a maximum value of 1.17Mpa, marked by the red arrow in Figure 5.30. Both top and bottom see an increase in stress in the nonlinear analysis. This is due to the higher strains that occur with a nonlinear analysis from to the change in stiffness matrix. A higher strain generally leads to higher stresses based on the material properties set out. At the top part of the beam, there is no longer a linear distribution, and the higher stresses are seen slightly below the top of the beam, at 8.2m. There is a redistribution of stresses and tension softening that is happening after what appears to be the onset of cracking, following the Hordijk model set in the concrete material properties.

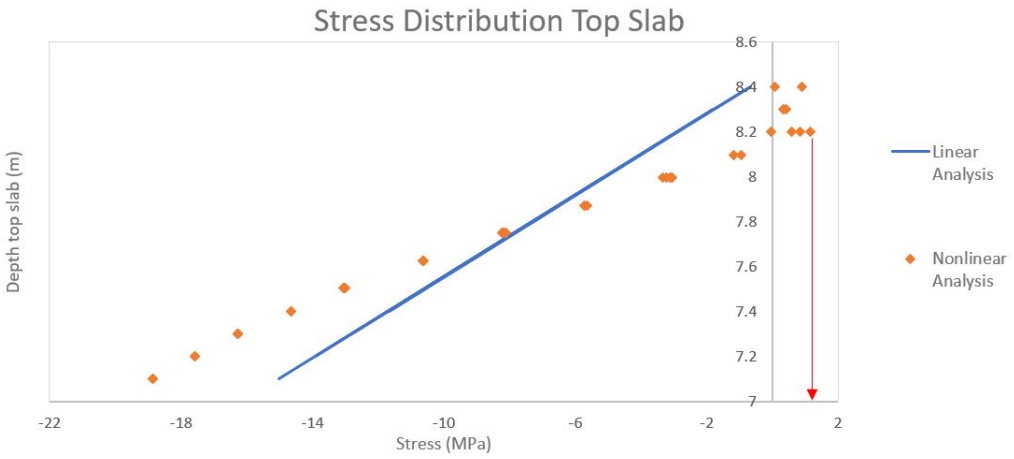

Figure 5.30: Stress distribution for the dry dock stage at midspan top slab

Similarly to the final immersed stage, a load deflection curve is seen in Figure 5.31 which shows the global behaviour of the structure at the dry dock stage. In this scenario however, the load that is being increased is the post-tensioning. Due to the implementation of the post-tensioning load as a start step, the load was not able to be increased in an iterative manner within the same analysis. Alternatively, the post-tensioning load was increased in increments of 20% for each analysis, keeping a constant self-weight load. A 40% loading was taken as the initial step, up to 210%, since 220% exhibited failure of the structure.

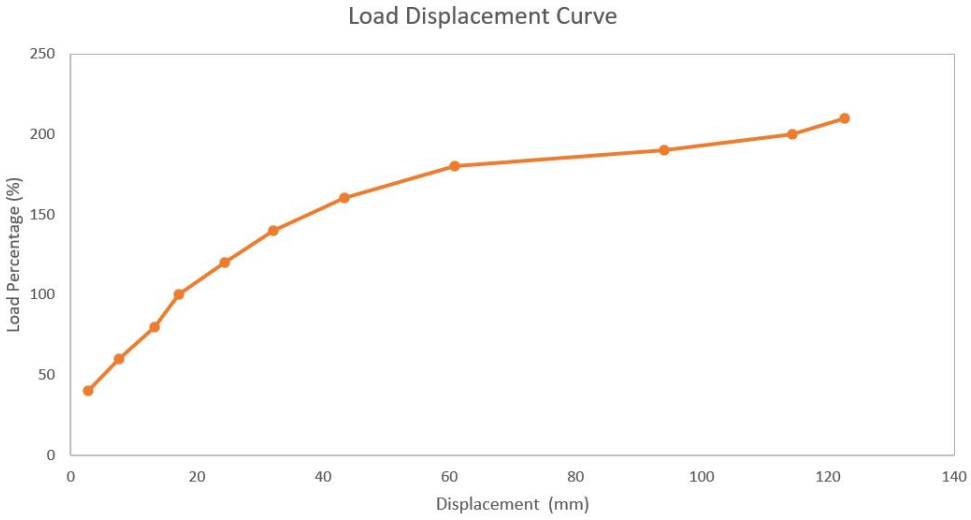

Figure 5.31: Load displacement curve for the dry dock stage

To validate the assumption that the current loading is in in fact in the nonlinear stage, Figure 5.32 shows the stress strain curve for that region of the structure. The red arrow points to the current loading stage, a compression of -18.87, which is taken to be 100%, and has visibly past the linear elastic stage. The linear elastic behaviour ends around -15.0Mpa which corresponds in this scenario to roughly 80% of the initial loading.

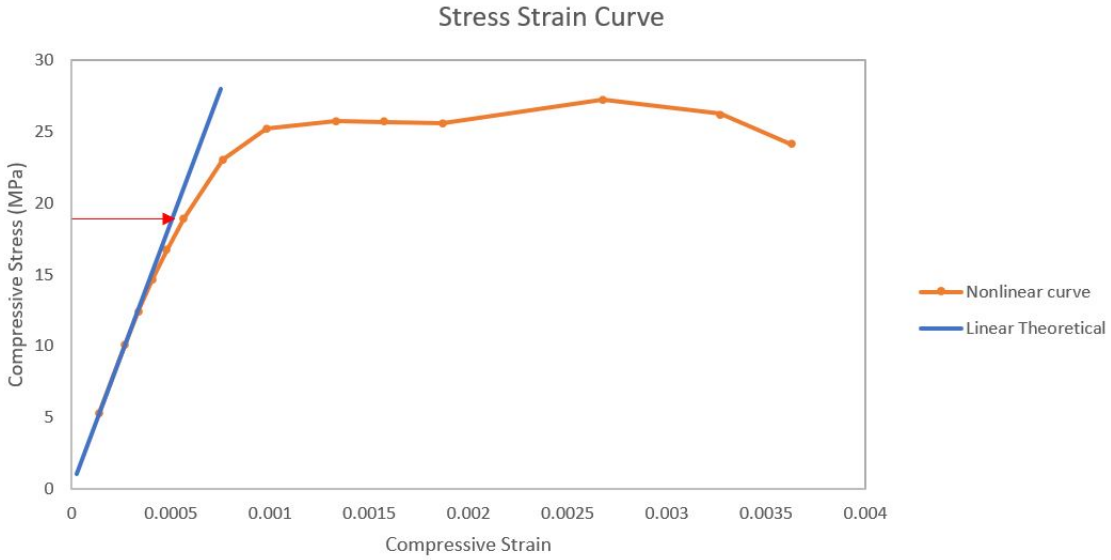

Figure 5.32: Stress strain curve for the dry dock stage at midspan

Figure 5.33 shows the crack strain results of the dry dock stage at 100%. The cracks are primarily present as expected at the opposite face of where the post tensioning force is located. The highest crack strains are present at the corners, where there is not high ductility of the section and the post-tensioning force is introduced. The area above the gallery also has some cracking, which means more reinforcement must also be allocated in these areas, which are affected by the post-tensioning distributed load. The load from the tendon situated above the gallery is pointing downwards, adding on to the self-weight distributed load. Based on the lack of ductility from the connection, the area is prone to crack as the deflections are limited by the gallery walls.

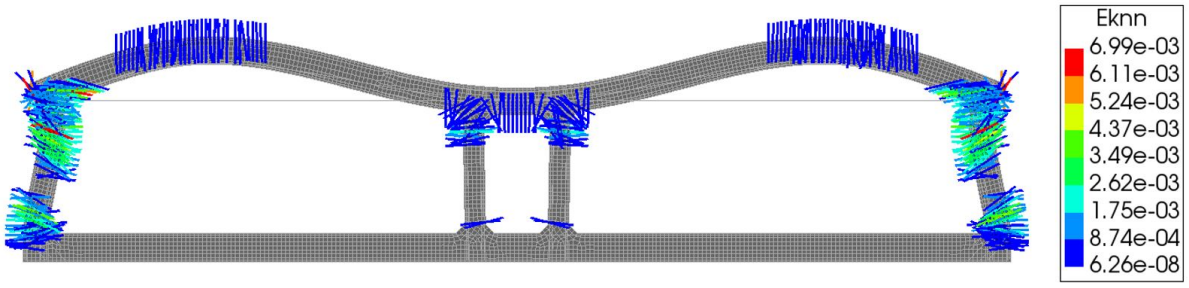

Figure 5.33: Crack strain at dry dock stage at 100% loading

The yielding of the reinforcement is shown in Figure 5.34,at the top side of the roof and at the corner with the gallery, with a maximum value of reinforcement stress of 465.69 N/mm^2 at a load of 200%. These stresses are in line with the cracking occurring in those regions. The yielding of the steel is a benefit of the nonlinear analysis, and it allows for the redistribution of forces to occur, and more accurately represent what the effect of the reinforcement has on the section.

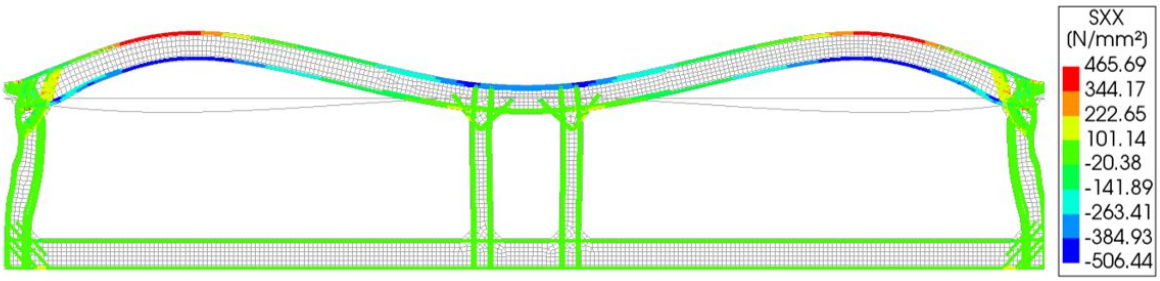

Figure 5.34: Reinforcement yielding at dry dock stage- 200% loading

5.10. Conclusion

A numerical model was created to simulate the behaviour of the immersed tunnel, and evaluate the structure in response to the application of transverse post-tensioning forces. This was done for both the final immersed stage, where 85% of the post-tensioning is modelled and the dry dock stage, where 100% is modelled.

The linear analysis gained insight into the stiffness and rigidity of the structure as a whole, which resulted in some differences over the assumed analytical model. The main differences are seen in the outside corners and inner corners where an increase of less than 30% is observed from the analytical values. The second observation, related to the post-tensioning force moments, sees a smaller moment over the gallery due to the downward distributed load the tendons are generating over the gallery. The two changes modified the overall analytical moment distribution.

The stress distributions from both the final and dry dock stage showed similar values and distributions to the analytical ones for the top slabs. Tensile stresses were observed in the top of the midspan during the dry dock stage, when observing only the effect from the post-tensioning force. When the self weight was added, a compressive stress of -0.63MPa was observed, a favourable results for the dry dock camber. High tensile and compressive forces of 16.22MPa and -69.37MPa respectively, were seen at the entry points of the post tensioning forces due to the concentration of high stresses at the outer elements. A point of concern in the final immersed stage, was the bottoms slab. High tensile forces were observed at the bottom corners and gallery.

This led to the implementation of bottom post-tensioning also being investigated using a linear analysis. When observing the stresses at the final immersed stage, due to the distributed loading upwards on the bottoms slab, stresses at the top of midspan exceeded the tensile limits with no post-tensioning. By adding post-tensioning in the bottom slab, the results showed a decrease by approximately 6MPa, making it a favourable outcome, since there was a clear overall compressive behaviour. When adding bottom post-tensioning there is a stiffening effect throughout the whole structure, which must be taken account additionally in the top slab at the dry dock stage. There was an increase in stress which generated a tensile stress of 0.20MPa, in this particular case below the material limit set in the model.

The nonlinear analysis allowed a glimpse into what stage each loading condition is in. For the final immersed loads, the structure response was in line with the linear analysis, visible through the moment and stress distributions. A closer look at the load displacement for the structure by increasing the external loads, validated that the loading conditions were still in a linear elastic stage and thus the linear analysis accurately represented the response of the structure. A similar analysis was performed for the dry dock stage, where the actual loading conditions were observed to just pass the linear elastic stage and the nonlinearities were exhibited in both the moment and stress distributions. The moment distribution showed large redistribution,

especially at the outside corners, due to subsequent deformations from the camber. The stress distribution showed tension softening at the top of the midspan due to the onset of cracking. The dry dock loading condition, thus is better represented from a nonlinear analysis, since the linear model underestimated the response of the structure.

The numerical model allows for a more accurate representation of the response when implementing post-tensioning forces in the structure. Especially when considering the boundary conditions and the moment distributions that are actually taking place. A nonlinear analysis was able to give a snapshot of where the two loading conditions were when looking at the overall structure's response. The investigation concluded that the dry dock stage loading conditions is no longer in the linear elastic stage of the structure behaviour, thus it is critical when it comes to the design of post-tensioning forces.

6

Parametric Study

Chapter 5 used finite element modelling to validate that the onset of cracking occurred when implementing post-tensioning for a concrete immersed tunnel at the dry dock, which was the case for the analytical calculations in Chapter 4. When designing the post-tensioning based on the requirements of the final immersed stage, the element sees an upward camber due to the lack of external loads that are present at the dry dock stage. Since the loads, specifically hydrostatic and backfilling pressures, are quite substantial, the post-tensioning camber can lead to large cracks at the top of the beam, along the midspan. One option to mitigate this is by adding reinforcement at the top of midspan, which will be referred to in this study as additional reinforcement, since it is separate from the longitudinal compressive reinforcement for the final stage. Another option is to further minimize the impact of the tendon drape force, while still obtaining enough to counteract the loading on the structure.

The primary objective of this chapter is to perform a parametric study on the main influences that can lead to an optimized solution, where the final immersed stage has enough structural capacity while minimizing the cracking in the dry dock stage. The optimal solution is defined as the combination of parameters that yields the least amount of cracking, while keeping the required prestressing force to a minimum and maintaining the structural capacity of the element.

When looking at the amount of additional reinforcement required for the dry dock stage, this can easily reach a high and unrealistic value when implementing high levels of prestressing force. There are two parameters that have an influence on the amount of reinforcement required; the curvature of the tendon profile and the percentage of total prestressing implemented. If both of these parameters are at their maximum, the highest amount of additional reinforcement at the dry dock will be required. By altering the curvature and the partial prestressing the minimum amount of additional reinforcement required can be achieved, hence obtaining an optimal design.

The analytical calculations found in Chapter 4 will be used, however the variations from the finite element model in Chapter 5 from the moment distributions will be implemented in the calculations. These include the reduction of moment at the corner and above the gallery from the distributed loads and a reduction of moment above the gallery for the prestressing force moment distribution.

6.1. Input Parameters

The parameters used in this analysis are consistent with the ones adapted in the finite element model and analytical calculations as seen in Tables, 6.1 and 6.2.

Table 6.1: Post Tensioned Base Case Dimensions

Dimensions		
Width of Gallery	3	m
Height of tunnel	5.7	m
Thickness of outer walls	1.2	m
Thickness of inner walls	1.0	m
Water Table Height	10	m
Rock Layer Height	1	m
Thickness of section	1	m
Cover	60	mm
Distance to Reinforcement	81	mm
Max distance to Post tensioning cables	113.5	mm

Table 6.2: Material properties implemented in parameter analysis

Post-Tensioning Steel		
Strength Class	Y1860S7	
f_{pk}	1860	N/mm^2
f_{pk}/Υ_s	1691	N/mm^2
e_{pu}	35	%
σ_{pm0}	1395	N/mm^2
Elastic Modulus	195000	N/mm^2

Steel & Concrete		
Steel		
f_{yd}	435	N/mm^2
Elastic Modulus	200000	N/mm^2
Concrete		
f_{ck}	35	N/mm^2
Elastic Modulus	34000	N/mm^2

6.2. Initial Curvature Analysis

The initial step in this process is to understand the influence that the curvature has related to the prestressing force and to optimize the shape of the post tensioning tendon. The main consequences of varying the tendon shape is the amount of prestressing force required and distributed force generated. The tendon profile will consist of two equal parabolas over the traffic envelope and the third over the gallery, as seen in Figure 6.1. For the analysis of the curvature, the tendon eccentricity is assumed to remain constant at the centre of the section, right above the gallery.

The first parameter that will be varied is the eccentricity at midspan. The centre parabola above the gallery, will have a constant eccentricity of 0.1m to avoid having a radius that is too small that generates large distributed loads in the region. In addition, this will simplify the model and always adhere to the limitations of the duct cover when closer to the external side of the tunnel, covered in Chapter 4.

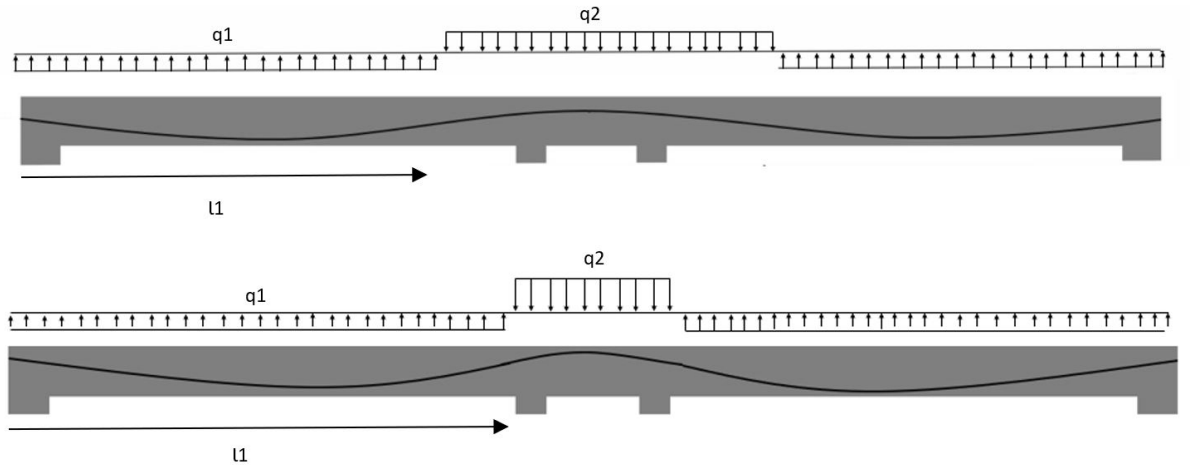

Figure 6.1: Two different scenarios with varying tendon profiles

The second parameter that will be altered, is the length of the parabolas, with the first scenario having three equal parabola lengths, and the last scenario having the middle parabola spanning the gallery width, as represented in Figure 6.1.The analysis will look at the effects that curvature has on the required prestressing force, distributed load of tendons, and prestressing losses. In the analysis, curvature relates to the change in eccentricity at midspan. A greater curvature, equates to a larger eccentricity.

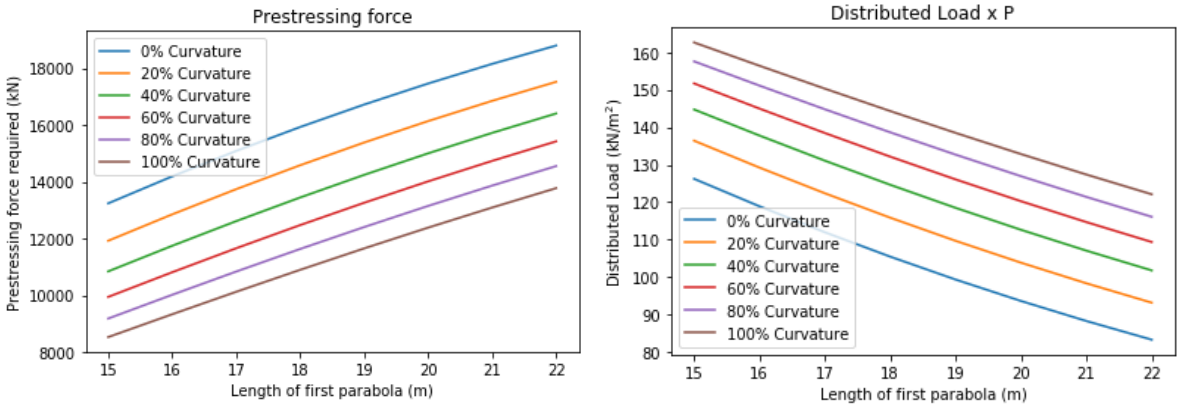

(a) Prestressing Force

(b) Distributed Load

Figure 6.2: Effects of changing curvature on prestressing force and distributed load

The key observations from Figure 6.2a are the increase in required prestressing force as the parabola length is increased, contrary to an increase in curvature which reduces the need for a higher prestressing force. This can be explained by the fact that larger curvature of the tendon shape decreases the radius, which yields higher distributed loads. The distributed loads that are transferred to the concrete by the curved tendons are essential to counteracting the loads on the structure and thus, less applied prestressing force is required. This is evident in Figure 6.2b, as the distributed load increases with curvature, and smaller parabola lengths that also lead to a decrease in radius size.

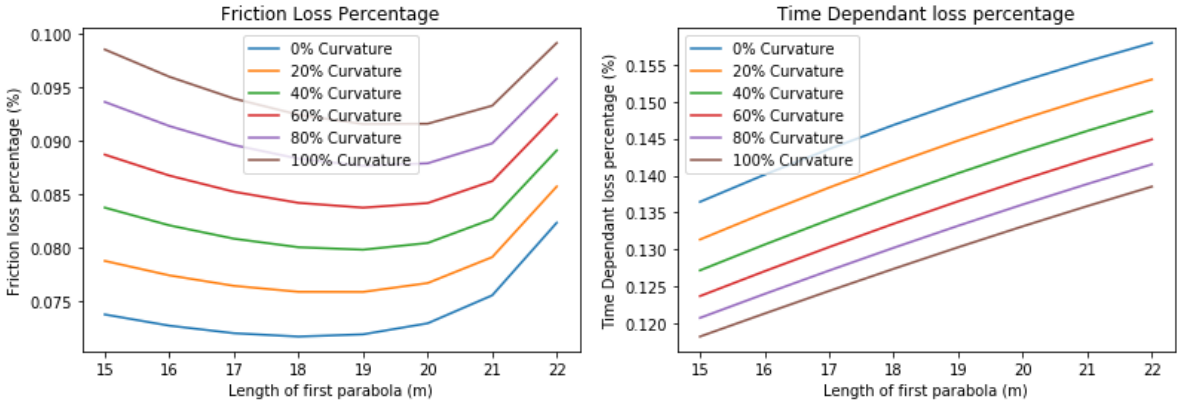

(a) Total Friction Loss

(b) Time dependant losses

Figure 6.3: Effects of changing curvature on prestressing losses: friction and time dependant

$$P_m(x) = P_m \cdot e^{-\mu(\theta+kx)} \tag{6.1}$$

The friction loss equation depends on the position along the tendon as well as the angle of the tendon drape. It is therefore logical, that the change in eccentricity have much larger effect than the change in parabola length. The increase around 20m parabola length in Figure 6.3a is due to the increase in the angle of second parabola, above the gallery. The time dependant loss percentage increases with increasing prestressing force, as Figures 6.2a and 6.3b depict with their uniform curves.

The above figures demonstrate that the change in drape height has a larger effect than the horizontal dimensions of the tendon parabola. Based on this analysis, moving forward the length of the parabolas will remain 7/8 of the span, which will be around 18m for a 20m span. The height of the drape of the outer parabolas will be varied from 0-100% to analyze the behaviour of the structure and optimize the need for any additional reinforcement.

The following section will go over the goal of the optimization script, the inputs required, and the results obtained from it. The main output that will be observed and used to compare the different scenarios is the amount of additional reinforcement required in the dry dock stage to reach an acceptable crack width due to the prestressing camber. Figure 6.4 shows two types of reinforcement; in red, the additional reinforcement mentioned, and in blue, the regular reinforcement. Regular reinforcement refers to the longitudinal tensile reinforcement required when designing the final immersed stage of the tunnel. The typical sagging moments at midspan and hogging moments at the supports are used to design the regular reinforcement. The crack width at the dry dock is utilized for the additional reinforcement amounts.

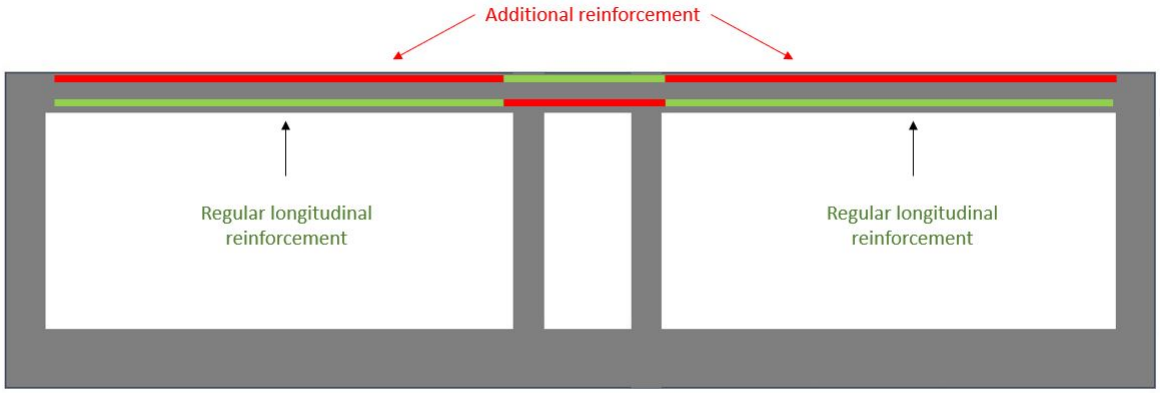

Figure 6.4: Layout showing location of additional vs. regular reinforcement

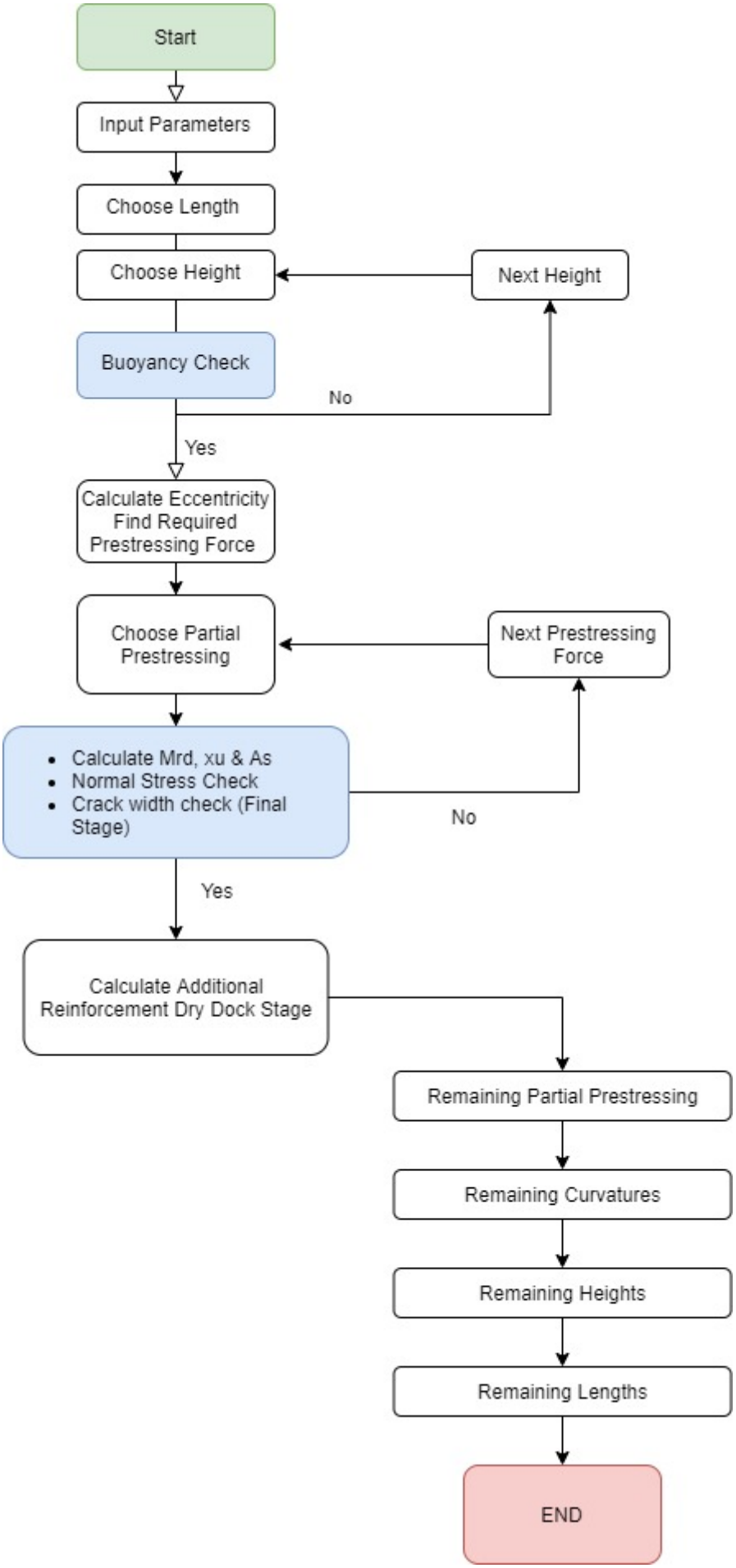

Figure 6.5: Flowchart of parameter analysis

6.3. Optimization Script

This section further analyzes the parameter relations, as well as finding an optimum combination that will allow for a longer span. The steps are outlined in chronological sequence in Figure 6.5. The Python script relies initially on a number of tests relating to the structural capacity of the element passing. If these are successful, the additional reinforcement to control the cracking at the initial stage is calculated. As mentioned, there are four parameters : span length, span height, tendon curvature and percentage partial prestressing. For this, a 4-dimensional matrix is created, where the reinforcement calculated can then be allocated and indexed based on the parameters. If any of the tests did not pass, there would be no number associated to that combination of parameters.

Test 1- Freeboard

The first test checks if the freeboard is over 15cm. There is no upward limit to this condition as freeboard values can be up to 1m, typically due to the large waves that can be encountered during transportation. Dimensioning of the tunnel is then complete if the freeboard test is passed, if not, the next height will be used. Loading on the structure and design moments are then calculated, using the same procedure and calculations as are seen in Chapter 4 for the post-tensioning Base Case. At this point the eccentricity of the tendons is chosen from the array, which will control the amount of curvature that the is implemented into the design. The required prestressing force is computed and the final parameter, partial prestressing, is defined at this point. The friction loss is also calculated, one for the location at midspan and the other above the first inner wall.

Test 2- ULS Capacity

Calculating As and xu is done utilizing a loop, that equates the moment capacity to the maximum design moment, at the connection with the inner wall of the gallery. An issue encountered with this, occured at high level prestressing and low curvature. Due to the low curvature, a higher value of prestressing is required based on the concrete strength calculations. When combined with a high percentage, the P_{m0} is extremely large. Since xu is calculated from the equilibrium of the cross section, a very large compressive height is needed to compensate for the high prestressing force. The value given in this scenario is larger than the height of the section itself. Due to this error, a very large reinforcement area was also calculated. To avoid this, the maximum compressive height is implemented that adheres with the ductility check:

$$\frac{x_u}{d} \leq \frac{500}{500+f} \tag{6.2}$$

The test will always be passed since the loop is designed that it can only end once Mrd is greater than Med. The shear was not included as one of the tests, due to the low probability of it being the governing failure of the structure, based on the analytical calculations.

Test 3- Normal stress capacity

The compressive stress of the concrete is checked with the following formula, taking into account the axial design force and prestressing force for N, and the applied bending moment and prestressing moment for M. The value must be lower than design compressive strength, $f_{cd} = -33.33MPa$.

$$\sigma(c) = -\frac{N}{A_{ceff}} - \frac{M}{W_{top}} \tag{6.3}$$

Test 4- Cracking at final stage

The cracking is checked as SLS for the final stage with all loads incorporated, and grouted tendons. Again, the same procedure seen in the Base Case in Section 4.4 is followed within the script. First the compressive height is found, using the maximum concrete stress. The steel stress is then calculated based on the section distribution and implemented into the crack width calculation. A limit of 0.15mm was used for the crack width based on as explained in Section 4.4.

Computing Reinforcement

The initial step was to calculate again the compressive height of the section with the initial condition at the dry dock. The assumption is made that there are no time dependant losses and is grouted shortly after prestressing. A loop is created to calculate the amount of additional reinforcement, using the crack width formula, and stating a maximum of 0.15mm width is required. The reinforcement is increased to lower the crack width until the condition is met. A maximum number of runs is set as not to exceed 20,000mm^2 of reinforcement, which generally will adhere to the 2% limit for the section, given that span heights will vary. If the reinforcement reaches the maximum count before the acceptable crack width, this implies that the condition would most likely not be met, and an alternative modification must be made. Some options for this are decreasing the size of reinforcement diameter, minimizing the allowable cover or increasing concrete strength.

6.4. Results and Observations from Optimization

The overall matrix formed was 4-dimensional, which creates complexity to the system. In order to simplify the results, several smaller snapshots are graphed in this section, providing insight into the different effects of each parameter. The script and an example of some of the output that was given is seen in Appendix D.

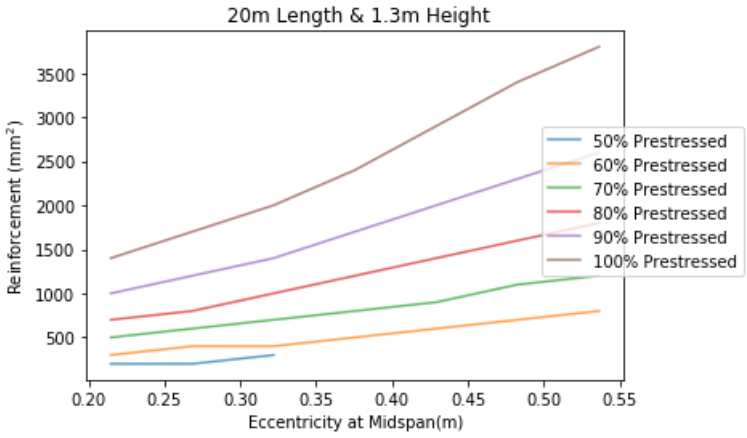

Figure 6.6: Curvature changes with constant length and height

Figure 6.6 helps visualize the effect the curvature has on the extra reinforcement required to keep the dry dock crack width under the limit. An increase in curvature means an increase in additional reinforcement required. At lower prestressing percentages, in this example 50%, there were crack width failures at the final stage since there was insufficient prestressing and steel stress.

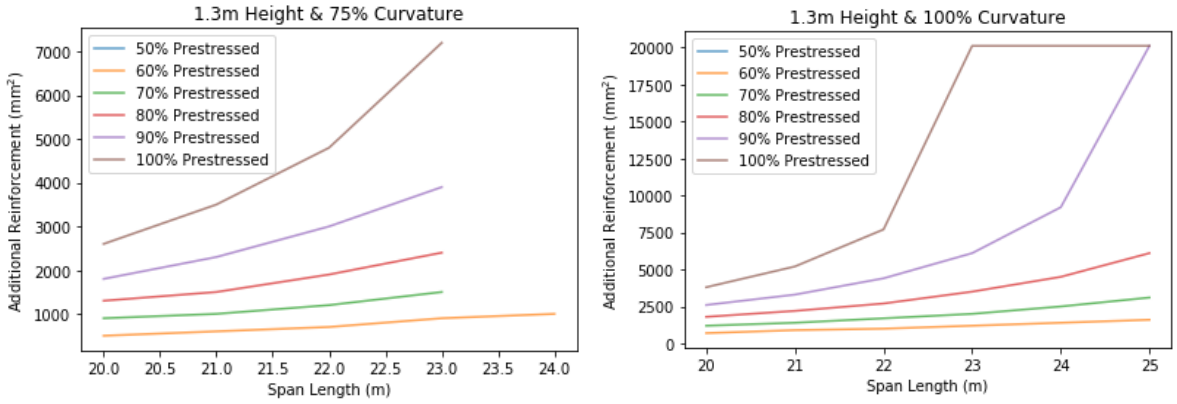

(a) 75% Curvature

(b) 100% Curvature

Figure 6.7: Testing span length variations with 1.3m height

The length of 26m was also included in the run where Figure 6.7 was generated however, for all percentages of prestress, the normal stress test failure occurred. Even with 100% prestressing, the normal stress exceeded the limit of the concrete compressive stress of 28.3MPa. This failure means a higher span height is required to accommodate the stresses that arise from the longer spans since the increment is proportional to the span length squared.

The 50% prestressing, not visible in either graph of Figure 6.7, failed at lower span lengths by not passing the final crack width check, and at higher spans due to the normal stress exceeding the limits. The crack width failed under low percentage prestressing, since there was not enough prestressing force, and the steel stress in the tensile area increased, affecting the crack width negatively. In this scenario, an increase of regular reinforcement would be required however, one of the script's limitations is that it only calculates the flexural reinforcement based on the design moment requirements. The normal stress check failures for lower prestressing percentages fail due to the stress contribution from the prestressing moment, which is positive, being too low, and the stress from the design moment not being compensated enough, making the normal stress exceed the limit.

By lowering the curvature to 75% seen in Figure 6.7a the maximum span length with a 1.3m height is 24m. Past this, the normal stress failed for all percentages of prestressing as the lower curvature was unable to compensate for the high stresses due to increased design moment. The 60% prestressing was the only successful value that passed all the tests. Above 60%, the normal stress check failed as the prestressing moment stress was not sufficient to compensate the negative stress from the larger axial prestressing force required to the smaller curvature.

Comparing the 75% to 100% curvature in Figure 6.7, the amounts of additional reinforcement are overall higher with increasing curvature, and the limit is reached much sooner, meaning that at higher curvature, other measures will also have to be taken to control the crack width at the dry dock stage. The figures show that as the length of the span increases, the amount of reinforcement required, will increase at a faster rate.

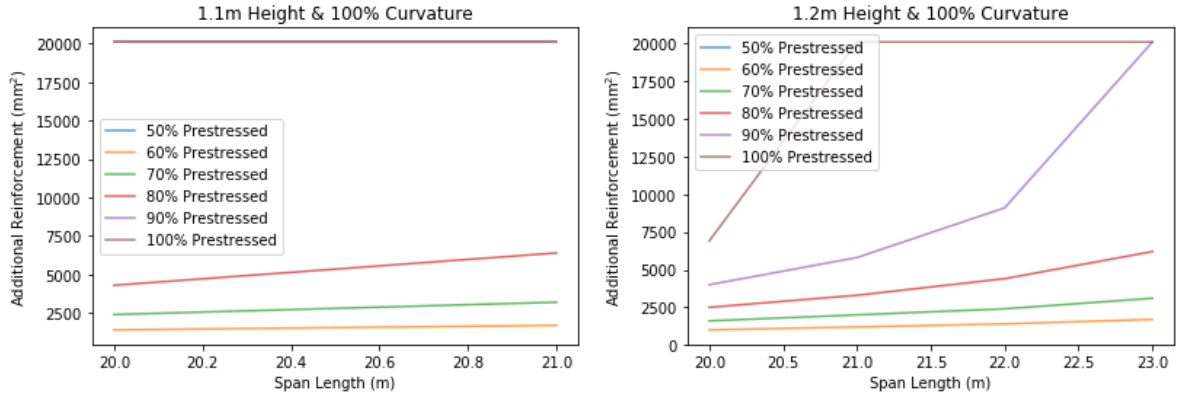

(a) 1.1m

(b) 1.2m

Figure 6.8: Testing increasing span lengths with lower heights

When there is lower curvature, the calculated required prestressing force is higher as seen in section 6.2 . Very high prestressing forces will sometimes mean that when calculating xu, the required concrete height to compensate for the high prestressing forces is too high, consequently calculating a required xu higher than the section itself. When this occurs in the script, the prestressing force will generate a very high compressive normal stress, and the test will subsequently fail.

Figure 6.8a shows the 1.1m height being limited to a 21m span, based on the normal stress check failing, which requires a larger section with increasing prestressing forces. Demonstrated by Figure 6.8b, where the 1.2m height, reaches a span of 23m.

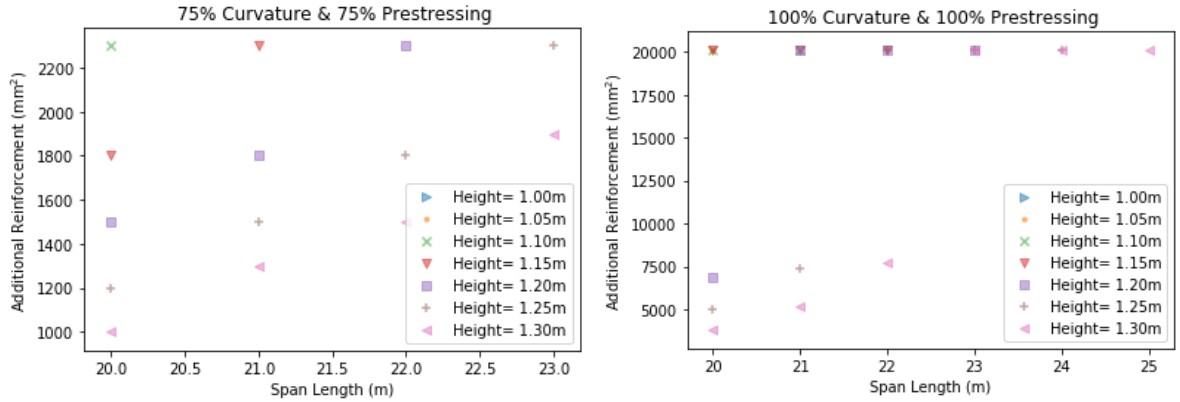

(a) Smaller height spans

(b) Larger height spans

Figure 6.9: Height of slab and span length variation with constant prestressing and curvature

Figure 6.9 focuses on the varying span heights with corresponding span lengths that pass all the tests. Figure 6.9a on the left, has heights from 1m-1.3m using 75% for both curvature and prestressing, and on the right in Figure 6.9b at 100%. When using 100% of both curvature and prestressing, a longer span can be achieved, in this case, 25m compared to the 23m when using 75%. The amount of additional reinforcement is significant when looking at the values in the vertical axis. Thus, the cracking generated using 100% is substantially higher.

An approximate maximum slenderness can be obtained from the results of Figure 6.9. This is achieved when using 100% prestressing and curvature, where the 25m span length and 1.3m height give a slenderness of 19.23, the maximum out of all the options which had passed the tests. A significant improvement from the reinforced concrete slenderness from Chapter 3 with a maximum slenderness of 15.4.

Analysing Figure 6.9a 75% for both curvature and prestressing was chosen to observe a more extensive variety since the maximum of both parameters yielded an additional reinforcement of 20,000mm^2 for a reduced number of heights that could pass all tests.

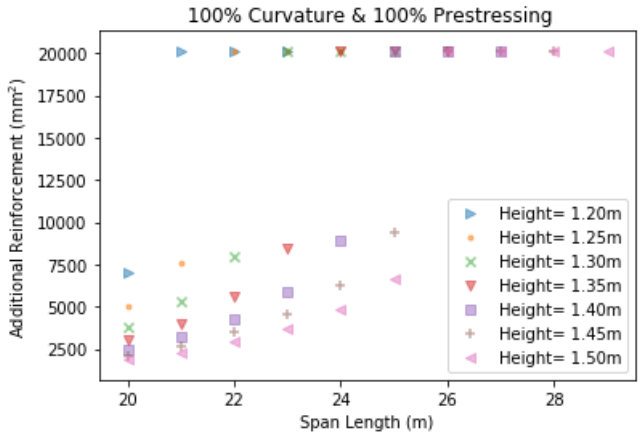

Figure 6.10: Height of slab and span length variation with a larger inner tunnel height

One of the limitations encountered when optimizing the span length of the element is the freeboard test. In order to avoid a buoyancy check failure, the inner tunnel height is increased to 7m. Consequently, the area inside the tunnel is then increased, thus allowing for a larger hydrostatic force while keeping the amount of concrete constant. A wider range of span lengths are now possible and seen in Figure 6.10.

With the parameters set in place, 25m length span was the maximum considering an inner height of the tunnel of 5.9m. When this value is increased to 7.0m, the span length can go to 29m. The maximum slenderness when looking at Figure 6.10 is 19.33 which is with a 29m span and 1.5m height. Although the increase in span length is positive, it is important to consider the height which, goes from 1.3m to 1.5m, a 0.2m increase. The total additional dredging would be of 1.3m considering the inner height change as well as the slab change.

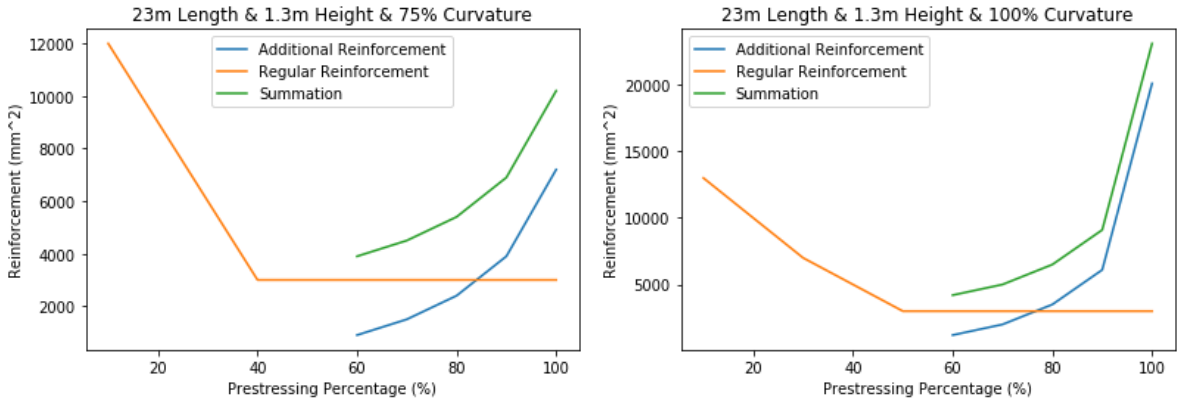

(a) 75% Curvature

(b) 100% Curvature

Figure 6.11: Comparison with regular and additional reinforcement at 23m span

Figures 6.11 show the comparison between regular reinforcement and additional reinforcement. Again, regular reinforcement refers to the positive bending moment reinforcement implemented in a beam at the opposing side of the concrete compressive stress block at the final stage. The additional reinforcement refers to the reinforcement required only to mitigate the cracking from the prestressing camber. These are both positioned at opposite sides from each other. From the figures, the trend is clear; as prestressing force percentage is increased, the amount of additional reinforcement to mitigate cracking increases, and the need for

regular reinforcement decreases. The regular reinforcement is calculated based on the design moment; however, with a high amount of prestressing, this can take up most of the moment and then the reinforcement is redundant in this aspect.

In this example the 23m span is used, only to see the effects of lowering from 100% curvature to 75%. The relation is very similar, but the values decrease considerably. In this case, the lowering of the curvature is a benefit to the amount of steel seen overall. However, when comparing the optimised solution in both graphs, in Figure 6.11a 60% prestressing requires the lowest overall reinforcement with a total of 4,100mm^2, whereas for 100% Figure 6.11b, again at 60% is slightly higher at 5,100mm^2. As mentioned, when lowering the curvature, this will inevitably increase the amount of prestressing cables required. The difference in this case is from 12,525kN, to 10,319kN which is a difference in 1,581mm^2 when translating it to area of prestressing steel. Thus, in this scenario, going with a higher curvature and slightly higher additional reinforcement would be the optimal outcome.

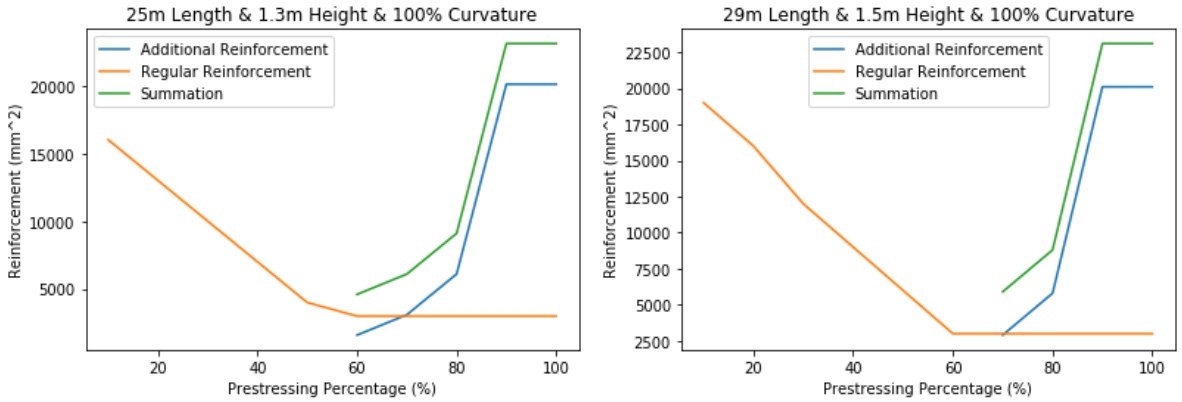

(a) 75% Curvature

(b) 100% Curvature

Figure 6.12: Comparison with regular and additional reinforcement at 25m and 29m span

Figures 6.12 look into the optimized span lengths that were found in Figure 6.9b with a maximum of 25m and Figure 6.10 with a maximum of 29m. In both these scenarios a 100% prestressing and curvature are used. The change in prestressing amounts is explored, which has a positive effect for both span lengths, in lowering the amount of additional reinforcement required. For the 25m span in Figure 6.12a, a 60% optimal percentage is seen, whereas the 29m span in Figure 6.12b, only reaches a 70% prestressing amount. Below that, the prestressing amounts failed, due to the crack width at the final stage exceeding the limit. When observing both the 25m and 29m spans with a lower curvature, similar to what was done in Figure 6.11 with 23m, all tests failed. Since these were the maximum spans that were obtained, already reaching the limit, when lowering the curvature, all normal stress tests failed, due to the very high prestressing forces calculated.

6.5. Conclusion

As the dry dock is the critical stage when considering the implementation of post-tensioning in concrete immersed tunnels, further analysis was done into minimizing these effects. The amount of additional reinforcement that is required in the dry dock to mitigate the camber cracking is used as a means of comparing the different scenarios and their effectiveness. The lower reinforcement required leads to a more optimal scenario. When the maximum curvature and percent of prestressing are simultaneously present, the reinforcement is either too high, or no amount of reinforcement will help close the cracks. When slightly lowering either of these parameters, a more feasible value is observed. Since lowering the curvature implies an increase in prestressing force, the more economical option is to be lowering the percentage of prestressing instead of the curvature.

Considering the external parameters, which are water depth and inner tunnel dimensions constant, the maximum length and slenderness were found. For these, the maximum span length was 25m with a height of 1.3m using 100% curvature. When varying heights to identify maximum slenderness, the maximum span of 25m, happened to also be the most slender with the height of 1.3m. In order to achieve a longer span, this requires still a greater height, which resulted in a failed buoyancy check due to the high amounts of concrete. When increasing the inner tunnel height, buoyancy check passed, and a length of 29m could be reached with a corresponding slab height of 1.5m, again making up the maximum slenderness. When analyzing the sum of both regular and additional reinforcement, the minimum can be determined as the optimal solution. This varies depending on the curvature put in place, but based on the analysis performed, ranging from 50-70%.

.

7

Fehmarnbelt Fixed Link

7.1. Introduction

The following section will go over a case study related to the Fehmarnbelt fixed link tunnel. The case study aims to use the findings from Chapter 5 and 6 to evaluate the possible optimization of the Fehmarnbelt Tunnel. In Chapter 5 finite element models were use to observe the tunnel elements behaviour to the addition of post-tensioning. In this case study however, finite element modelling will be used to analyze and compare the effects of two crack mitigating methods; the first is to add the reinforcement at the top of midspan, and the second is the implementation of temporary tendons.

The tunnel will connect Rødbyhavn on Lolland and the German island of Fehmarn. Once completed, it will be the longest immersed concrete tunnel, with approximately 18km in length. This tunnel will allow the travel time to be reduced from a 45-minute ferry ride between both points to a 10-minute car ride [27]. It contains a 2x2-lane highway and 2 railway tracks. A unique design characteristic in the Fehmarnbelt tunnel is the addition of special elements, which consist of a two-story cross section, located every 1.8km. The alignment of the tunnel is illustrated in Figure 7.1, where the special elements are depicted with the solid black line. The interval at which these elements are used throughout the tunnel is clearly seen. The other important detail is the depth at which these special elements reach, marking the difference in height, where the lowest depth according to Figure 7.1 is approximately 45m below sea level. The Fehmarnbelt link was ultimately chosen to be an immersed tunnel, primarily due to the planning benefits and the environmental impact studies [1].

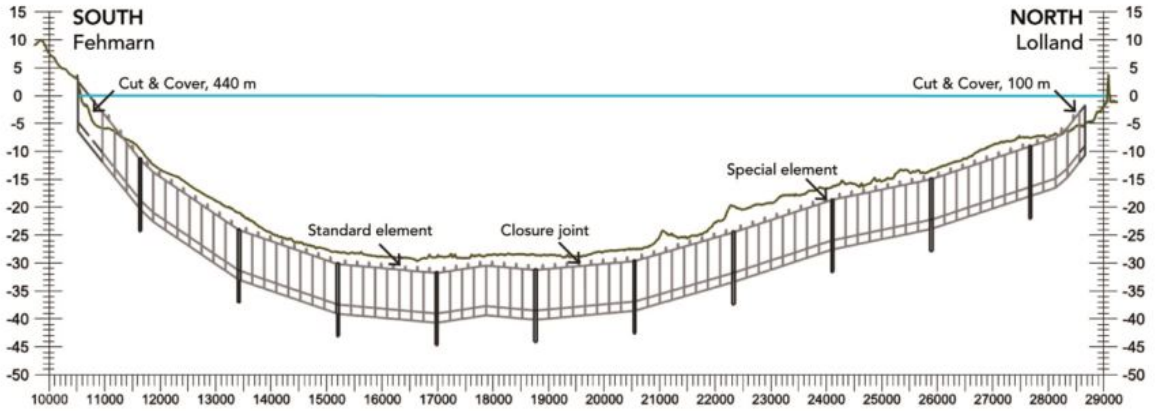

Figure 7.1: Alignment of Fehmarnbelt tunnel [11]

Out of a total of 89 elements, there will be 10 special elements, which will house all the operations and maintenance equipment, such as climate installations and pumping facilities, on the additional lower floor.

This innovative design will allow for lower maintenance cost in addition to an optimized size for standard elements [28]. Figures 7.2 and 7.3, show the standard and special element cross-sections respectively. The dimensions of the special elements are both higher and wider than the standard elements. In the location of the special elements, the dredging will have to accommodate the excess depth and width. The design of these elements optimizes the use of space so that the required equipment can be concentrated in the special elements. This allows for the standard elements to have an overall reduction in size. This means that the Fehmarnbelt tunnel will be cheaper and easier to maintain and will require significantly less concrete since the standard elements can be made smaller. The elements are also much shorter than the standard elements, with 39m compared to 217m [1], illustrated in Figure 7.1.

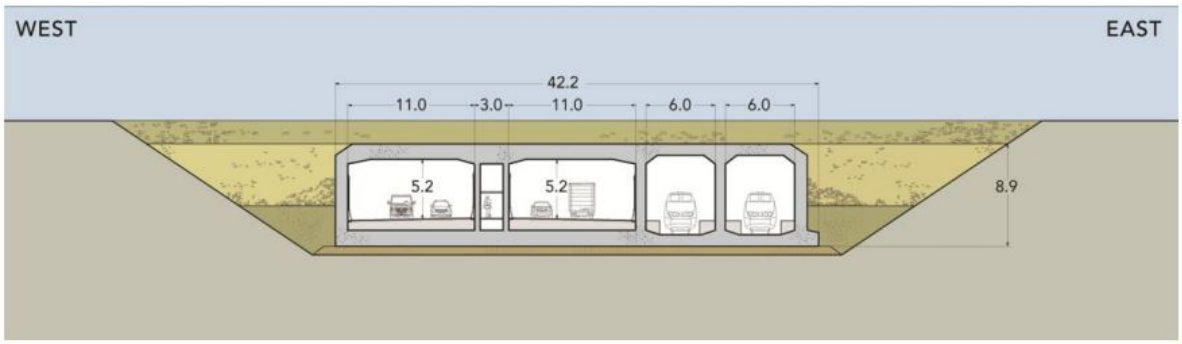

Figure 7.2: Standard element cross-section of Fehmarnbelt tunnel [m][11]

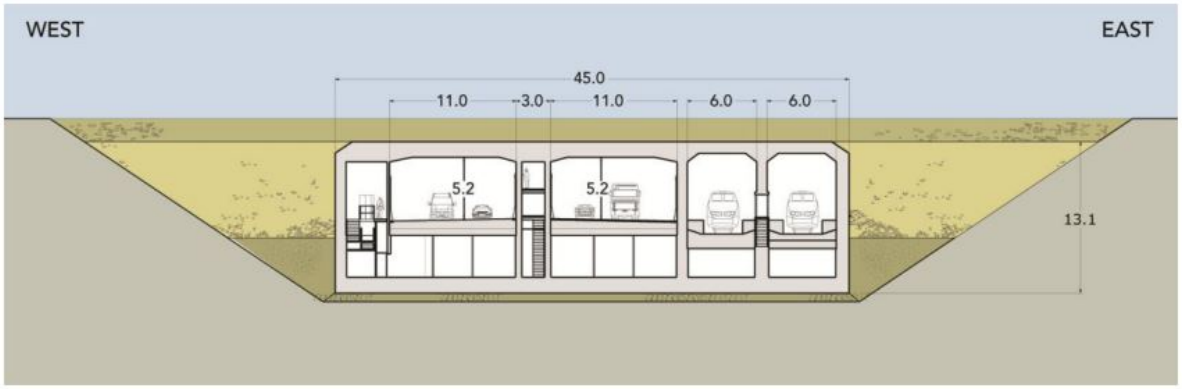

Figure 7.3: Special element cross-section of Fehmarnbelt tunnel [m] [11]

Observing the special element cross-section in Figure 7.3, the west side of the tunnel shows a wall separating the access point to the lower level from the first traffic envelope. A more accurate structural representation is shown in Figure 7.4 where it is clear that the wall is non-structural, therefore the total span of the first traffic envelope is in fact, a little over 16m. Figure 7.4 has revision clouds around the bottom slab, these indicate that there was a change made to the drawing at the time, however it is not mentioned in the Design Report [12] and has no influence on this study.

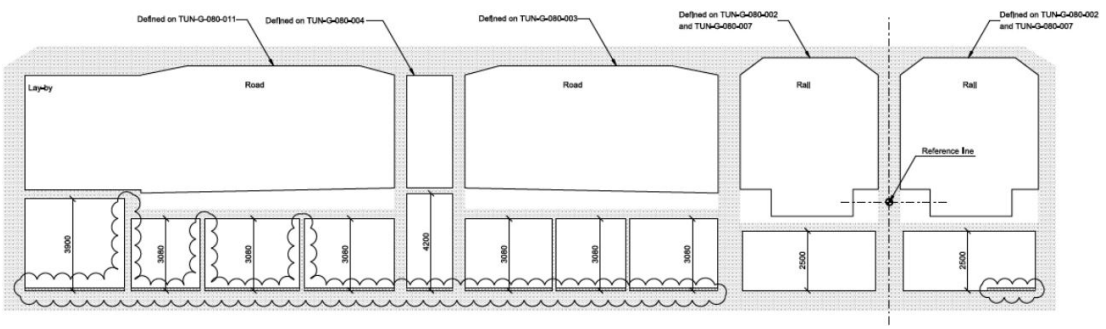

Figure 7.4: Special element detailed cross-section [mm] [12]

The tunnel has recently begun construction on the dry dock, which in itself has an innovative design, as it has to accommodate the production of both elements and the allowable draught [27].

7.2. Case Study

The initial step in this case study aims to use the tools from Chapter 6 and optimize the top slab of the Fehmarnbelt immersed tunnel by implementing post-tensioning forces. The following step will look at the means of mitigating cracking in the dry dock, which was determined to be a critical stage when adding post-tensioning. Due to the implementation of the special elements, an opportunity to analyze an alternate method to control the extreme camber in the dry dock stage is possible. The first method, previously discussed in this thesis, is to add more reinforcement at the top part of the beam at midspan, where the cracking is prone to initiate. The second method, explored further in this section, is the use of temporary tendons, to connect the top and middle span, as seen in Figure 7.16.

In the standard element, the option of implementing temporary tendons is not favourable due to the constructability issues that arise since the ballast tanks will be located where the connection is required to the base. This implies separating the tank in two, and adding a connection for the tendon between them, which adds complications. When looking at the special elements, the two storey design allows for the ballast tanks to be placed at the bottom level, freeing up space above the middle span for an easier connection. Even though this is still an additional cost to implement temporary solutions for the elements, the additional reinforcement that would permanently stay in the structure is no longer required.

Given the fact that the Fehmarnbelt link is a working design, the reinforced concrete option is has sufficient capacity. This case study will not compare the use of post tensioning and reinforced concrete, but rather use the unique design to explore optimizing it and dry dock crack mitigation design alternatives. In Chapter 6 the solution of adding additional reinforcement was used to mitigate cracking. In this case study, this additional reinforcement will be compared with the temporary tendons that connect top and middle span.

First the top slab will be optimized in terms of height by adding post-tensioning and a numerical model for the dry dock stage will be performed. From this base model, two subsequent numerical models will allow the comparison of both crack mitigation methods; adding additional top reinforcement and adding temporary tendons. The goal is to observe the response of the structure and to identify the efficiency of both methods. This will be done by identifying analytically the amount of reinforcement and temporary tendons that would be required to control the cracking caused by the camber. These values will be implemented into the numerical model and the responses of the structure will be observed and compared to the original model.

Initial Model

To simplify the cross-section, Figure 7.5 illustrates with the red square, the section that will be used, and making it symmetrical as seen in Figure 7.6. The inner span will be 16.025m as set out in the final design of the actual structure and the original top slab height is of 1.33m. The railway envelopes were also eliminated

for simplicity.

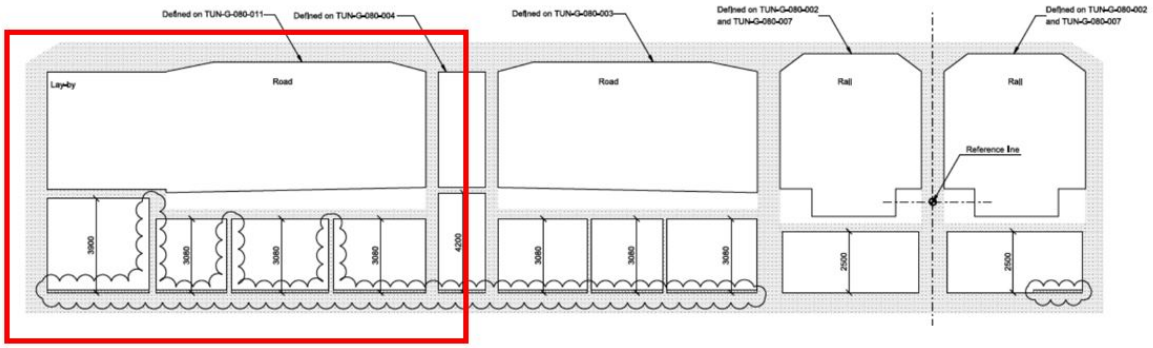

Figure 7.5: Case study cross-section focus

Bottom prestressing was not incorporated in this case study, as the focus was the observation of the camber in the top beam. The issue of excessive camber is not of great concern on the bottom, due to the thicker element of the base slab, less prestressing force required, and the fact that the element will be supported by the dry dock floor. As seen in Section 5.7 bottom prestressing improved the overall capacity of the bottom slab and it can also be used when there is a need to make the element more slender or reinforce the section more.

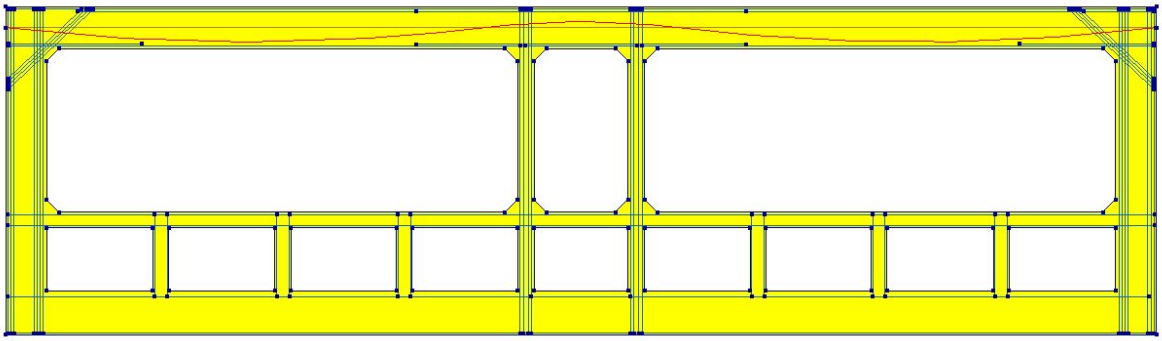

Figure 7.6: Special element cross-section DIANA model

In modifying the cross-section as seen in Figure 7.6, the total width is 38.4m compared to the actual design, which is 46.15m. The main point of concern in the actual design would be the tendon design and consequential additional losses. Since the rail track envelopes are only 6m, the post tensioning force is would not bring much added capacity at those locations. In order to minimize the post tensioning losses in that section, the curvature would have to be kept to a minimum. Nevertheless, careful attention would have to be paid to that additional loss, which is not considered in this case study.

In the Montreal Louis Hippolyte tunnel mentioned in Chapter 2, there was both top and bottom prestressing, and the temporary tendons installed were providing support to both slabs [23]. The middle slab in the special element will be where the connection of the temporary tendon would be located as seen in Figure 7.16. The consequence of this being that the slab must be able to bare the force of the tendon. Close attention to has to be paid to this detail since the slab is considerably less thick.

Determining slenderness

Following the same procedure of Chapter 6 an investigation is done into the possibility of making the top slab more slender by implementing post-tensioning forces. The primary differences from the model in Chapter 6

and the Fehmarnbelt is the geometry of the section itself, and the depth at which the element is immersed. The first step is to find the most slender option possible and then find an alternative that will be viable in terms of construction. Therefore, initially a 100% curvature and prestressing is used, as seen in Figure 7.7b. 100% curvature refers to the use of the maximum eccentricity at midspan, and 100% prestressing refers to the total amount of prestressing force calculated for the section as described in section 4.3.1. The option with the lowest height, of 1.2m, corresponds to the maximum amount of reinforcement in the midspan area, which as mentioned in Chapter 6 means that the loop reached its maximum without achieving the acceptable crack width limit. Heights, 1.2m, 1.25m and 1.3m were passed by the prestressing percentages of 70-100%. Below that, the tests failed at crack width ranging from 100% to 60% as seen for height 1.3m. Decreasing the curvature to 80% in Figure 7.7a has an overall decrease in additional reinforcement required. However, the lowest height available in this analysis is of 1.25m. Moving forward, a height of 1.25 will be used as it successfully reached the crack width limit with 60% prestressing, a slight reduction from the original 1.33m.

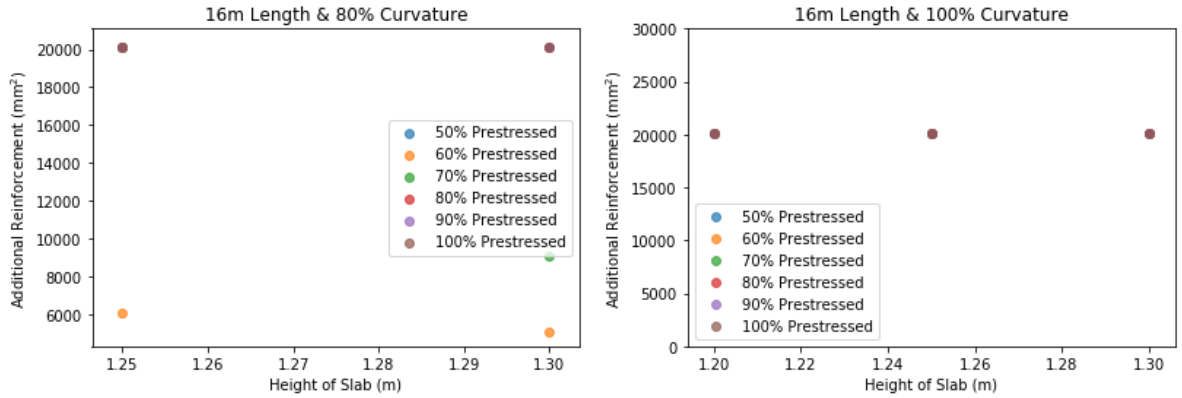

(a) 80% Curvature

(b) 100% Curvature

Figure 7.7: Optimized heights for Fehmarnbelt top slab

Running the model, with the corresponding length and height of 16.025m and 1.25m respectively, the varying prestressing percentages and curvatures were found and are illustrated in Figure 7.8. From the plot, the optimal scenario as seen in the previous chapter is that with the least additional reinforcement, considering the largest possible curvature. This will yield the smallest prestressing force required, whilst keeping the additional reinforcement area low.

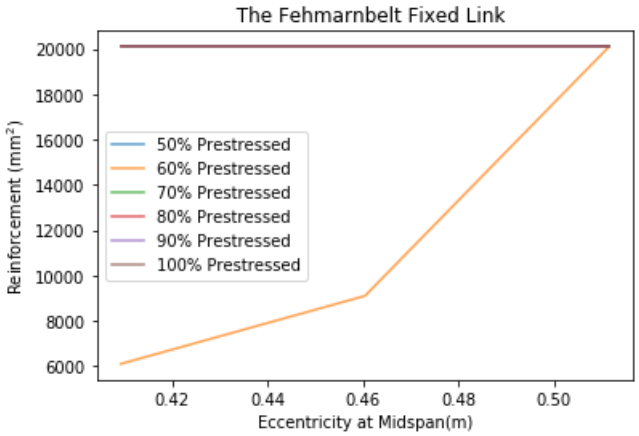

Figure 7.8: Fehmarnbelt prestressing force and curvature options

The value of 60% prestressing was chosen, with an eccentricity at midspan of 0.4m, which corresponds to an 80% of the maximum allowable eccentricity. The amount of additional reinforcement corresponding to

this combinations is 6,100mm^2. From the same method used in Chapter 6, the total amount of required prestressing force is 20,111kN, and applying 60% leads to 12,066kN. When looking at the option with 90% curvature was 11,324 kN- the additional prestressing force results in a 531mm^2 increase in area which equates to 4 strands. For the additional reinforcement the difference in from 9,100mm^2 to 6,100mm^2, which is 3,000mm^2 increase. Although steel is significantly cheaper, the economic benefit was not carried out, and therefore the 80% was chosen based on only adding 4 strands.

7.3. Numerical Models

As seen in Chapter 5 both linear and nonlinear analysis were performed to model the tunnel cross-section and to observe if a linear analysis validated the analytical results. To see the behaviour of the structure, the linear analysis presented the overall response accurately. In the dry dock stage, however, the nonlinear analysis showed an increase in accuracy due to the loading conditions being past the linear elastic stage of the structure behaviour. Redistribution of stresses were present, and to properly capture the real values, a nonlinear analysis was required. To model the effect of the additional reinforcement, a linear analysis is limiting. When adding reinforcement and observing the effects this has on the structure's response, the importance of modelling the material nonlinearities becomes crucial [29]. Most structures are designed using linear principles, however the insight into the overall structural behaviour and redistribution effects provides the nonlinear analysis with added benefits for this study.

Steel and concrete are assumed to deform together, when cracking occurs, steel then takes over the stresses and this relation is no longer in unison. This becomes critical, as additional reinforcement could mean a decrease in the concrete stress and subsequently less cracking.

Based on the findings in Chapter 5, which concluded that the dry dock stage was a critical stage to analyze when implementing post-tensioning forces. The focus in this chapter will be on the dry dock stage, and the response of the structure when implementing the post-tensioning forces with the reinforcement designed for the final immersed stage. Thus, nonlinear analyses will be performed on three separate models;

1. The original reinforcement calculated for the final stage
2. Additional reinforcement in critical top slab areas
3. Temporary tendons

7.3.1. Results Model 1: Original Design

The first model includes the reinforcement designed for the final immersed stage. The loading in the dry dock stage is composed of the self-weight of the structure and the post-tensioning forces designed for the immersed stage. In the initial trials, it was clear that additional reinforcement was required at the corners, shear reinforcement in the walls and longitudinal reinforcement on the inner side of the outer walls. This model and the following models, all contain this additional reinforcement to the corner and walls. The analysis was done by evaluating the initial state with the implementation of the post-tensioning forces, as seen in Chapter 5 for the dry dock stage.

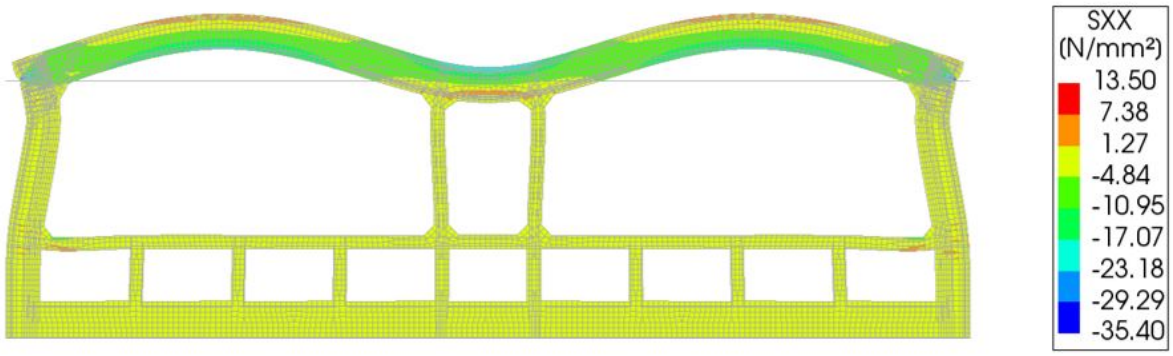

Figure 7.9: Stress distribution

The stress distribution for the first model is shown in Figure 7.9. The top of the midspan as well as the area right above the gallery, is seen to have tensile stresses. The high tensile stresses of 13.50 MPa visible on the legend, are concentrated at the entry point of the post-tensioning force, along with the high compressive stress due to the discrete effect of the force introduction of the tendon. These stresses are also related to the bursting stresses occurring at the anchorage zones of the post-tensioning forces, and are mitigated using reinforcement specific to this scenario, for example spiral reinforcement.

Focusing on the stresses at midspan, Figure 7.10 shows the distribution along the height of the slab, from 5.7, to 6.95m. It is important to note, that the model has its y-axis origin starting at the bottom of the middle slab and not at the bottom of the structure. The nonlinear behaviour is apparent at the top of the slab. Similarly to the nonlinear behaviour seen in the dry dock model in Chapter 5, the tensile distribution follows the Hordijk stress strain relation model. Each node has four values associated to it, from the four elements that it is connected to, except for the first and last points which only have two elements. The stress is obtained at the integration points and then extrapolated to the corresponding node. If there is a crack in one of the elements, there will be redistribution of stresses and the element containing the crack will have have a stress reduction, whilst the others have to compensate in terms of load carrying. Depending on the location of the crack, the elements will redistribute the stresses differently and consequently the node will have disparate values. From Figure 7.10 at approximately 6.8m, the 4 values at that node are visibly different, and there are two that have smaller values, which leads to believe that a larger crack is present in those two elements. The maximum stress reached is 0.97MPa in Figure 7.10 , which is below the 1.93MPa design limit for C50/60 concrete assumed, however since there is redistribution of stresses visible, this entails that the tensile stress has been reached and the onset of cracking has therefore caused a redistribution of stresses.

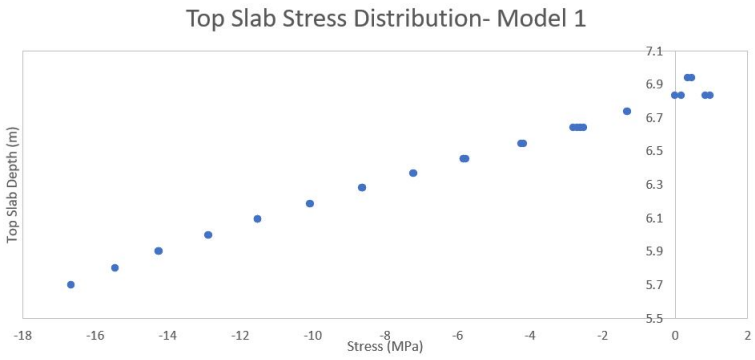

Figure 7.10: Stress distribution down width of midspan

The cracking model used is the same as described in Chapter 5. Figure 7.11, shows the crack strain, where the entry of the post tensioning force generates the highest strains. The higher strain in the walls cannot be observed by looking at the stress distribution in the x-direction in Figure 7.9. Due to the rigid connection,

high forces are expected on the inner side of the outer walls, which is visible by looking at the crack strains. In this particular design due to the presence of the midpsan slab, the walls are stiffer, which leads to less flexible corner.

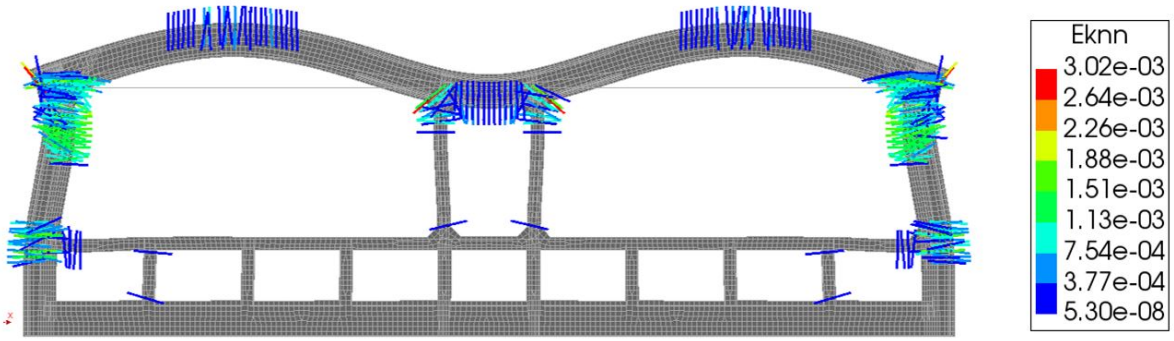

Figure 7.11: Crack strain for Model 1- no additional reinforcement

Based on the model seen, the tensile stresses close to the allowable limits and a redistribution of stresses due to the onset cracking is visible. Two methods are mentioned to mitigate the cracking will be implemented in the models in the following section.

7.3.2. Results Model 2: Additional Top Reinforcement

The first method to improve the structures capacity is to implement 6,100mm^2 of reinforcement at the locations marked in Figure 7.12, which is given by 10x 28∅ bars.

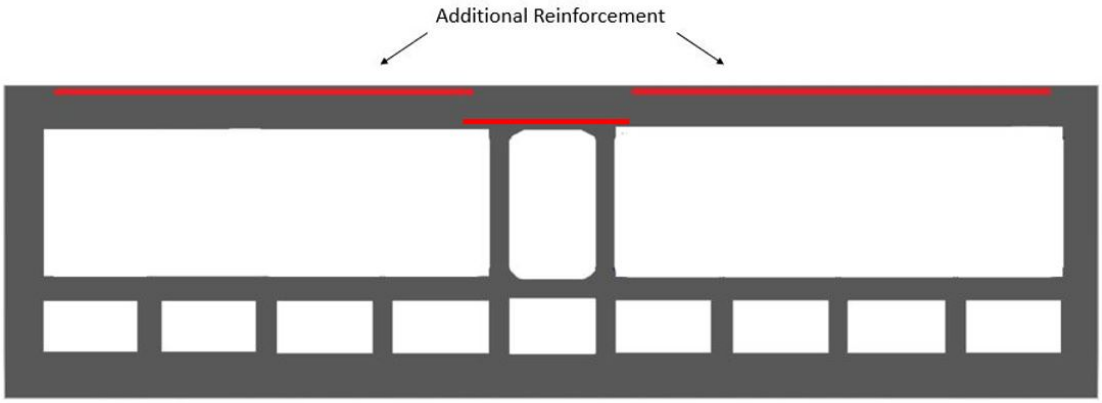

Figure 7.12: Location of additional reinforcement placement for the Fehmarnbelt tunnel

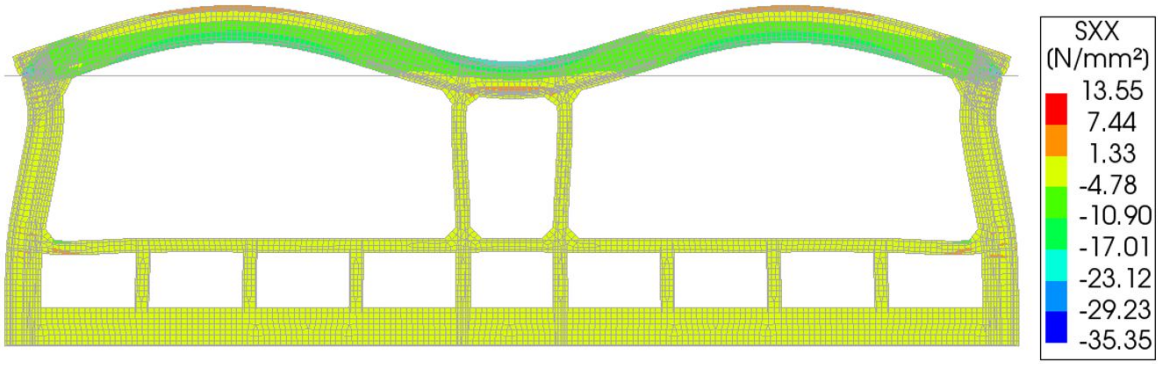

Figure 7.13: Stress distribution of the Fehmarnbelt tunnel with additional reinforcement

A more homogeneous distribution is seen at the top of midspan in Figure 7.13 compared to Model 1, and when looking at the stress distribution in Figure 7.14, it follows a more linear pattern. The stress above 6.8m is still in a tensile region, but has not yet undergone visible redistribution of stresses.

The slab has higher capacity and resistance due to the increase in steel, which is seen when observing the compressive stress at the bottom if the slab of -15.2MPa seen in 7.14, there is a 10% decrease when comparing it to Model 1. A weaker slab will reach its compressive strength limit at a smaller load than with a slab with higher capacity. The higher compressive stress signifies a weaker slab, that is further along in reaching its compressive strength capacity for the same load. The stress at 6.95m seen in 7.14 is 1.03MPa, 6% higher than the tensile stresses in Model 1, however, the lack of visible redistribution of stresses signifies it has not yet reached the tensile limit.

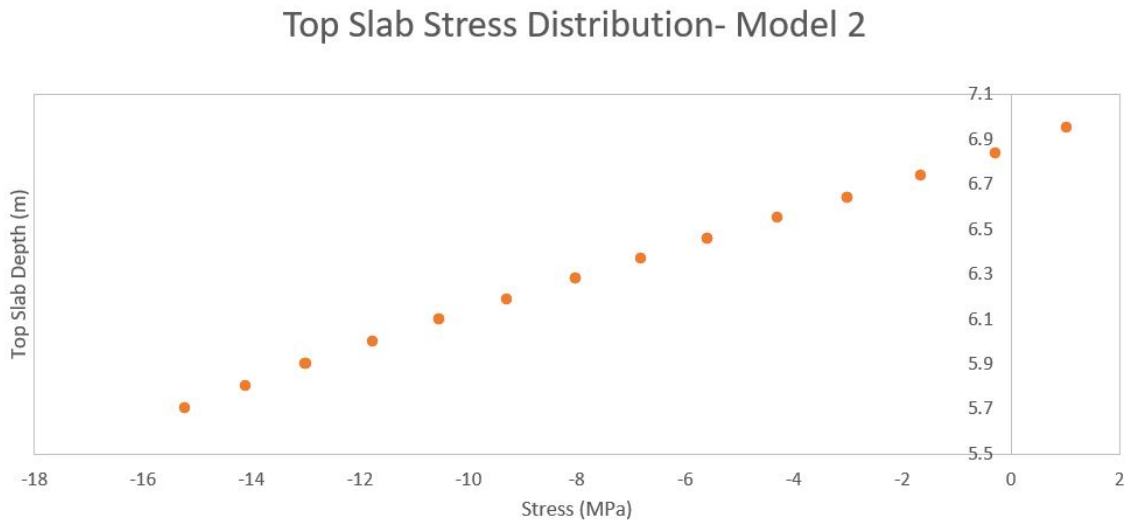

Figure 7.14: Stress distribution down height of top slab with additional reinforcement

Figure 7.15 shows the crack strains of this model. A small improvement on the top of the midspan crack strains are visible, with only the minor dark blue strains corresponding to 9.26E-08, compared to the strains in Figure 7.11 which applies to Model 1, that reach a value of 3.77E-04. The higher strains in the corner are still present and governing at this stage.

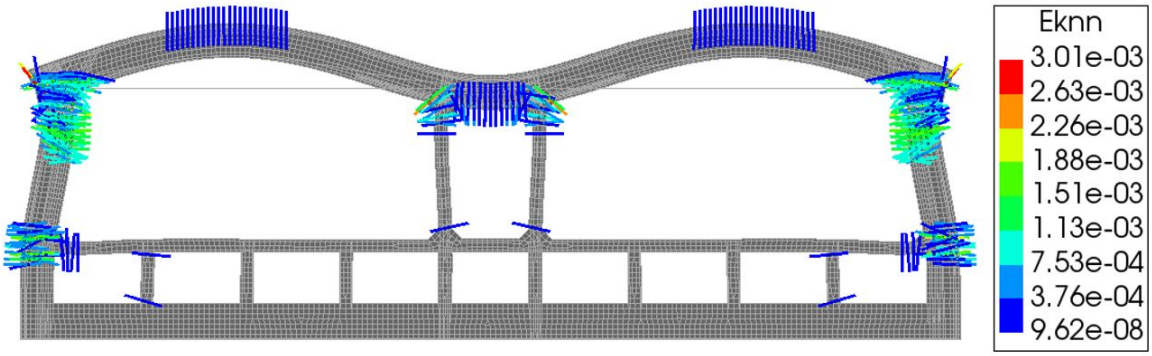

Figure 7.15: Crack strain of Model 2 - with additional Reinforcement

From the numerical model, the effect of applying additional reinforcement is clearly seen from the decrease in crack strain and lack of stress redistribution at midspan. Sufficient reinforcement in the rest of the structure must also be ensured when designing the tunnel elements. Due to the deflections caused by the prestressing forces, ductility of the structure also plays an important role, and too much reinforcement might cause a brittle failure of the structure, which is to be avoided. The crack strains are still highest at the walls since the additional reinforcement added affects the top slab directly.

7.3.3. Results Model 3: Temporary tendons

The second method to increase capacity of the structure, which was used in the Montreal Louis Hippolyte tunnel, is the implementation of temporary tendons [23]. These are connected at opposite ends inside the inner tunnel, from the top slab to the middle as illustrated in Figure 7.16. They are referred to as temporary since as the external forces of the tunnel begin to be present, the tendons can be relaxed to accommodate them and avoid overloading the segments. When the tunnel is then completely submerged, these tendons are removed, and the final stage is designed with no excess inner reinforcement. To model this situation with finite element analysis, a spring was used to connect the top and middle slab.

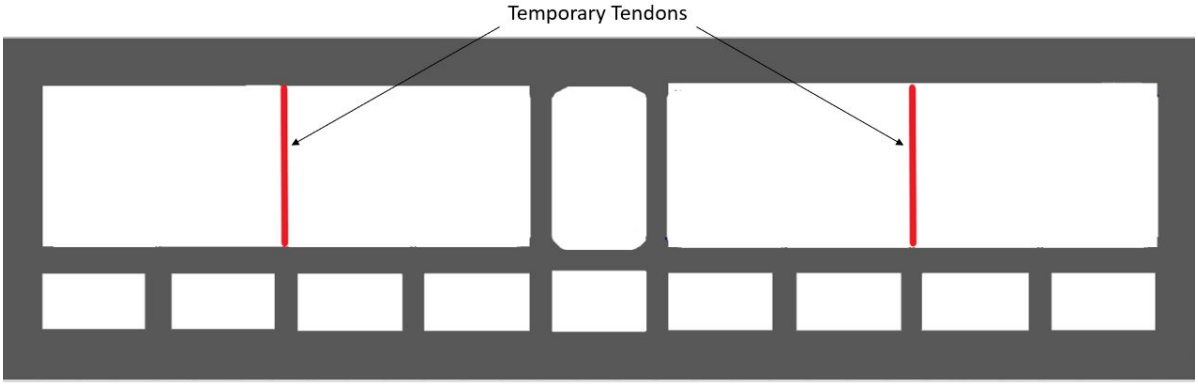

Figure 7.16: Temporary tendon placement layout

The analytical force required was calculated based on the additional moment needed to lower the concrete stress at the top of the beam. This value was back calculated from an acceptable crack width taken as 0.15mm, the limit taken from Eurocode. The steel stress, concrete strain and ultimately concrete stress were calculated based on the calculations below. Identifying the maximum steel stress that is required to have a crack width of 0.15mm. This is done by forming a loop where the steel stress is reduced until the condition is met. By reducing the steel stress, the ϵ_{sm} is recalculated and then the crack width is subsequently:

$$w_k = S_r \cdot \epsilon_{sm} \tag{7.1}$$

With the steel stress known, the concrete strain is calculated assuming a linear relation. By following the equation below, the concrete stress at the top of the beam is found.

$$\sigma_s = \epsilon_c \cdot E_c \tag{7.2}$$

where σ_s is the steel stress
ϵ_c is the concrete strain
E_c is the concrete elastic modulus

The required moment accounting for this scenario is calculated using the formula below, used in Chapter 4 when finding the required prestressing force, where 1.0 MPa is the allowable concrete tensile stress.

$$\sigma_c = -\frac{P_{m\infty}}{A_c} - \frac{M_p}{W} + \frac{M_{req}}{W} \leq 1.0MPa \tag{7.3}$$

where M_{req} $Msw + Ft \cdot \frac{L}{2}$
$P_{m\infty}$ is the working prestress prestress

For the springs in the numerical model, Hooke's law is used assuming a spring extension of 5mm.

$$Ft = -k \cdot x \tag{7.4}$$

where k is defined as spring stiffness
x is the spring displacement

This value is approximately half of the upward deflection of the beam without using any additional reinforcement. This gave a stiffness of 206,200kN/m. When equating this value to EA/L, and considering a bar length of 5.2m, the area required would be 5,336mm^2. This corresponds to a diameter of 83mm.

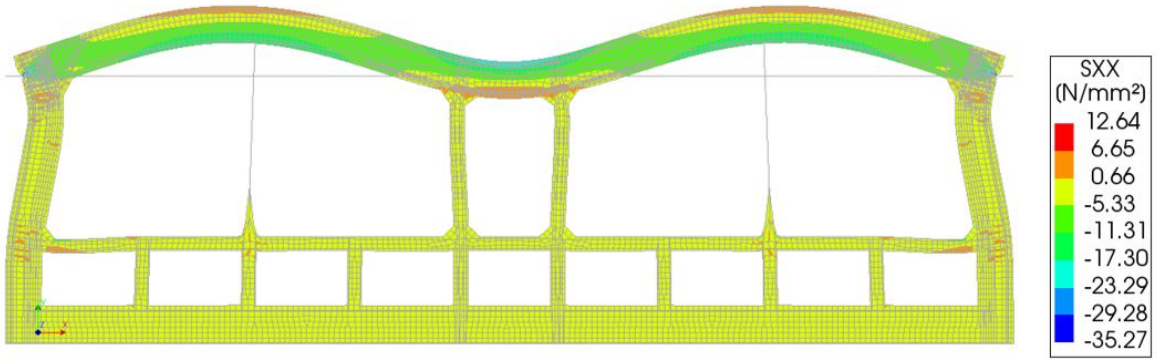

Figure 7.17: Stress distribution Model 3 - temporary tendons

There is a clear deformation at the middle slab seen in Figure 7.17 , where the spring is connected which is a singularity of the model. In order to avoid a singularity when modelling, a plate consisting of several nodes has to be chosen. The singularity is occurring at the lower side of the spring. A reason for this could be the that the top is connected to a region where the concrete has a higher compressive stress than at the middle slab. Since concrete is stronger in compression there is higher capacity to withstand it, and therefore the singularity appears at a point where it is in tension.

The distribution down the height of the slab for Model 3 is shown in Figure 7.18. Similar to the Model 1 without any additional reinforcement, there were nodes that had two different values, more prominent at

the top of the beam around 6.85m. However, no significant difference and redistribution of stresses is visible. The very initial stages of some nonlinearities are thus exhibited. The stress at 6.95m is of 1.15MPa, 10% higher than Model 2.

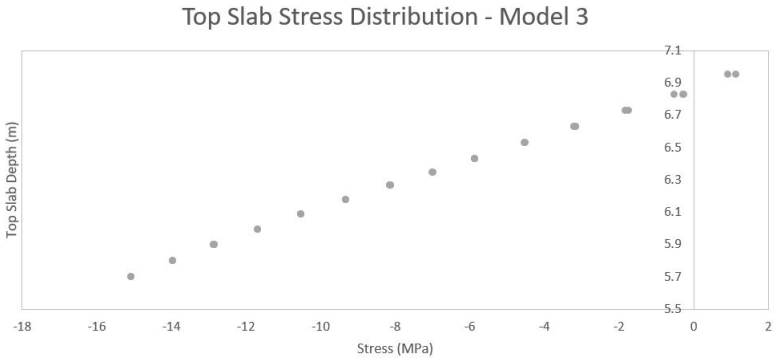

Figure 7.18: Stress distribution down the height of top slab with temporary tendons

In this particular case, as mentioned, the tendons can be implemented due to the two storey layout and the fact that the balanced tanks can be placed elsewhere. However, in the Montreal tunnel the connection was placed at the bottom slab. One of the points of concern using this procedure, is that the middle slab, to which the tendon is connected to, will have insufficient capacity. This would manifest in the deformation of the middle slab, however, from the stress distribution in Figure 7.17, the middle slab seems to undergo no large deformations. From the crack strains in Figure 7.19, similar locations to the Models 1 and 2 are subject to higher crack strains, with the addition of the bottom spring connection. The singularity also generates the highest crack strain, which exceeds the other two models by a factor of 10.

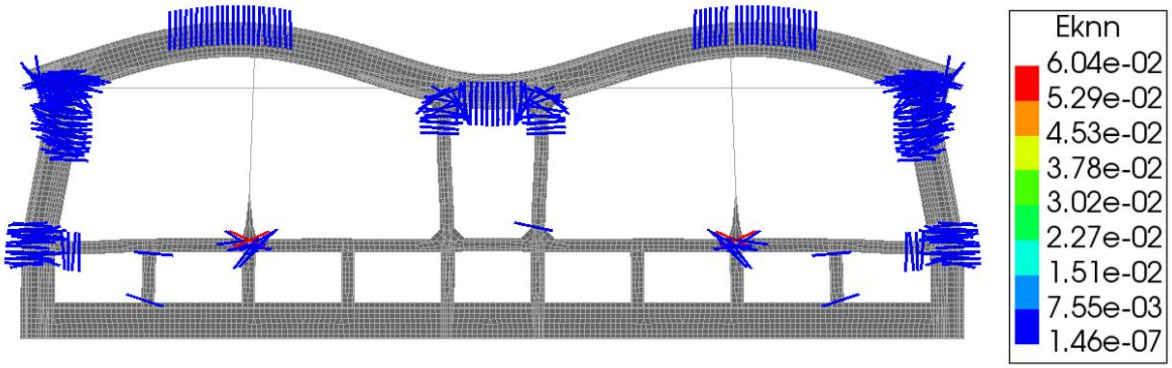

Figure 7.19: Crack strain for Model 3 - temporary tendons

7.3.4. Evaluation of global capacities

Following the same procedure as Chapter 5, the loading of the prestressing was increased until failure, which was done in separate individual analyses. Since the prestressing was added as an initial state rather than a load in the analysis, when increasing the prestressing load, this required a new analysis for each incremented load. Starting at 60% of the original load, increments of 40% were carried out, with additional loads closer to failure.

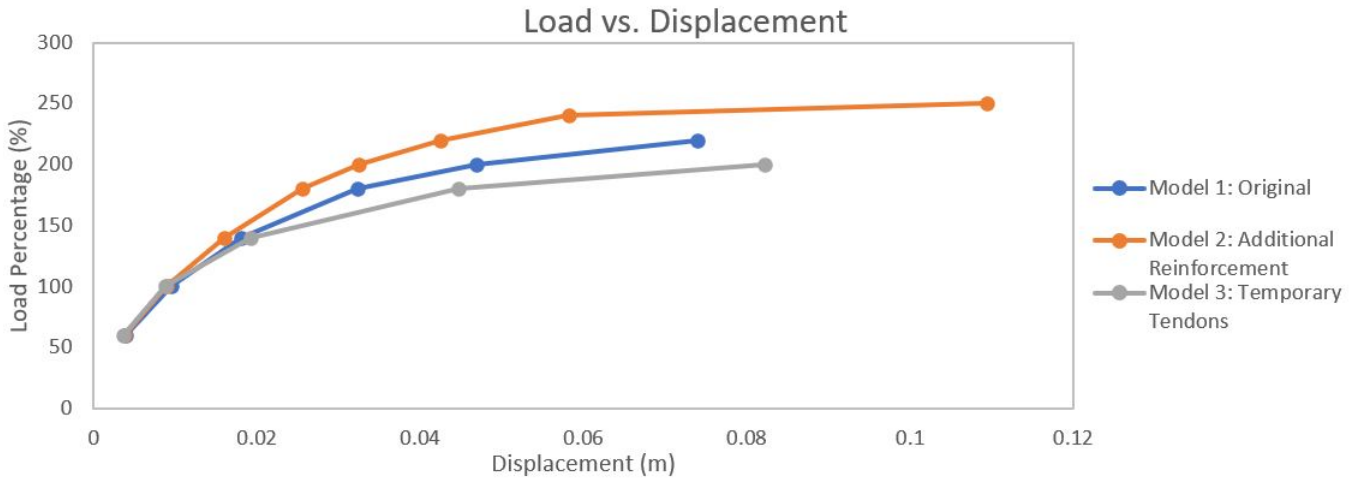

Figure 7.20: Load Percentage vs Displacement for all three models

A load-displacement graph for the three nonlinear models is seen in Figure 7.20. The global displacement at midspan was taken, considering that the relative displacement between corners and midspan, were not too different for the varying models. The graph shows at what load percentage each model could reach before failure occurred. Model 2, which has the additional top reinforcement, exceeded the other two with the failure happening at 250%.

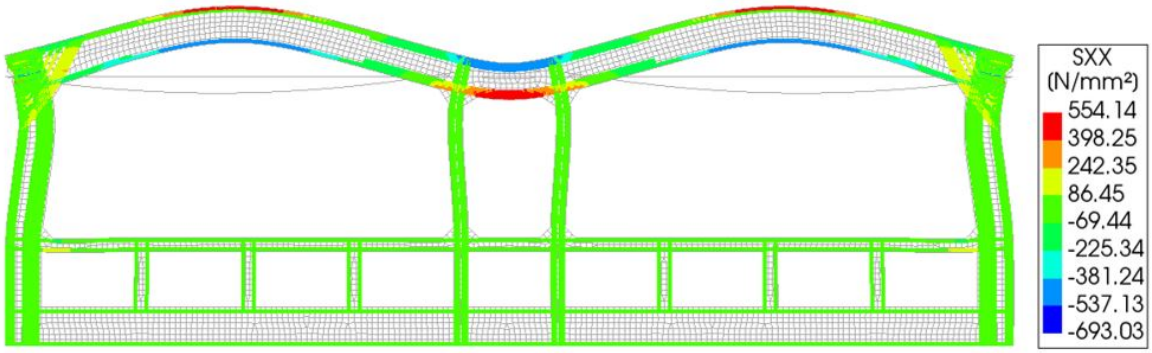

Figure 7.21: Yielding of steel - Model 1

The failure of Model 1 was at the weak spots of the midspan shown by the yielding of the steel in Figure 7.21, where the steel has a a yield strength of 435MPa. In contrast, Figure 7.22 shows the step before the failure of Model 2, which occurred closer to the walls due to the high stresses near the anchor, which are where the high stresses are concentrated. The fact that the failure is now not at the midpsan, is a clear benefit to the implementation of additional reinforcement.

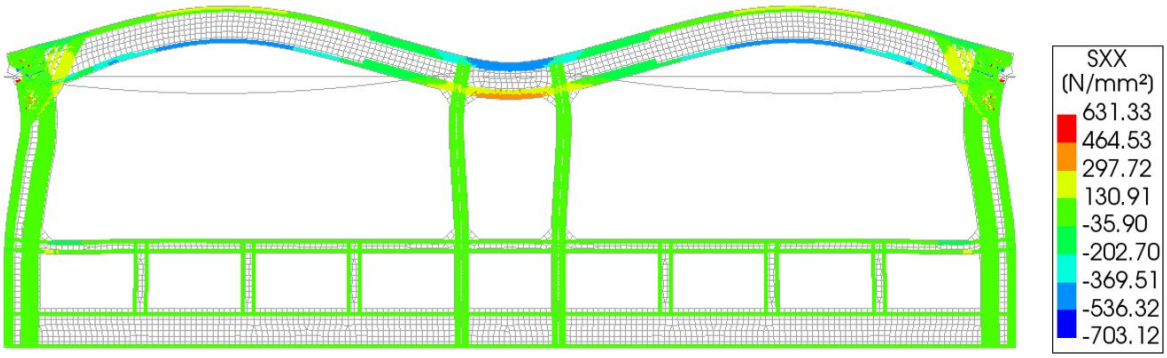

Figure 7.22: Yielding of steel - Model 2

Model 3, using the springs, has less capacity, which is seen by looking the lower load percentages that the structure requires for the same deflections as the other two models, and the fact it failed earliest at a loading of 200 %. The failure occurred at the connection with the spring on the top slab, where the singularity is present in Figure 7.23. Based on this there cannot be a clear conclusion since the presence of the singularity and the subsequent failure at that location are causing a premature failure. From the yielding of the steel, however, it is clear that some additional reinforcement is nevertheless required when using the solution of temporary tendons. This is seen from the steel yielding at the top of the midspan.

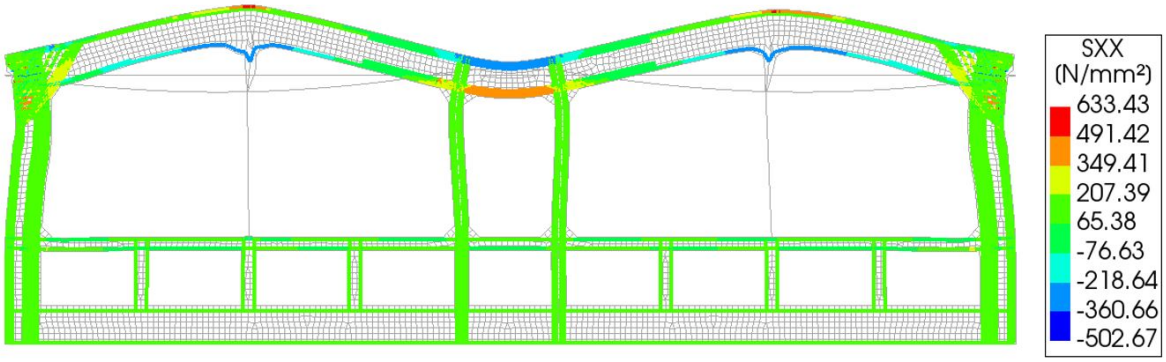

Figure 7.23: Yielding of steel - Model 3

7.4. Conclusion

The special elements of the Fehmarnbelt tunnel, which are a two storey concrete element, were used as the base of this case study. The option to post-tension provided an opportunity to optimize the section by making it more slender. The second part of this case study consisted in analyzing two methods for mitigating the cracks at the dry dock stage: adding reinforcement at the top of the beam at midspan and the use of temporary tendons. The optimization of the top slab reduced the height from the original design of 1.33m to 1.25m, taking into account a feasible structural design for the dry dock stage, where the post-tensioning curvature and percentage were reduced to 80% and 60% respectively.

Due to the findings in Chapter 5, where the dry dock was the critical stage when implementing post-tensioning, three different models were analysed, all in the dry dock section using nonlinear numerical models. The first with the original design, the second adding additional reinforcement and third using temporary tendons.

Model 1 was done with the reinforcement determined for the final immersed stage. The analysis showed that there was a redistribution of stress at the top of the beam. This suggest that there is an on set of cracking in that section. The two methods were investigated to help increase the capacity of the section, predominantly

in the top midspan where the post-tensioning caused an onset of cracking. Model 2 revealed an improvement in the particular section at midspan, where there was now a linear distribution present and a lower compressive strength. The capacity of the midspan is increased by the addition of the reinforcement. Model 3 was run using springs to represent the stiffness of the temporary tendons, which connect the top slab to the middle slab. There was an increase again in the capacity of the midspan for these loading conditions, with similar linear distribution to Model 2.

When observing the structural capacity of the whole cross-section, a load-displacement diagram revealed a greater capacity in Model 2. Implementing additional reinforcement in the critical areas, Model 2 showed an increase in overall capacity marked by the failure at the corners, instead of midpsan of top slab. It also reached a higher failure load of 260%, approximately 50% higher load than Model 3. Due to the singularity at the springs and consequential failure in that location, Model 3 with the temporary tendons was inconclusive in terms of overall structural capacity.

Overall, the efficiency of implementing additional reinforcement is clearly seen through this study, in the increase in capacity of the midspan and in the overall section. Due to the singularity present in the model concerning the temporary tendons, a conclusion of the overall capacity of the section could not be made. Given the additional constructability issues with adding temporary tendons, and the less favourable outcome in terms of capacity, adding reinforcement at the top of midspan is the easiest and most efficient option when it comes to mitigating cracks that form from the post-tensioning camber at the dry dock stage.

8

Conclusions

What parameters limit the design widths of reinforced concrete immersed tunnels?

The primary limitations governing the reinforced concrete design width are the buoyancy of the elements and the normal stress of the top slab. A simple parametric design showed that increasing the span width led to high normal stress and required increased slab height. In terms of the external parameters, the tunnel's water depth and inner height played a role helped in defining the available dimensions and additional constraints on the minimum height or slenderness required.

What are the governing stages of the element when considering the effects of post-tensioning on the cross section?

The post-tensioning force is designed for the final stage of the element when it is fully immersed. In addition to the reinforcement in the section, the chosen amount of prestressing force must pass the structural criteria that ensure the capacity of the section. These are the moment, shear and normal capacities, in addition to the crack width verification. Once the slab has been designed with the corresponding prestressing force, the critical stage is at the dry dock after the elements undergo the jacking of the strands. At this stage, the hydrostatic and backfilling loads are not present. Only the self-weight is counteracting the upward distributed load generated by the draped tendons against the concrete. By applying the total amount of prestressing force required for the final stage, with the maximum curvature available, the crack widths at the top of the midspan slab exceeded the allowable limits due to the upwards camber generated by the prestressing loads.

Finite element modelling was used to observe the behaviour of the structure and validate the moment distribution and stresses of the top slab using a linear analysis. In addition, a nonlinear analysis was performed for both final immersed and dry dock stages. The loading was increased and a global insight into the structure's capacity and behaviour was observed. The final stage exhibited linear elastic behaviour, whereas the dry dock stage showed some nonlinearities. The nonlinear behaviour was predominantly visible at the top of midspan, leading to the assumption that there had been an onset of cracking in this location.

From these analyses, both final immersed and dry dock stages are found to be imperative for the design of post-tensioning forces. The design must adhere to the capacity of the structure at the final immersed stage, while minimizing the camber to avoid cracks that exceed the limit during the dry dock stage. Thus, both final immersed and dry dock stage are critical in the design of post-tensioning.

What are the governing sections influenced by the implementation of post-tensioned loading?

The self-weight, hydrostatic and backfilling loads generate the highest moments at the connection between the inner walls and top slab. When looking at the prestressing loads, higher moments were exerted at the outside corners and at the midspan. At the final stages, the areas of concern are the corners, whereas at the dry dock, the midspan experiences the initial failures when no additional reinforcement is implemented due to the cracking caused by the upward prestressing camber. When calculating the analytical moment distribution, the frame's rigidity plays a vital role in determining the value of the moments in the corners. The

analytical assumptions overestimated these values and therefore adjustments were made to the subsequent analytical calculations.

What methods can be used to increase the capacity in the governing sections?

Two methods of mitigating the cracking at the midspan during the dry dock stage were covered in this study: the implementation of additional reinforcement and installing temporary tendons from top to bottom slab. Based on the case study performed, implementing additional reinforcement at midspan has a clear benefit to the overall structural capacity at the dry dock stage and locally at the midspan based on the reduction of nonlinear behaviour in the section which had cracked. Similarly, using temporary tendons improved the midspan section in the same manner by reducing the onset of cracking. However, the overall structural capacity of the section was inconclusive due to a singularity caused in the connection from the springs.

Optimize the degree of curved tendons in relation to the additional reinforcement required and prestressing losses. What is the optimal balance between amount of prestressing and curvature to minimize the impact at the dry dock stage?

For the specific external conditions - mainly the tunnel's depth and inner height - the use of post-tensioning force can be optimized to reduce cracking at midspan. The curvature and percentage of prestressing were the two main criteria modified, since they both have a substantial effect on the subsequent camber due to prestressing.

By diminishing the curvature, the amount of required prestressing to obtain the same stress level in the section increased. A larger prestressing force is not economic; the ideal situation would be to use the highest curvature and least prestressing force. However, in terms of structural capacity lowering the curvature reduces the cracking at the midspan since the distributed prestressing load is directly related to the curvature. Therefore, based on minimizing both the prestressing force and the additional reinforcement required, the optimal scenario found is a curvature around 80-100%, along with a more significant reduction in prestressing force closer to 60%. The case study of Fehmarnbelt link added an extra level of complexity due to the increased depth of the tunnel. This increased the post-tension force required considerably, which created high normal stresses, limiting the options available for optimizing the section. Nevertheless, by reducing the curvature and prestressing amounts, a 0.08m reduction of the height was still possible.

Main Question: What is the overall feasibility of implementing transverse post tensioning in concrete immersed tunnels?

The overall intention of adding post-tensioning to an immersed tunnel is to increase the structure's capacity. This comes into play when an increase in width is required, a reduction of slab height, or presence of high depth. It aids the final stage in mitigating the loads and not requiring as much reinforcement. In the scope of this research, the implementation of a post-tensioning force was observed to have a positive effect on the capacity of the structure at the final stage. Modifying the curvature of the tendons and the amount of prestressing, ensures the structure at the dry dock does not exceed cracking limits due to the upwards camber. Furthermore, the use of post-tensioning becomes a more feasible option. In doing so, the opportunity for more slender tunnels is available when considering the use of concrete, revealing the opportunity for larger capacity fixed links, as well as an economic benefit from having lower approaches.

9

Recommendations

The following recommendations are made regarding future research in transverse post tensioning based on observations and findings made throughout this research.

1. This research focused primarily on the cracking area at midspan due to the distributed post-tensioning load. From the model evaluated, the outside corners and gallery area, also require attention and more in depth evaluation into the effects the anchorage area is affected.
2. Investigate further the effect of eccentricity above the gallery, since it remained constant in this study.
3. Further optimize the shape of the tendon for different cross sections and additional losses for the tunnels that have railway traffic envelopes.
4. Determine a feasible crack width limit for the dry dock stage, taking into account the possibility of cracks closing when the remaining loads are applied.
5. Investigate and further optimize the amount of prestressing force compared to adding ore reinforcement from an economic standpoint.
6. Further analysis and modelling of the potential ground settlements and the effects on the bottom slab when implementing post-tensioning.
7. Improve the temporary tendon analysis singularity in order to evaluate global structure behaviour more accurately.
8. Investigate the maximum water depth that is feasible when implementing transverse post-tensioning in concrete immersed tunnels.

Bibliography

[1] JCWM De Wit and E Van Putten. Immersed tunnels: Competitive tunnel technique for long (sea) crossings. Under City 2012 Dubrovnik, 12, 2012.

[2] A. Claeys Em. Coene J. Blondeé. De j.f. kennedy-tunnel te antwerpen. 1969.

[3] Jon Excel. Total immersion: the world's longest immersed tunnel, 11 2015.

[4] Mtr shatin to central link hk, 2015.

[5] Yong-Il Kim. Busan-geoje fixed link immersed tunnel. DAEWOO EC.

[6] C.R. Braam J.C. Walraven. Prestressed Concrete. TU Delft, 2019.

[7] ASC Bruggeling. Partially prestressed concrete structures—a design challenge. PCI JOURNAL, 30(2):140–171, 1985.

[8] Bernard Lamarre. Highways built with prestressed concrete in montreal. JOURNAL PRESTRESSED CONCRETE INSTITUTE, 12(5):67, 1967.

[9] Gang Wei, Shi-jie Lu, Zhe Wang, and Xu Huang. A theoretical model for the circumferential strain of immersed tunnel elements under tidal load. Geotechnical and Geological Engineering, 36(3):1633–1645, 2018.

[10] DIANA. Diana-10.4 user's manual – diana documentation (v). 2020.

[11] Consolidated technical report fehmarn, 2011.

[12] Søren Christian Nielsen Jelmer Veldhuizen Amani Al Qadi. Design report of fe-model of special element 04, 2021.

[13] A. Doorduyn J. Bergsma. Immersed tunnel: A viable option for the orlovsky crossing. In ITA WTC 2015 Congress and 41st General Assembly, 2015.

[14] Armand van Wijck. Reflecting on europe's first immersed tunnel. Tunnel Talk, 2013.

[15] Jan Saveur and Walter Grantz. Structural design of immersed tunnels. Tunnelling and Underground Space Technology, 12(2):93–109, 1997.

[16] Zhang Zhigang, Lin Wei, Ji Hai, and Liu Xiaodong. Layout and design techniques of cross section for the large immersed tunnel. Procedia engineering, 166:37–44, 2016.

[17] Richard Lunniss and Jonathan Baber. Immersed tunnels. CRC Press, 2013.

[18] DM Rogowsky and P Marti. Detailing for post-tensioned. Bern: VSL International LTD, 1996.

[19] S Quanke, C Yue, Y Li, and H de Witt. Hongkong zhuhai macao bridge link in china stretching the limits of immersed tunnelling. Dostępny w Internecie.

[20] EN 1992-1-1 Eurocode 2: Design of concrete structures—. Part 1-1: General rules and rules for buildings,EN, 2004.

[21] LH Hoang and M Pasquignon. Essais de flexion sur des poutres en beton precontraintes par des cables exterieurs. Contrat SETRA CEBTP, 1, 1985.

[22] Johannes Van Greunen and Alexander C Scordelis. Nonlinear analysis of prestressed concrete slabs. Journal of Structural Engineering, 109(7):1742–1760, 1983.

[23] Graham Earle Per Hall, Armand Couture. Prestressed concrete in sub- aqueous tunnel construction. PCI Journal v10 n4 (19650801): 44-53, 1965.

[24] European Committee for Standardisation. NEN-EN 1990+A1+A1/C2, 12 2011.

[25] Osamah Ibrahim Mahmood. Camber control in simply supported prestressed concrete bridge girders. 2013.

[26] VSL. Vsl strand post tensioning system. Brochure, 2015.

[27] Susanne Kalmar Pedersen and Søren Brøndum. Fehmarnbelt fixed link: the world's longest road and rail immersed tunnel, 2018.

[28] The fehmarnbelt tunnel, another danish connection. World Highways, 2017.

[29] Hsuan-Teh Hu and William C Schnobrich. Nonlinear analysis of cracked reinforced concrete. Structural Journal, 87(2):199–207, 1990.

[30] Michael P Collins and Denis Mitchell. Prestressed concrete basics. Canadian Prestressed Concrete Institute, 1987.

[31] Maha Alqam and Fadi Alkhairi. Numerical and analytical behavior of beams prestressed with unbonded internal or external steel tendons: a state-of-the-art review. Arabian Journal for Science and Engineering, 44(10):8149–8170, 2019.

Appendices

A

Grouting of Tendons in DIANA

In the dry dock stage, the tendons are stresses once the concrete has achieved sufficient stress, using a hydraulic jack. Once the tendons have been stressed and secured, the grout is inserted into the ducts. The grouting of the tendons is not often done immediately. At this point the tendons are unbonded to the concrete. With DIANA, a material property is available to choose to have tendons bonded or unbonded to the mother element. This is implemented specifically for the post-tensioning tendons, as some structures have tendons that are designed to be unbonded. In this case, this property would be used to analyze the structure prior to grouting being inserted in the tendon at the dry dock stage.

When analyzing the differences using a linear analysis, how both material properties behave can be observed. Firstly, when looking at the moment distribution at the dry dock stage in Figures A.1 for bonded and A.2 unbonded, these values show varying values in the legend. Although a very similar distribution is seen between both figures, the unbonded tendons exhibit higher moments. Figure A.2. with unbonded tendons shows a maximum moment at the outer edges of -3,515.85kNm, whereas with bonded tendons in Figure A.1 the moment is -3,228.27kNm. Similarly, unbonded tendons have a higher moment at the midspan.

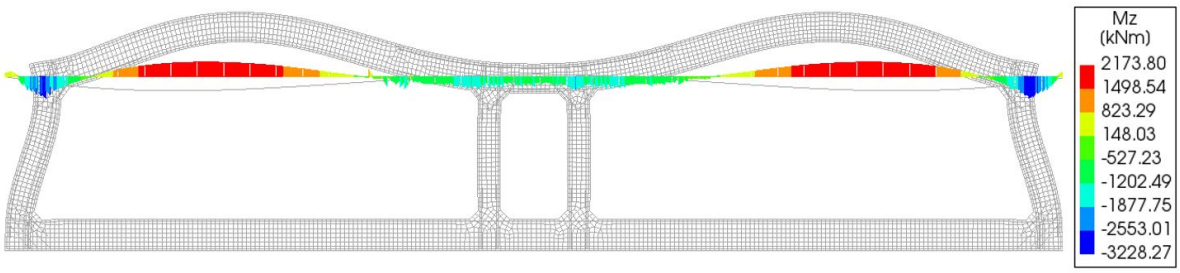

Figure A.1: Moment distribution linear analysis with bonded tendons

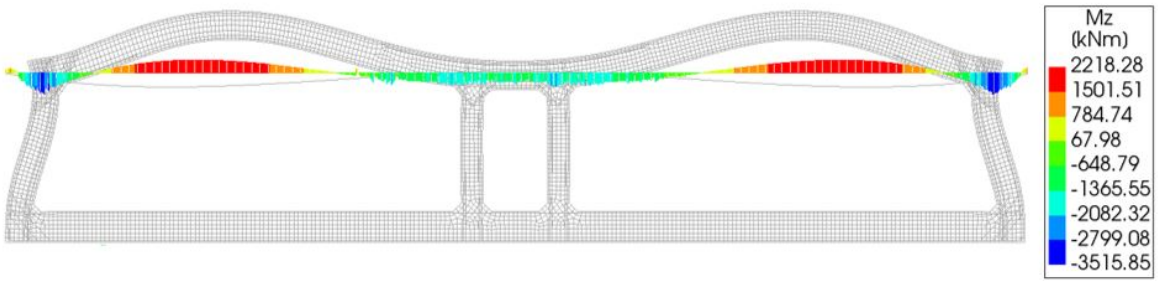

Figure A.2: Moment distribution linear analysis with unbonded tendons

Figure A.3 shows the stress distribution in the initial dry dock stages, with boned tendons. The maximum

stresses seen are overall lower than those of the unbonded tendons in Figure A.4, seen firstly by the wider range covered in the legend of 19.43MPa to -84.07. These of course are the stresses that are exhibited in the corners. This shows that the discrete effect for the unbonded tendons is larger and the forces in the numerical model are higher than with bonded tendons.

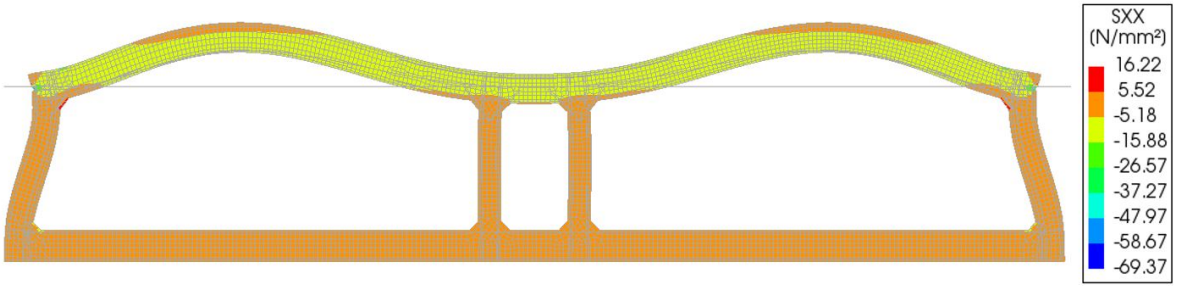

Figure A.3: Stress distribution linear analysis with bonded tendons

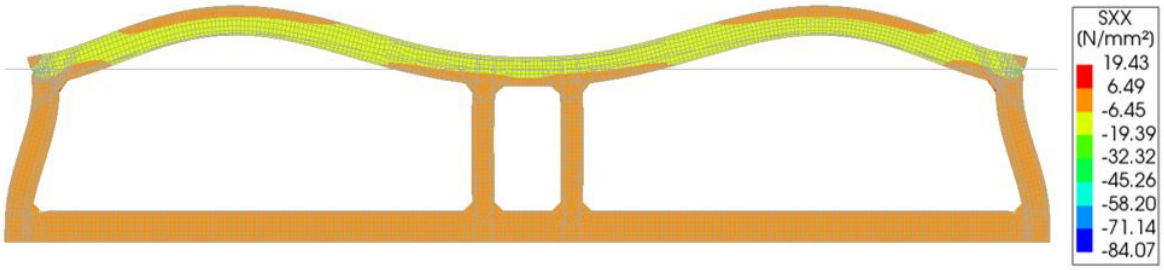

Figure A.4: Stress distribution linear analysis with unbonded tendons

When looking at the top slab behaviour in Figure A.5, the unbonded tendons have an overall larger stress distribution, both in the bottom and top of the slab. With bonded tendons, the assumption that there is a perfect bond between the tendons and concrete is made and the cross sectional analysis then incorporated the change in stress of the post tensioning forces[30]. This is because the concrete and the tendons can be assumed to have equal strain at the location. However, this is not the case with unbonded tendons where that assumption is not true. The change in stress of the unbonded tendon is distributed throughout the entirety of it, due to the lack of bond. This can be directly seen from the relative elongation of the tendon along the whole member, which is related to the deformation of the structure. Thus, a section analysis is much harder to be realized than that with bonded tendons[31]. The higher stresses seen in Figure A.5 from the unbonded tendon model, could be due to the fact that the strain calculated based on the elongation of the tendon is greater than the strain calculated for the bonded tendons, which is based on the concrete strain.

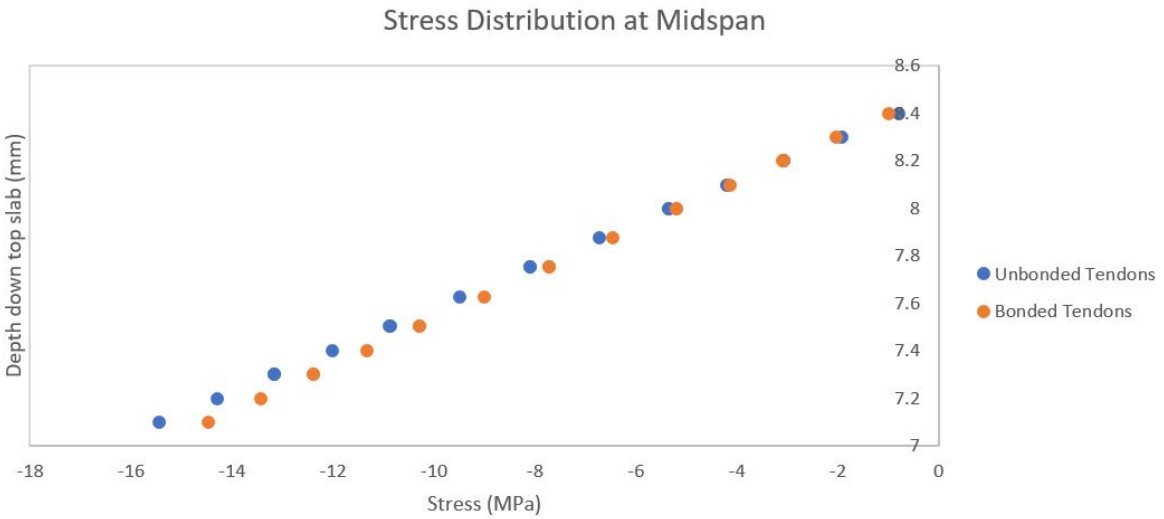

Figure A.5: Stress distribution for both bonded and unbonded tendons in linear analysis, at the midspan of top slab

When performing a nonlinear analysis, the unbonded selection showed a similar pattern when comparing it to bonded tendons. The moment distribution of unbonded tendons in Figure A.7 showed overall significantly larger moments and a clear redistribution further from the corner. This could be due to the fact that using DIANA, the unbonded tendons do not have any connection to the mother element. The stiffness of the steel and concrete are not dependant on each other, which is a concern when cracking of concrete is present. The prestressing steel stiffness is not taken into account at the nodes where it is present, which causes larger crack strain changes leading to a diverged result. As mentioned by Van Greunen [22] in the nonlinear study of ungrouted tendons, the stiffness of the tendons is not incorporated into the stiffness matrix of the structure, and the elongation of these tendons are only calculated at the anchor points. As mentioned in section 5.5, DIANA might also have inaccuracies related to the wedge set losses when using nonlinear analysis.

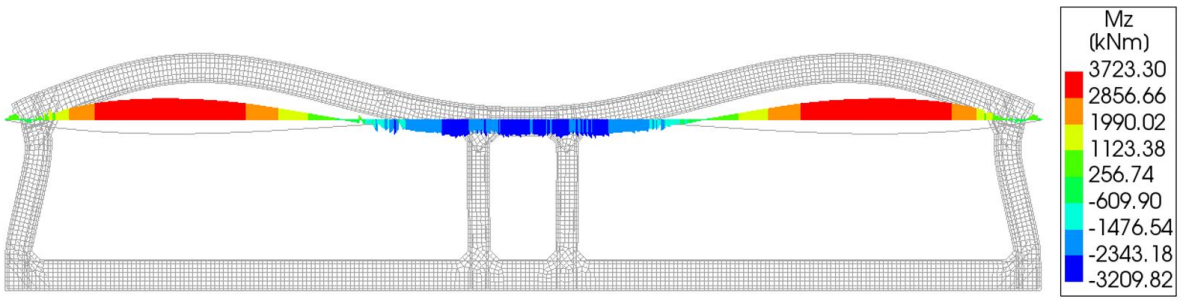

Figure A.6: Moment distribution at dry dock stage with bonded tendons

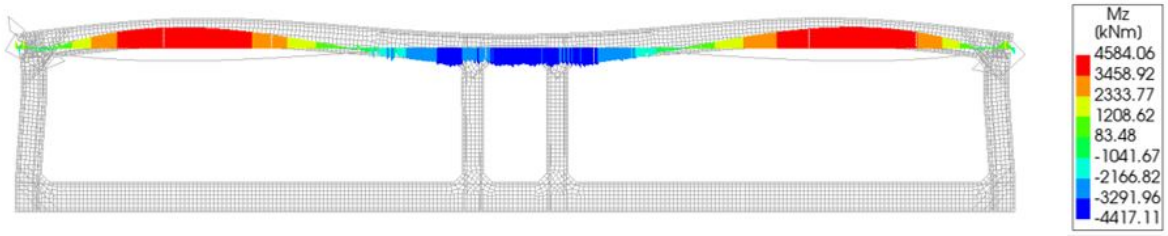

Figure A.7: Moment distribution at dry dock stage with unbonded tendons

The corner steel stress, close to where the post-tensioning force is implemented, has yielded as seen in Figure A.8, and has caused failure in parts of the steel.

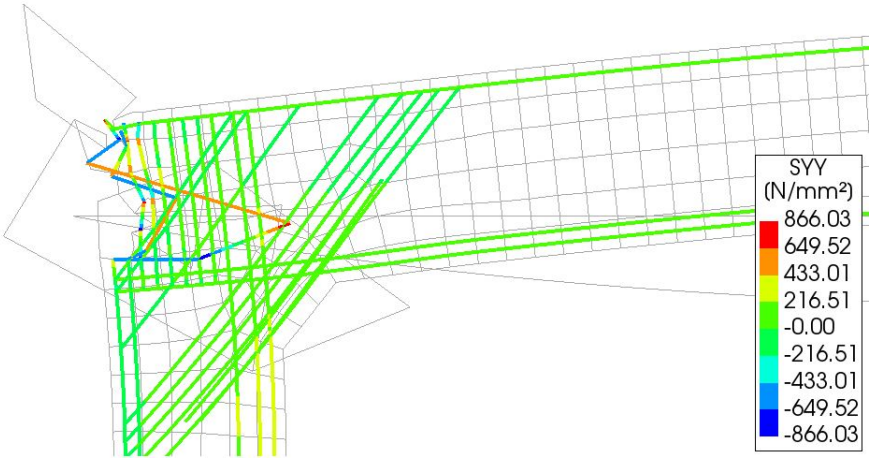

Figure A.8: Yielding steel corner unbonded tendons-nonlinear analysis

Due to the uncertainty in the accuracy of unbonded tendons, the numerical models in this study were done using bonded tendons.

B

Reinforcement Tables

The table below shows the moments in both ULS and SLS that correspond to the bottom floor of the model seen in Chapter 4. The loading used for these values is seen in Table 4.4.

Table B.1: Moments in SLS and ULS for floor slab at the final immersed stage with no prestressing

	Midspan		**Left Edge**		**Right Edge**	
	SLS	ULS	SLS	ULS	SLS	ULS
Self-weight Moment (kNm)	754.36	678.92	-977.44	-879.70	-1,385.44	-1,246.90
Variable Load Moment (kNm)	-6,127.72	-7,371.24	2,733.17	3,563.44	7,088.71	8,747.74
Total Moment at Final Stage (kNm)	**-3,526.76**	**-4,478.15**	**3,053.93**	**4,176.67**	**5,703.27**	**7,500.84**

Table B.2 summarizes the initial reinforcement used in the numerical model seen in Chapter 5.

Table B.2: Initial reinforcement for Chapter 4 FEA model

Roof			**Floor**			**Walls**		
Tensile	2,568.80	mm^2	Tensile	5,717.00	mm^2	Tensile	4,040.00	mm^2
Compresisve	1,256.00	mm^2	Compresisve	1,256.00	mm^2	Compresisve	1,256.00	mm^2
Total	3,824.80	mm^2	Total	6,973.11	mm^2	Total	5,295.91	mm^2
Ratio	0.30	%	Ratio	0.50	%	Ratio	0.45	%
Rebar Distribution			**Rebar Distribution**			**Rebar Distribution**		
Tensile (bot)			Tensile (bot)			Tensile (bot)		
9x20	2,826.00	mm^2	10x28	6,160.00	mm^2	9x24	4,068.00	mm^2
Compressive (top)			Compressive (top)			Compressive (top)		
4X20	1,256.00	mm^2	4X20	1,256.00	mm^2	4X20	1,256.00	mm^2

C

Reinforced Concrete Paramater Analysis Resutls

Table C.1: RC parameter analysis table of results

Span Length	Span Height	Tunnel Height	Slenderness	Total Width	AS	xu	M	Buoyancy check	Med Roof ULS	Ned ULS	xe	Mrd	Iyy	Wc top	Normal force check	ec	Steel Stress	ecr	Sr, max	wk
10.00	0.70	9.44	14.29	25.70	0.01	0.30	1,447.65	0.86	1,758.75	1,046.70	0.35	2,908.36	0.03	0.08	-23.03	-0.00109	218.40	0.0009	405.94	0.31
11.00	0.77	9.59	14.29	27.70	0.02	0.33	1,781.33	0.85	2,154.28	1,063.77	0.38	3,577.21	0.04	0.10	-23.16	-0.00103	205.88	0.0008	395.31	0.30
12.00	0.84	9.75	14.29	29.70	0.02	0.37	2,149.36	0.85	2,594.94	1,080.85	0.42	4,314.79	0.05	0.12	-23.31	-0.00097	194.73	0.0008	386.45	0.28
13.00	0.92	9.92	14.13	31.70	0.02	0.41	2,612.01	0.85	3,087.27	1,100.36	0.46	5,241.89	0.06	0.14	-23.02	-0.00091	183.38	0.0007	377.97	0.26
14.00	0.99	10.08	14.14	33.70	0.02	0.44	3,053.64	0.86	3,622.93	1,117.44	0.49	6,126.75	0.08	0.16	-23.24	-0.00087	174.47	0.0007	371.68	0.25
14.50	1.04	10.19	13.94	34.70	0.02	0.47	3,390.12	0.87	3,918.84	1,129.64	0.52	6,800.86	0.09	0.18	-22.75	-0.00084	168.63	0.0007	367.71	0.24
15.00	1.07	10.25	14.02	35.70	0.02	0.48	3,600.41	0.87	4,214.64	1,136.95	0.53	7,222.17	0.10	0.19	-23.07	-0.00082	165.30	0.0006	365.50	0.23
17.00	1.23	10.61	13.82	39.70	0.02	0.56	4,828.55	0.89	5,556.47	1,175.98	0.61	9,682.31	0.16	0.25	-22.89	-0.00074	149.58	0.0006	355.55	0.20
17.00	1.24	10.63	13.71	39.70	0.02	0.56	4,911.27	0.90	5,565.40	1,178.42	0.62	9,847.99	0.16	0.26	-22.56	-0.00074	148.70	0.0006	355.01	0.20
19.00	1.39	10.96	13.67	43.70	0.03	0.64	6,236.13	0.92	7,119.40	1,215.01	0.69	12,501.53	0.22	0.32	-22.86	-0.00068	136.59	0.0005	347.89	0.18
20.00	1.47	11.13	13.61	45.70	0.03	0.68	7,007.22	0.94	7,987.49	1,234.53	0.73	14,045.80	0.26	0.36	-22.89	-0.00065	130.91	0.0005	344.68	0.17
22.00	1.63	11.49	13.50	49.70	0.03	0.76	8,683.98	0.97	9,904.35	1,273.56	0.81	17,403.63	0.36	0.44	-23.01	-0.00060	120.85	0.0004	339.22	0.15
23.00	1.71	11.66	13.45	51.70	0.03	0.80	9,589.65	0.98	10,956.08	1,293.07	0.85	19,217.21	0.42	0.49	-23.09	-0.00058	116.38	0.0004	336.87	0.14
25.00	1.88	12.04	13.30	55.70	0.04	0.88	11,663.16	1.02	13,272.91	1,334.54	0.93	23,369.10	0.55	0.59	-23.09	-0.00053	107.89	0.0004	332.54	0.13
27.00	2.10	12.52	12.86	59.70	0.04	0.99	14,647.24	1.06	15,977.49	1,388.21	1.04	29,343.88	0.77	0.74	-22.24	-0.00049	98.59	0.0003	327.98	0.11
28.00	2.14	12.61	13.08	61.70	0.04	1.01	15,226.25	1.07	17,279.91	1,397.96	1.06	30,503.14	0.82	0.76	-23.13	-0.00048	97.07	0.0003	327.25	0.11
29.00	2.23	12.81	13.00	63.70	0.04	1.06	16,570.03	1.08	18,770.30	1,419.92	1.11	33,193.53	0.92	0.83	-23.12	-0.00046	93.81	0.0003	325.71	0.10
30.00	2.32	13.00	12.93	65.70	0.05	1.10	17,970.59	1.10	20,337.62	1,441.87	1.15	35,997.54	1.04	0.90	-23.12	-0.00045	90.77	0.0003	324.28	0.10

D

Python Script and Result Table

```
import matplotlib.pyplot as plt
import matplotlib
from mpl_toolkits.mplot3d import Axes3D
import numpy as np
import pandas as pd

from Finalclasses import Model, compute_eccs

lengths = [20,21,22,23,24,25,26]
heights = [1,1.05,1.1,1.15,1.2,1.25,1.3]
PPs = [50,60,70,80,90,100]
n_eccs = 9 #number of ecc values for matrix size

# LENGTH, HEIGHT, ECCENTRICITY, PP
reinforcements = np.zeros((len(lengths),len(heights),
                           n_eccs,len(PPs)))
As1s=np.zeros((len(lengths),len(heights),
                           n_eccs,len(PPs)))

slenderness=np.zeros((len(lengths),len(heights),
                           n_eccs,len(PPs)))
rows = [] #empty row for excel sheet


for a, length in enumerate(lengths):
    for b, height in enumerate(heights):
        eccs =compute_eccs(height) #calculating the eccentricity based on the height


        for c, ecc in enumerate(eccs):
            for d, PP in enumerate(PPs):

                model1=Model(length,height,ecc,PP)

                As1=model1.compute_loads()
                As1s[a,b,c,d]=As1*1000000
                slenderness[a,b,c,d]=length/height

                if model1.test_passed()== True:
                    print("PASSED",length, height, ecc, PP)
                    reinforcement = model1.compute_reinforcement()

                else:
                    print("Test failed",length, height, ecc, PP)
                    values = model1.compute_reinforcement()
                    reinforcement = np.nan# not a number


                reinforcements[a,b,c,d] = reinforcement
                rows.append(model1.result_table())



header = ['length', 'height', 'ecc','PP', 'self.Freeboard>0.15','xu', 'As1','Pm', 'Mrd','abs(self.signcheck)<fcd' ,'self.wk_F·
df = pd.DataFrame(np.array(rows), columns=header)
df.to_excel(excel_writer = "results1.xlsx",float_format="%.2f")


from Finalconsts1 import *
from sympy import symbols, solve, Eq
import math
from tabulate import tabulate

def compute_eccs(height):
    #Percentage of eccentricity at midspan
    percs=[20,30,40,50,60,70,80,90,100]
    eccs=[]
    for perc in percs:
        eccs.append((height/2-coverPT)*perc/100)
    return eccs

class Model:
    def __init__(self, length, height,ecc,PP):
        self.length = length
        self.height = height
        self.ecc=ecc
        self.PP=PP



    def compute_loads(self):
        self.tests=[]

        Floor_height = self.height+0.1
        Total_height = Inner_height + self.height + Floor_height
        Total_width=2*self.length+2*Outer_wall+2*Inner_wall+Gallery_width
```

```
        #=======================================================
        #2. Buoyancy check

        Hydro_force=Total_height*Total_width*water
        Concrete_force=(Total_height*Total_width-(self.length*Inner_height*2+Gallery_width*Inner_height))*cdens
        Steel_force=(Total_height*Total_width-(self.length*Inner_height*2+Gallery_width*Inner_height))*sdens*0.02
        water_ballast=(Hydro_force-Concrete_force-Steel_force)*0.8
        self.Freeboard=(Hydro_force-Concrete_force-Steel_force-water_ballast)/(Total_width*water)

        print("height",self.height,"length",self.length)
        self.tests.append(self.Freeboard>0.15) #test 1
        if self.Freeboard>0.15:
            print('Freeboard passed')
        else:
            print('Freeboard failed')
        print("Freeboard=", self.Freeboard) #test
         #print(Freeboard if Freeboard>0 else 0)
        #Water_ballast

        #=======================================================
        #Loads
        #hydroloads kept constant- same distance to water level-10m
        #only roof loads
        Hydro_height=Water_table+Total_height+rock_height
        C_roof=self.height*cdens
        S_roof=self.height*sdens*0.02
        Hydro_roof=water*(Water_table+rock_height) #from spread sheet - change when heigh changes?
        Rock_roof=(Rdens-water)*rock_height
        Tot_roofload=C_roof+S_roof+Hydro_roof+Rock_roof
        Tot_roofload_ULS=1.2*C_roof+1.2*S_roof+1.15*Hydro_roof+1.2*Rock_roof

    #side loads
        Side_roof= (Hydro_roof+Rock_roof/2)+Rock_roof/2
        Side_floor=Hydro_height*water+(Rdens-water+(Total_height*(rdens-water)))
    #Normal Forces
        Side_f=Total_height*(Side_roof+Side_floor)/2
        Side_dist=Total_height*(Side_roof+2*Side_floor)/(2*(Side_roof+Side_floor))
        N_roof=Side_f*Side_dist/Total_height
        N_floor=Side_f-N_roof
        N_roof_ULS=1.15*N_roof
        N_floor_ULS=N_floor*1.15
    #=================
    #Design Moment Calculation
    #Edge 1 SLS
        coef=(1.2*6*(2+0.285*1.2714))
        Msw_sls_B1= -(1/coef)*(C_roof+S_roof)*self.length**2
        Mvar_sls_B1=-(1/coef)*(Hydro_roof+Rock_roof)*self.length**2
        Mtot_sls_B1=-(1/coef)*(Tot_roofload)*self.length**2
        Msw_uls_B1= -(1/coef)*(1.2*C_roof+1.2*S_roof)*self.length**2
        Mvar_uls_B1=-(1/coef)*(1.15*Hydro_roof+1.2*Rock_roof)*self.length**2
        Mtot_uls_B1=-(1/coef)*(Tot_roofload_ULS)*self.length**2

    #=================
    #Edge #2
        Msw_sls_B2= -(1/12)*(C_roof+S_roof)*self.length**2
        Mvar_sls_B2=-(1/12)*(Hydro_roof+Rock_roof)*self.length**2
        Mtot_sls_B2=-(1/12)*(Tot_roofload)*self.length**2

        Msw_uls_B2= -(1/12)*(1.2*C_roof+1.2*S_roof)*self.length**2
        Mvar_uls_B2=-(1/12)*(1.15*Hydro_roof+1.2*Rock_roof)*self.length**2
        self.Mtot_uls_B2=-(1/12)*(Tot_roofload_ULS)*self.length**2
    #=================
    #Midspan
        self.Msw_sls_mid= (Msw_sls_B1+Msw_sls_B2)/2+(1/8)*(C_roof+S_roof)*self.length**2
        Mvar_sls_mid=(Mvar_sls_B1+Mvar_sls_B2)/2+(1/8)*(Hydro_roof+Rock_roof)*self.length**2
        Mtot_sls_mid=(Mtot_sls_B1+Mtot_sls_B2)/2+(1/8)*(Tot_roofload)*self.length**2

        Msw_uls_mid= (Msw_uls_B1+Msw_uls_B1)/2+(1/8)*(1.2*C_roof+1.2*S_roof)*self.length**2
        Mvar_uls_mid=(Mvar_uls_B1+Mvar_uls_B1)/2+(1/8)*(1.15*Hydro_roof+1.2*Rock_roof)*self.length**2
        Mtot_uls_mid=(Mtot_uls_B1+Mtot_uls_B1)/2+(1/8)*(Tot_roofload_ULS)*self.length**2


        MgA=Msw_uls_mid
        MgqA=Mtot_uls_mid
        MgB=-Msw_uls_B2
        MgqB=-self.Mtot_uls_B2
        self.N=abs(N_roof_ULS)
        self.N_sls=abs(N_roof)
        Med=-self.Mtot_uls_B2
        Iyy=(1/12)*b*self.height**3
        self.Wtop=Iyy/(self.height/2)
        self.Ac=self.height*b


        l1=Outer_wall+(7/8)*self.length
        l2=Total_width-2*l1
        a1=0
```

```
        f1=e1+self.ecc
        f2=0.1
        perc=(self.ecc/(self.height/2-coverPT))*100
        R1=l1**2/(8*f1)
        R2=(l2)**2/(8*f2)
        q1=1/R1
        q2=1/R2

    #calculate Pmo

        eB1=(Inner_height/self.length)*(self.height**3/Outer_wall**3)
        eB=0.8*(1/(6*(2+eB1)))*q1*self.length**2
        eC=(1/12)*q1*self.length**2-(1/12)*q2*l2**2
        self.eA=(eB+eC)/2-(1/8)*0.93*q1*self.length**2

        #t=0,
        #midspan
        PmA1b=symbols('PmA1b')
        expr1=-PmA1b/self.Ac+(-PmA1b*self.eA + MgA)/self.Wtop-1000
        sol1=solve(expr1)
        PmA1t=symbols('PmA1t')
        expr2=-PmA1t/self.Ac + (PmA1t*self.eA - MgA)/self.Wtop - 1000
        sol2=solve(expr2)
        #edge
        PmB1b=symbols('PmB1b')
        expr3=-PmB1b/self.Ac + (PmB1b*eC - MgB)/self.Wtop - 1000
        sol3=solve(expr3)
        PmB1t=symbols('PmB1t')
        expr4=-PmB1t/self.Ac + (-PmB1t*eC + MgB)/self.Wtop - 1000
        sol4=solve(expr4)

        #t=infinity
        #midspan
        PmA2b=symbols('PmA2b')
        expr5=-0.85*PmA2b/self.Ac + (-0.85*PmA2b*self.eA + MgqA)/self.Wtop - 1000
        sol5=solve(expr5)
        PmA2t=symbols('PmA2t')
        expr6=-0.85*PmA2t/self.Ac + (0.85*PmA2t*self.eA - MgqA)/self.Wtop - 1000
        sol6=solve(expr6)
        #edge
        PmB2b=symbols('PmB2b')
        expr7=-0.85*PmB2b/self.Ac + (0.85*PmB2b*eC - MgqB)/self.Wtop - 1000
        sol7=solve(expr7)
        PmB2t=symbols('PmB2t')
        expr8=(-0.85*PmB2t-self.N)/self.Ac + (-0.85*PmB2t*eC + MgqB)/self.Wtop - 1000
        sol8=solve(expr8)
        print("Pmo is > ", sol8)

        #prestressing loss calculation
        k=0.01
        mu=0.19 #
        theta=2*(f1/(l1/2))+f2/(l2/2)
        theta2=l1/R1+(l2/2)/R2
        x=Total_width/2
        self.pmx=math.exp(-mu*(theta2+k*x))

        #Percent Prestress
        self.Pm0=self.PP*sol8[0]/100
        self.Ap=self.Pm0/(1395*1000)
        self.Pm=self.pmx*0.85*self.Pm0
        self.ds1=self.height-cover
        self.ds2=cover
        self.dp=self.height/2+self.ecc
        self.As2=1256/1000000
        self.As1=2000/1000000
        self.Mrd=1
        Fs2=self.As2*fy
        count1=0
        #Moment capacity and steel area calculation
        while self.Mrd<=abs(self.Mtot_uls_B2)and count1 <20:
            count1=count1+1
            self.As1=self.As1+0.001
            Fs1=self.As1*fy
            Fs2=self.As2*fy
            Fp=self.Ap*fyp
            self.xu=(Fs1-Fs2+Fp+self.N)/(fcd*b*0.75)
            Fc=fcd*b*0.75*self.xu
            es2=0.0035*(self.xu-self.ds2)/self.xu
            if es2>0.002:
                Fs2=self.As2*fy
            else:
                Fs2=self.As2*Es*es2
            z1=self.ds1-0.39*self.xu
            z2=0.39*self.xu-self.ds2
            zp=self.dp-0.39*self.xu
            self.Mrd=(Fs1*z1+Fs2*z2+self.Ap*(1606*1000-1080*1000)*zp+abs(self.N)*(self.height/2-0.39*self.xu)+self.Pm*(self.h
```

```
        self.tests.append(self.Mrd>self.Mtot_uls_B2) #test 2
        self.signcheck=-(self.Pm+abs(self.N))/self.Ac+(self.Mtot_uls_B2+eC*self.Pm)/self.Wtop
        if abs(self.signcheck)<fcd:
            print('Normal stress passed')
        else:
            print('Normal stress failed')
        self.tests.append(abs(self.signcheck)<fcd) #test 3

        #============================================
        #Final stage cracking
        #ULS compression zone height
        Mmax_final=abs(Mtot_sls_B2+eC*self.Pm)
        sigmc1=-(self.Pm+self.N_sls)/self.Ac-(Mmax_final/self.Wtop)
        ec_1=-sigmc1/Ec
        xe_F=symbols('xe_F')
        Fs_Fin1=Es*self.As1*ec_1*(self.ds1-xe_F)/xe_F
        Fs_Fin2=Es*self.As2*ec_1*(xe_F-self.ds2)/xe_F
        Fp_Fin=0.5*Ep*self.Ap*ec_1*(self.dp-xe_F)/xe_F
        Fc_Fin=0.5*Ec*b*xe_F*ec_1
        eq_Fin=Eq(Fc_Fin+Fs_Fin2-Fs_Fin1-Fp_Fin-self.Pm-self.N_sls)
        sol=solve((eq_Fin),(xe_F))
        xe_F=sol[1]

        #crack width at final stage test

        sigs=min(Es*ec_F*(self.ds1-sol[1])/sol[1],500*1000)
        ae=Es/Ec
        squig=0.5
        kt=0.6 #short term loading
        fcteff=(0.3*(fck/1000)**(2/3))*1000
        k1=0.8
        k2=0.5
        k3=3.4
        k4=0.425
        diam=15/1000
        if 2.5*(self.height-self.ds1)<(self.height-xe_F)/3:
            heff=2.5*(self.height-self.ds1)
        else:
            heff=(self.height-xe_F)/3
        Aceff=heff*b
        ppeff_F=self.As1/Aceff
        Sr_F=k3*cover2+k1*k2*k4*(diam/ppeff_F)
         print(Sr_F)
        esm_F=(sigs-kt*(fcteff/ppeff_F)*(1+ae*ppeff_F))/Es
        if esm_F<0.6*sigs/Es:
            esm_F=0.6*sigs/Es
            self.wk_F=esm_F*Sr_F
        else:
            esm_F=(sigs-kt*(fcteff/ppeff_F)*(1+ae*ppeff_F))/Es
            self.wk_F=esm_F*Sr_F

        #test4
        if self.wk_F<0.15/1000:
            print('crack width passed')
        else:
            print('crack width failed')
        self.tests.append(self.wk_F*1000< 0.15)
        return self.As1

    def test_passed(self):

        if all(self.tests) == True:
            print("PASSED")
            return True
        else:
            print("FAIL")
            return False

    def compute_reinforcement(self):
        #SLS compression zone height
        Mmax=abs(self.Msw_sls_mid+self.eA*self.Pm0)
        sigmc=(-(self.Pm0)/self.Ac-(Mmax/self.Wtop))
        ec=-sigmc/Ec
        xe=symbols('xe')
        Fs_1=Es*self.As1*ec*(xe-self.ds2)/xe
        Fs_2=Es*self.As2*ec*(self.ds1-xe)/xe
        Fp_e=0.5*Ep*self.Ap*ec*(xe-coverPT)/xe
        Fc_e=0.5*Ec2*b*xe*ec
        eq1=Eq(Fc_e+Fs_1+Fp_e-Fs_2-self.Pm0)
        sol=solve((eq1),(xe))
        self.xed=sol[1]

      #=======================================
     #CALCULATING ADDITIONAL REINFORCEMENT FROM CRACK WIDTH
        self.sigsb=min(Es*ec*(self.ds1-sol[1])/sol[1],500*1000)
        ae=Es/Ec
```

```
    squig=0.5
    kt=0.6 #short term loading
    fcteff=(0.3*(fck/1000)**(2/3))*1000
    k1=0.8
    k2=0.5
    k3=3.4
    k4=0.425
    diam=15/1000
    if 2.5*(self.height-self.ds1)<(self.height-self.xed)/3:
        heff=2.5*(self.height-self.ds1)
    else:
        heff=(self.height-self.xed)/3

    Aceff=heff*b
    self.As=1/10000
    self.wk=0.3
    count=0
    while self.wk>=0.15/1000 and count <200:
          count=count+1
          self.As=self.As+0.0001
          ppeff=self.As/Aceff
          Sr=k3*cover2+k1*k2*k4*(diam/ppeff)
          esm=(self.sigsb-kt*(fcteff/ppeff)*(1+ae*ppeff))/Es
          if esm<0.6*self.sigsb/Es:
              esm=0.6*self.sigsb/Es
              self.wk=esm*Sr

          else:
              esm=(self.sigsb-kt*(fcteff/ppeff)*(1+ae*ppeff))/Es
              self.wk=esm*Sr
    reinforcement=self.As*1000000
    return reinforcement


def result_table(self):
    self.rows=[self.length, self.height, self.ecc, self.PP, self.Freeboard>0.15 ,self.xu*1000, self.As1*1000000,self.Mrd,
```

Table D.1: Python results for 20m length and 1.2 & 1.3m heights

Length (m)	height (m)	ecc (m)	PP (%)	Freeboard	xu (mm)	As1 (mm^2)	Pm (kN)	Mrd (kNm)	Normal Stress	Final CW	wk (mm)	As (mm^2)
20	1.2	0.24	50	TRUE	597.98	3000	8,539.99	8,482.69	True	True	0.13	300
20	1.2	0.24	60	TRUE	697.72	3000	10,247.99	9,119.71	True	True	0.14	500
20	1.2	0.24	70	TRUE	797.47	3000	11,955.99	9,560.40	True	True	0.15	800
20	1.2	0.24	80	TRUE	897.21	3000	13,663.98	9,804.74	True	True	0.15	1200
20	1.2	0.24	90	TRUE	996.95	3000	15,371.98	9,852.75	True	True	0.15	1900
20	1.2	0.24	100	TRUE	1,096.69	3000	17,079.98	9,704.42	False	True	0.15	2800
20	1.2	0.29	50	TRUE	548.66	3000	7,666.97	8,084.16	True	True	0.12	400
20	1.2	0.29	60	TRUE	638.54	3000	9,200.36	8,753.42	True	True	0.14	600
20	1.2	0.29	70	TRUE	728.41	3000	10,733.75	9,263.66	True	True	0.14	1000
20	1.2	0.29	80	TRUE	818.29	3000	12,267.15	9,614.87	True	True	0.14	1500
20	1.2	0.29	90	TRUE	908.17	3000	13,800.54	9,807.05	True	True	0.15	2200
20	1.2	0.29	100	TRUE	998.05	3000	15,333.93	9,840.22	True	True	0.15	3400
20	1.2	0.34	50	TRUE	508.21	3000	6,951.18	7,720.76	True	False	0.14	400
20	1.2	0.34	60	TRUE	590.00	3000	8,341.42	8,400.33	True	True	0.14	700
20	1.2	0.34	70	TRUE	671.79	3000	9,731.66	8,948.55	True	True	0.15	1100
20	1.2	0.34	80	TRUE	753.58	3000	11,121.89	9,365.41	True	True	0.15	1700
20	1.2	0.34	90	TRUE	835.37	3000	12,512.13	9,650.91	True	True	0.15	2600
20	1.2	0.34	100	TRUE	917.15	3000	13,902.37	9,805.05	True	True	0.15	4000
20	1.2	0.39	50	TRUE	474.45	3000	6,353.69	7,392.12	True	False	0.13	500
20	1.2	0.39	60	TRUE	549.48	3000	7,624.43	8,069.18	True	True	0.14	800
20	1.2	0.39	70	TRUE	624.52	3000	8,895.17	8,635.97	True	True	0.14	1300
20	1.2	0.39	80	TRUE	699.55	3000	10,165.91	9,092.46	True	True	0.15	1900
20	1.2	0.39	90	TRUE	774.59	3000	11,436.64	9,438.66	True	True	0.15	3000
20	1.2	0.39	100	TRUE	849.62	3000	12,707.38	9,674.58	True	True	0.15	4800
20	1.2	0.44	50	TRUE	445.83	3000	5,847.42	7,095.63	True	False	0.14	500
20	1.2	0.44	60	TRUE	515.14	3000	7,016.91	7,762.65	True	True	0.14	900
20	1.2	0.44	70	TRUE	584.46	3000	8,186.39	8,335.80	True	True	0.15	1400
20	1.2	0.44	80	TRUE	653.77	3000	9,355.88	8,815.08	True	True	0.15	2200
20	1.2	0.44	90	TRUE	723.08	3000	10,525.36	9,200.48	True	True	0.15	3500
20	1.2	0.44	100	TRUE	792.39	3000	11,694.85	9,492.02	True	True	0.15	5800
20	1.2	0.49	50	TRUE	421.27	3000	5,412.98	6,828.02	True	False	0.13	600
20	1.2	0.49	60	TRUE	485.67	3000	6,495.58	7,480.62	True	True	0.14	1000
20	1.2	0.49	70	TRUE	550.07	3000	7,578.18	8,052.39	True	True	0.15	1600
20	1.2	0.49	80	TRUE	614.47	3000	8,660.78	8,543.32	True	True	0.15	2500
20	1.2	0.49	90	TRUE	678.87	3000	9,743.37	8,953.41	True	True	0.15	4000
20	1.2	0.49	100	TRUE	743.27	3000	10,825.97	9,282.67	True	True	0.15	6900
20	1.3	0.27	50	TRUE	551.14	3000	7,681.52	9,071.31	True	True	0.13	200
20	1.3	0.27	60	TRUE	641.02	3000	9,217.83	9,887.08	True	True	0.13	400
20	1.3	0.27	70	TRUE	730.91	3000	10,754.13	10,543.59	True	True	0.14	600
20	1.3	0.27	80	TRUE	820.79	3000	12,290.43	11,040.86	True	True	0.15	800
20	1.3	0.27	90	TRUE	910.68	3000	13,826.74	11,378.88	True	True	0.15	1200
20	1.3	0.27	100	TRUE	1,000.57	3000	15,363.04	11,557.64	True	True	0.15	1700
20	1.3	0.32	50	TRUE	507.05	3000	6,899.79	8,600.22	True	True	0.11	300
20	1.3	0.32	60	TRUE	588.12	3000	8,279.74	9,411.98	True	True	0.15	400
20	1.3	0.32	70	TRUE	669.18	3000	9,659.70	10,094.55	True	True	0.14	700
20	1.3	0.32	80	TRUE	750.25	3000	11,039.66	10,647.94	True	True	0.15	1000
20	1.3	0.32	90	TRUE	831.32	3000	12,419.61	11,072.15	True	True	0.15	1400
20	1.3	0.32	100	TRUE	912.39	3000	13,799.57	11,367.18	True	True	0.15	2000
20	1.3	0.38	50	TRUE	470.84	3000	6,257.83	8,183.97	True	False	0.13	300
20	1.3	0.38	60	TRUE	544.66	3000	7,509.39	8,979.51	True	True	0.14	500
20	1.3	0.38	70	TRUE	618.49	3000	8,760.96	9,668.21	True	True	0.14	800
20	1.3	0.38	80	TRUE	692.31	3000	10,012.52	10,250.07	True	True	0.14	1200
20	1.3	0.38	90	TRUE	766.14	3000	11,264.09	10,725.09	True	True	0.15	1700
20	1.3	0.38	100	TRUE	839.97	3000	12,515.65	11,093.28	True	True	0.15	2400
20	1.3	0.43	50	TRUE	440.56	3000	5,721.26	7,815.70	True	False	0.14	300
20	1.3	0.43	60	TRUE	508.34	3000	6,865.51	8,588.74	True	True	0.14	600
20	1.3	0.43	70	TRUE	576.11	3000	8,009.76	9,272.00	True	True	0.15	900
20	1.3	0.43	80	TRUE	643.88	3000	9,154.01	9,865.46	True	True	0.14	1400
20	1.3	0.43	90	TRUE	711.65	3000	10,298.26	10,369.14	True	True	0.15	2000
20	1.3	0.43	100	TRUE	779.42	3000	11,442.51	10,783.04	True	True	0.15	2800
20	1.3	0.48	50	TRUE	414.88	3000	5,266.11	7,488.78	True	False	0.13	400
20	1.3	0.48	60	TRUE	477.52	3000	6,319.33	8,236.35	True	True	0.14	700
20	1.3	0.48	70	TRUE	540.15	3000	7,372.55	8,907.44	True	True	0.15	1000
20	1.3	0.48	80	TRUE	602.79	3000	8,425.78	9,502.05	True	True	0.14	1600
20	1.3	0.48	90	TRUE	665.42	3000	9,479.00	10,020.18	True	True	0.15	2300
20	1.3	0.48	100	TRUE	728.06	3000	10,532.22	10,461.82	True	True	0.15	3300
20	1.3	0.54	50	TRUE	392.82	3000	4,875.18	7,197.33	True	False	0.14	400
20	1.3	0.54	60	TRUE	451.04	3000	5,850.21	7,918.34	True	True	0.15	700
20	1.3	0.54	70	TRUE	509.26	3000	6,825.25	8,573.45	True	True	0.14	1200
20	1.3	0.54	80	TRUE	567.48	3000	7,800.28	9,162.66	True	True	0.15	1800
20	1.3	0.54	90	TRUE	625.71	3000	8,775.32	9,685.96	True	True	0.15	2600
20	1.3	0.54	100	TRUE	683.93	3000	9,750.36	10,143.36	True	True	0.15	3800